E-ISSN: 2147-1959

MIRT

Molecular Imaging and Radionuclide Therapy

February 2025 Volume 34 Issue 1 www.tsnm.org

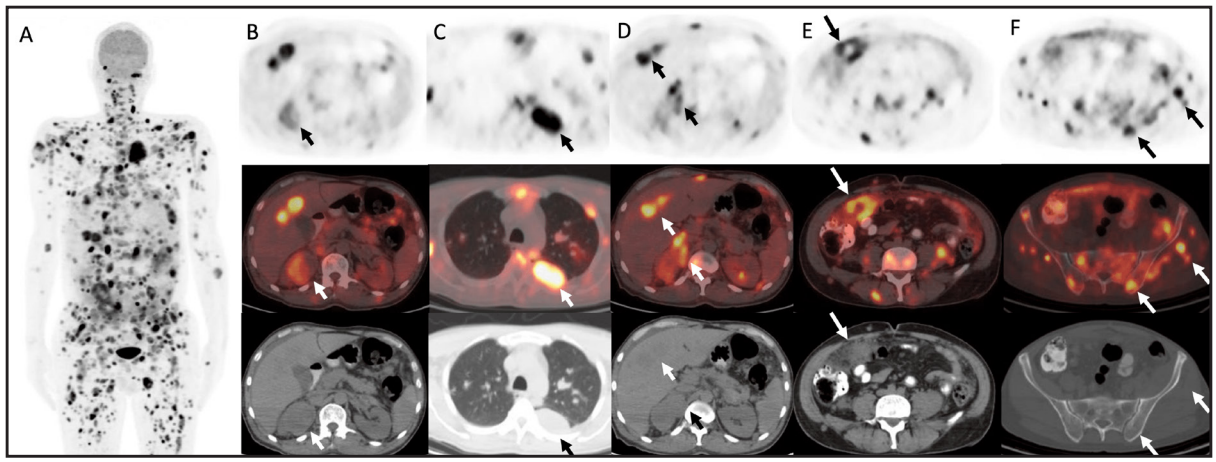

"Official Journal of the Turkish Society of Nuclear Medicine"

galenos yayınevi

TURKISH SOCIETY OF NUCLEAR MEDICINE 1975

MIRT

Molecular Imaging and Radionuclide Therapy

MIRT

Molecular Imaging and Radionuclide Therapy

Turkish Society of Nuclear Medicine
Cinnah Caddesi Pilot Sokak No: 10/12 Çankaya 06650 Ankara, Türkiye **Phone:** +90 312 441 00 45 **Fax:** +90 312 441 12 95 **Web:** www.tsnm.org **E-mail:** dernekmerkezi@tsnm.org
"Formerly Turkish Journal of Nuclear Medicine"

Reviewing the articles' conformity to the publishing standards of the Journal, typesetting, reviewing and editing the manuscripts and abstracts in English, creating links to source data, and publishing process are realized by Galenos.

Publisher Contact
Address: Molla Gürani Mah. Kaçamak Sk. No: 21/1 34093 İstanbul, Türkiye
Phone: +90 (530) 177 30 97 / +90 (539) 307 32 03
E-mail: info@galenos.com.tr/yayin@galenos.com.tr
Web: www.galenos.com.tr
Publisher Certificate Number: 14521

Online Publication Date: February 2025
ISSN: 2146-1414 **E-ISSN:** 2147-1959
International scientific journal published quarterly.

MIRT

Molecular Imaging and Radionuclide Therapy

Please refer to the journal's webpage **(https://mirt.tsnmjournals.org/)** for "Aims and Scope", "Instructions to Authors" and "Ethical Policy".

The editorial and publication process of Molecular Imaging and Radionuclide Therapy are shaped in accordance with the guidelines of ICMJE, WAME, CSE, COPE, EASE, and NISO. The journal is in conformity with the Principles of Transparency and Best Practice in Scholarly Publishing.

Molecular Imaging and Radionuclide Therapy is indexed in **Pubmed, Pubmed Central (PMC), Emerging Sources Citation Index (ESCI), TUBITAK-ULAKBIM, Scopus, Gale/Cengage Learning, EBSCO databases, ProQuest Health & Medical Complete, CINAHL, Embase, J-Gate, IdealOnline, Türkiye Atıf Dizini-Turkiye Citation Index, Turk Medline, Hinari, GOALI, ARDI, OARE, AGORA** and **CNKI**.

The journal is published electronically.

Owner: Murat Fani Bozkurt on Behalf of Turkish Society of Nuclear Medicine

Responsible Manager: Murat Fani Bozkurt

MIRT
Molecular Imaging and Radionuclide Therapy

CONTENTS

Original Articles

Interesting Images

MIRT
Molecular Imaging and Radionuclide Therapy

CONTENTS

Letter to the Editor

Original Article

Mol Imaging Radionucl Ther 2025;34:1-9 *DOI:10.4274/mirt.galenos.2025.16023*

Improved Accuracy and Reliability of PRIMARY Scoring Using Delayed [^{68}Ga] Ga-PSMA PET/CT Imaging

Geç [^{68}Ga] Ga-PSMA PET/BT Görüntüleme Yöntemi İle PRIMARY Derecelendirmesinin Doğruluğunun ve Güvenilirliğinin Artırılması

Kaan Akçay[1], Gamze Beydağı[1], Onur Erdem Şahin[2], Reşit Akyel[3], Elife Akgün[4], Özgül Ekmekçioğlu[5], Nalan Alan Selçuk[1], Türkay Toklu[1], Asiye Işın Doğan Ekici[6], Kayra Kapran[1], Levent Kabasakal[1,2]

[1]*Yeditepe University Faculty of Medicine, Department of Nuclear Medicine, İstanbul, Türkiye*
[2]*İstanbul University-Cerrahpaşa, Cerrahpaşa Faculty of Medicine, Department of Nuclear Medicine, İstanbul, Türkiye*
[3]*Yedikule Chest Diseases and Chest Surgery Training and Research Hospital, Clinic of Nuclear Medicine, İstanbul, Türkiye*
[4]*University of Health Sciences Türkiye, Başakşehir Çam and Sakura City Hospital, Clinic of Nuclear Medicine, İstanbul, Türkiye*
[5]*University of Health Sciences Türkiye, Şişli Hamidiye Etfal Training and Research Hospital, Clinic of Nuclear Medicine, İstanbul, Türkiye*
[6]*Acıbadem University Faculty of Medicine, Department of Pathology, İstanbul, Türkiye*

Abstract

Objectives: Delayed [^{68}Ga]Ga-prostate-specific membrane antigen (PSMA) positron emission tomography/computed tomography (PET/CT) images show reduced PSMA uptake in benign lesions and increased PSMA uptake in malignant lesions. This study investigated the efficacy of PRIMARY scoring on [^{68}Ga]Ga-PSMA PET/CT images at standard versus delayed time points and assessed the potential added value of delayed imaging in PRIMARY scoring.

Methods: A total of 140 patients with biopsy results of International Society of Urological Pathology grade groups (ISUP) 1-2 who had standard (median 60 min) and delayed images (median 138 min) with [^{68}Ga]Ga-PSMA PET/CT before radical prostatectomy were included. Results were confirmed in pathological reports. For diagnostic parameters, two experienced nuclear medicine physicians, who were blinded to clinical data, independently reviewed the images, and a third physician provided consensus in cases of disagreement. PRIMARY scoring was also conducted by four nuclear medicine physicians on both images, with a 1-month interval between assessments for intraobserver agreement analyses.

Results: The percentage of lesions scored as 1-2 in PRIMARY scoring decreased from 29% to 10% in delayed images compared with standard images, whereas lesions scored as 3-5 increased from 71% to 90%. Additionally, agreement between two experienced nuclear medicine physicians regarding scoring was 66% for standard imaging and 77% for delayed imaging. The number of patients with PRIMARY score 5 increased from 31 to 46 in delayed imaging. All patients were confirmed to have clinically significant prostate cancer (csPCa). Furthermore, no csPCa of ISUP grade 3 or higher was detected in patients with a delayed PRIMARY score (dPRIMARY). The sensitivity of standard PRIMARY scoring was 71%, which increased to 92% with dPRIMARY scoring, with a consistent positive predictive value of 87% for both. Intraobserver agreement Cohen's kappa values for all observers were higher for delayed images than for standard images. Inter-observer agreement, assessed by Fleiss kappa, was 0.47 and 0.52 for standard images in rounds 1 and 2, respectively, and 0.61 and 0.72 for delayed images, respectively.

Conclusion: Decreased background activity and increased primary tumor uptake in delayed images improved differentiation between primary tumors and benign lesions, leading to better primary tumor identification. Enhanced reliability was also observed in both intraobserver and interobserver assessments of delayed images.

Keywords: Prostate-specific membrane antigen, prostate cancer, clinically significant prostate cancer, active surveillance, primary staging, prostate biopsy

Address for Correspondence: Levent Kabasakal, Yeditepe University Faculty of Medicine; İstanbul University-Cerrahpaşa, Cerrahpaşa Faculty of Medicine, Department of Nuclear Medicine, İstanbul, Türkiye
E-mail: lkabasakal@tsnm.org **ORCID ID:** orcid.org/0000-0002-4050-1972
Received: 26.08.2024 **Accepted:** 23.12.2024 **Epub:** 31.01.2025 **Publication Date:** 07.02.2025

Cite this article as: Akçay K, Beydağı G, Şahin OE, Akyel R, Akgün E, Ekmekçioğlu Ö, Alan Selçuk N, Toklu T, Doğan Ekici AI, Kapran K, Kabasakal L. Improved accuracy and reliability of PRIMARY scoring using delayed [^{68}Ga] Ga-PSMA PET/CT imaging. Mol Imaging Radionucl Ther. 2025;34:1-9.

Öz

Amaç: Yapılan çalışmalarda malign lezyonların prostat-spesifik membran antijeni (PSMA) tutulumunun geç [^{68}Ga]Ga-PSMA Pozitron emisyon tomografisi/bilgisayarlı tomografi (PET/BT) görüntülemede belirginleştiği bildirilmiştir. Bu çalışmanın amacı [^{68}Ga]Ga-PSMA PET/BT'nin PRIMARY derecelendirmesinde etkinliğini araştırmak ve PRIMARY derecelendirmesinde geç görüntülemenin olası katkısını değerlendirmektedir.

Yöntem: Radikal prostatektomi öncesi standart (ortalama 60 dakika) ve geç (ortalama 138 dakika) [^{68}Ga]Ga-PSMA PET/BT görüntüleri olan biyopsi sonucuna göre Uluslararası Ürolojik Patoloji Derneği Derece Grupları (ISUP) 1-2 (bISUP 1-2) prostat kanseri tanılı 140 hasta çalışmaya dahil edilmiştir. Sonuçlar radikal prostatektomi sonrası patoloji raporları ile doğrulanmıştır. Tanısal parametreler için klinik verilerden habersiz iki deneyimli nükleer tıp uzmanı görüntüleri bağımsız olarak incelemiş, anlaşmazlık durumunda üçüncü bir uzman ile uzlaşma sağlanmıştır. PRIMARY derecelendirmesinin gözlemci içi uyum analizleri dört nükleer tıp uzmanı tarafından, bir ay arayla ile standart ve geç görüntüler üzerinden gerçekleştirilmiştir.

Bulgular: PRIMARY derecelendirmesi sonuçlarına göre, geç görüntülerde PRIMARY 1-2 olarak derecelendirilen lezyonların yüzdesi standart görüntülerle karşılaştırıldığında %29'dan %10'a düşerken, 3-5 olarak derecelendirilen lezyonlar %71'den %90'a yükselmiştir. Ayrıca, iki deneyimli nükleer tıp uzmanı arasındaki derecelendirme uyumu, standart görüntülemede %66 iken, geç görüntülemede %77'ye çıkmıştır. Geç görüntülemede PRIMARY 5 olan hasta sayısı 31'den 46'ya yükselmiş ve tamamının klinik önemi olan prostat kanseri (csPCa) olduğu doğrulanmıştır. Ayrıca, geç görüntülerde PRIMARY derecelendirmesi 1-2 olan hastalarda ISUP 3 veya daha yüksek derecede csPCa tespit edilmemiştir. Standart görüntülerdeki PRIMARY derecelendirmesinin duyarlılığı %71 iken, geç görüntülerde bu oran %92'ye çıkmış, her ikisi için de pozitif öngörü değeri %87 olarak sabit kalmıştır. Gözlemci-içi uyumu için Cohen's kappa değerleri, geç görüntülerde standart görüntülere göre daha yüksek bulunmuştur. Gözlemciler-arası uyumu ise Fleiss kappa ile değerlendirilmiş, 1. ve 2. değerlendirme turunda sırasıyla standart görüntüler için 0,47 ve 0,52, geç görüntüler için ise 0,61 ve 0,72 olarak bulunmuştur.

Sonuç: Geç görüntülerde arka plan aktivitesindeki azalmanın ve primer tümör tutulumundaki artışın, primer tümörün daha net bir şekilde tanımlanmasına olanak sağladığı gözlemlenmiştir. Ayrıca, bu görüntülerde hem gözlemci içi uyumun hem de gözlemciler arası uyumun güvenilirliğinin belirgin şekilde arttığı tespit edilmiştir.

Anahtar kelimeler: Prostat-spesifik membran antijeni, prostat kanseri, klinik anlamlı prostat kanseri, aktif izlem, PRIMARY derecelendirme, prostat biyopsisi

Introduction

Positron emission tomography/computed tomography (PET/CT) with [^{68}Ga]-labeled prostate-specific membrane antigen (PSMA) inhibitors ([^{68}Ga]Ga-PSMA-11 PET/CT) has emerged as a valuable modality for both staging and restaging of clinically significant prostaate cancer (csPCa) (1,2,3). However, recent studies have suggested its potential utility in the primary diagnosis of csPCa, particularly in distinguishing clinically significant csPCa from indolent forms (4,5). Notably, PSMA expression correlates positively with csPCa grade, with higher expression associated with increased disease severity and poorer prognosis (6). Molecular imaging with [^{68}Ga]Ga-PSMA PET/CT provides insights into disease at the molecular level, with PSMA uptake reflecting PSMA expression levels. Studies have indicated a direct association between maximum standardized uptake value (SUV_{max}) on [^{68}Ga]Ga-PSMA PET/CT and PSMA expression, with SUV_{max} escalating alongside higher-grade groups of csPCa (7). The PRIMARY trial was undertaken to evaluate the diagnostic roles of [^{68}Ga]Ga-PSMA PET/CT and multi-parametric magnetic resonance imaging (mpMRI) in discerning csPCa (8). Notably, the PRIMARY trial revealed a higher sensitivity [^{68}Ga]Ga-PSMA PET/CT than mpMRI, with a marked improvement observed when both modalities were combined.

The introduction of the PRIMARY score signifies a remarkable advancement in csPCa diagnosis. Incorporating factors such as the uptake pattern within the prostate gland, location within the peripheral zone, and intensity of PSMA uptake, the PRIMARY score aims to enhance diagnostic accuracy (4). Reproducibility studies have demonstrated comparable reliability to that of MRI, suggesting the potential for predicting csPCa (9). Although the PRIMARY score has been reported to achieve successful results in the diagnosis of csPCa in a selected group of patients with low-grade csPCa (10), its applicability in patients with low-grade disease remains uncertain and requires further refinement (11).

PSMA uptake varies in benign prostate lesions and in normal prostate tissue on [^{68}Ga]Ga-PSMA PET/CT. Within the PRIMARY scoring system, the first three scores are primarily aimed at differentiating benign pathologies from csPCa, with a focus on lesions predominantly located in the peripheral zone (4). It has been postulated that increased PSMA uptake outside the peripheral zone predominantly indicates benign conditions. Early studies using [^{68}Ga]Ga-PSMA PET/CT demonstrated a reduction in PSMA uptake in benign lesions and background activity on delayed images obtained 2-3 hours after injection (12,13,14,15). In contrast, PSMA uptake was observed to be constant or increased in malignant lesions. Therefore, delayed imaging may allow for a more accurate classification of benign prostate lesions, potentially improving the efficacy of the PRIMARY scoring system.

This study aimed to investigate the comparative efficacy of PRIMARY scoring on [^{68}Ga]Ga-PSMA PET/CT images acquired at standard versus delayed time points and to ascertain the potential incremental value of delayed imaging in PRIMARY scoring assessment.

Materials and Methods

Patient Population and Study Protocol

We assessed 140 treatment-naive patient records diagnosed with International Society of Urological Pathology grade groups (ISUP) 1 and 2 PCa by biopsy (bISUP) and who underwent radical prostatectomy (RP) in different hospitals. The indications for RP were patient preference, physician preference, and high D'Amico risk. The final pathology results were compared with preoperative [^{68}Ga]Ga-PSMA PET/CT imaging PRIMARY scoring data. [^{68}Ga]Ga-PSMA PET/CT imaging was performed within 3 months before RP. The initial informed consent form also included consent for future retrospective analysis. The study was approved by the Yeditepe University Rectorate Non-Interventional Clinical Research Ethics Committee (number: E.83321821-805.02.03-377, date: 15.03.2024) and was carried out in accordance with the Declaration of Helsinki.

Imaging Protocol

Preoperative [^{68}Ga]Ga-PSMA PET/CT imaging was performed with a mean dose of 240.5±67.16 MBq of [^{68}Ga]Ga-PSMA-11. The mean start time of scanning after injection was 59.5±15.8 min (median 60.0 min). Whole-body [^{68}Ga]Ga-PSMA PET/CT imaging was performed using a GE Discovery 710 PET/CT scanner with 64 CT slices from the vertex to the mid-thigh. Additional delayed pelvic imaging, which is routine in our clinic, was also acquired using 3-bed pelvic imaging at a mean of 139.1±21.3 min (median 138.0 min) after injection. Standard and delayed imaging was performed with an acquisition time of 3 min per bed position (Figure 1). Low-dose CT images were obtained for anatomical localization and attenuation correction. [^{68}Ga]Ga-PSMA PET/CT images were analyzed using the Advanced Workstation (v4.7) (GE Healthcare, WI, USA). The prostate region of interest was manually delineated for SUV_{max} measurement. The standard uptake value (SUV) calibration of the scanner was performed every 3 months as recommended by the manufacturer. The other quality control checks were regularly performed according to the recommendations of the European Association of Nuclear Medicine Guidelines (16).

PRIMARY Scoring

[^{68}Ga]Ga-PSMA PET/CT images were independently assessed by two experienced nuclear medicine physicians to determine the PRIMARY scores of both standard (sPRIMARY score) and delayed imaging (dPRIMARY score). To ensure an unbiased assessment, these physicians were blinded to the patients' clinical and pathologic data. In case of disagreement in the assignment of PRIMARY scores, a third nuclear medicine physician was consulted to reach a consensus. To assess inter- and intra-observer reproducibility, initial scoring was performed on standard imaging by four distinct nuclear medicine specialists who were blinded to both each other and the patient's clinical information. Subsequently, the same specialists repeated the procedure using only delayed [^{68}Ga]Ga-PSMA PET/CT images, while remaining blinded to the standard [^{68}Ga]Ga-PSMA PET/CT images and initial scores. Intra-observer agreement analysis involved the specialists re-assessing all images after a 1-month interval, following the same protocol as described above. In the PRIMARY scoring system used, score 2 was not divided into two subgroups;

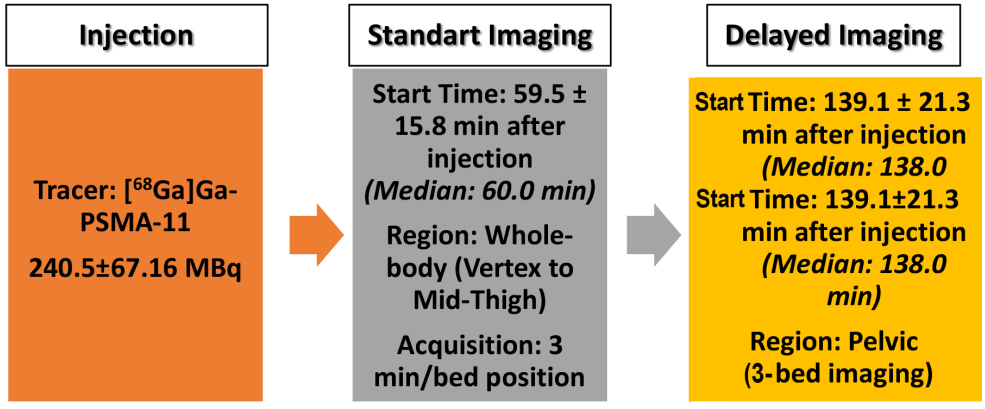

Figure 1. The imaging protocol for standard and delayed [^{68}Ga]Ga-PSMA PET/CT
PSMA: Prostate-specific membrane antigen, Min: Minimum, PET: Positron emission tomography, CT: Computed tomography

instead, both subgroups A and B were considered as group 2. Patients with a final pathological report indicating ISUP 2 or higher were diagnosed with csPCa.

Statistical Analysis

The descriptive data were used to calculate the median and mean values and the corresponding standard deviations(±). The values were analyzed using the Statistical Package for the Social Sciences, version 25.0 (IBM Corporation in Chicago, Illinois, USA). Sensitivity and specificity values for PRIMARY scoring were determined using pathologic ISUP results as a standard reference. Differences in diagnostic parameters between the sPRIMARY and dPRIMARY scores were assessed using the MedCalc proportional comparison calculator, which can be accessed at the following URL: https://www.medcalc.org. The relationship between ISUP and both sPRIMARY or dPRIMARY scores was analyzed using the Spearman correlation test. Cohen's kappa and Fleiss kappa were determined as 5 categories of the PRIMARY scoring for both imaging. Receiver operating characteristic (ROC) curves were also calculated for 5-level sPRIMARY and dPRIMARY scores. The paired samples t-test was used to compare the SUV_{max} of standard and delayed images. The Related-Samples Wilcoxon signed-rank test and McNemar's test were used to perform a comparative analysis between the sPRIMARY and dPRIMARY scores. Statistical significance was attributed to the values with a $p<0.05$ (two-sided).

Results

The mean age of the 140 men included in the study was 62.6±7.6 years (range, 43-80 years). The mean prostate-specific antigen (PSA) level was 8.5±7.2 ng/mL, with values ranging from 1.8 to 67.0 ng/mL. Regarding the preoperative biopsy results, 51 patients (36%) had bISUP 1, while 89 patients (64%) had bISUP 1 and 2, respectively. After RP, a 69% and 20% upgrade was observed in patients initially classified as bISUP 1 and a 20% upgrade in patients initially classified as bISUP 2. There was a 38% increase in bISUP in all patients to a higher value (Table 1).

Among the 140 patients, csPCa was detected in 34 (24%) patients with sPRIMARY scores 1-2 and in 86 (61%) patients with sPRIMARY scores 3-5 after RP (Tables 2,3). The sensitivity and specificity of sPRIMARY scoring in identifying csPCa were calculated to be 71% and 35%, respectively (Table 4). The positive predictive value (PPV) and negative predictive value were calculated to be 87% and 17%, respectively. The sensitivity of dPRIMARY scoring increased from 71% [confidence interval (CI): 63%-80%] to 92% (CI: 85%-96%) ($p<0.0001$) without any change in PPV. It is noteworthy that the number of patients with sPRIMARY score 5 increased from 31 to 46 with dPRIMARY score 5, all of whom were confirmed to have csPCa. Additionally, no csPCa of ISUP grade 3 or higher was detected in any of the patients with a dPRIMARY score of 1-2. The area under curves (AUCs) of sPRIMARY and dPRIMARY in the receiver operating characteristic curves (ROC) analysis were 0.616 and 0.721, respectively. The sPRIMARY and dPRIMARY scores were moderately correlated with ISUP, with Spearman-Rho values of 0.302 and 0.389, respectively.

The percentage of lesions scored as 1-2 in the PRIMARY scoring decreased from 29% in standard images to 10% in delayed images, whereas the percentage of lesions scored as 3-5 increased from 71% in standard images to 90% in delayed images ($p<0.001$ Table 2). In addition, the percentage of giving the same PRIMARY score by two experienced nuclear medicine physicians in standard imaging was 66%, which increased to 77% in delayed imaging ($p<0.05$). According to the results of Cohen's kappa analysis at standard imaging, intra-observer agreement was 0.536, 0.798, 0.593, and 0.638 for observers 1, 2, 3, and 4, respectively. The delayed images showed higher Cohen's

Table 1. Patient characteristics, biopsy findings, and histopathological findings

	Mean ± SD		**Median (range)**
Age (n=140)	62.6±7.6		63 (43-80)
PSA (n=138) (ng/mL)	8.5±7.2		6.9 (1.8-67.0)
	bISUP 1 (n=51)	bISUP 2 (n=89)	bISUP 1-2 (n=140)
ISUP 1	16 (31%)	4 (5%)	20 (14%)
ISUP 2	29 (57%)	67 (75%)	96 (67%)
ISUP 3	4 (8%)	15 (17%)	19 (14%)
ISUP 4	2 (4%)	1 (1%)	3 (2%)
ISUP 5	-	2 (2%)	2 (1%)
Upgrade	35 (69%)	18 (20%)	53 (38%)

ISUP: International Society of Urological Pathology Grade Groups, SD: Standard deviation, PSA: Prostate-specific antigen

Kappa coefficients of 0.697, 0.839, 0.769, and 0.740 for all observers, respectively, compared with the standard images, indicating better intraobserver reproducibility for delayed images (Figure 2). In the first assessment for PRIMARY scoring, the inter-observer Fleiss kappa coefficient was 0.47 for standard images and 0.61 for delayed images. In the second assessment, these coefficients increased to 0.52 for standard images and 0.72 for delayed images (Figure 3). Fleiss kappa coefficients were better for delayed images than for standard images in both sessions.

Table 2. Scanning time intervals of [^{68}Ga]Ga-PSMA PET/CT imaging and the results of the PRIMARY scoring obtained from standard and delayed imaging

	Standard imaging (n=140)	Delayed imaging (n=140)	Significance
Mean scan time ± SD (min)	59.5±15.8	139.1±21.3	
Median scan time (min)	60.0	138.0	
Mean SUV_{max}±SD	9.3±6.1	11.4±7.8	p<0.001*
PRIMARY score 1-2	**41 (29%)**	**14 (10%)**	**p<0.001****
ciPCa	7 (5%)	4 (3%)	
csPCa	34 (24%)	10 (7%)	
PRIMARY score 3-5	**99 (71%)**	**126 (90%)**	
ciPCa	13 (9%)	16 (11%)	
csPCa	86 (62%)	110 (79%)	

SD: Standard deviation, ciPCa: Clinically insignificant prostate cancer, csPCa: Clinically significant prostate cancer, PRIMARY: PRIMARY scoring system, SUV_{max}: Maximum standardized uptake value, *Paired-samples t-test **Related samples Wilcoxon signed-rank test for standard and delayed imaging PRIMARY scores

Table 3. ISUP grade groups of patients according to PRIMARY scores in patients diagnosed with bISUP 1 and 2

	PRIMARY Score	ISUP 1	ISUP 2	ISUP 3	ISUP 4	ISUP 5
Standard imaging (bISUP 1 and 2), n=140 (Spearmen Rho: 0.302)	**1**	2	19	2	-	-
	2	5	13	-	-	-
	3	2	3	-	-	-
	4	11	42	8	1	1
	5	-	19	9	2	1
Delayed imaging (bISUP 1 and 2), n=140 (Spearmen Rho: 0.389	**1**	3	8	-	-	-
	2	1	2	-	-	-
	3	1	1	-	-	-
	4	15	54	7	1	1
	5	-	31	12	2	1

ISUP: International Society of Urological Pathology Grade Group obtained after radical prostatectomy; bISUP: ISUP GG obtained after biopsy; PRIMARY: PRIMARY scoring system

Table 4. Diagnostic parameters for detecting csPCa from PRIMARY scoring in patients diagnosed as bISUP 1 and 2 (n=140) in both standard and delayed imaging

	Sensitivity	Specificity	PPV	NPV
	(95% CI)			
sPRIMARY score	71% (63%-80%)	35% (15%-59%)	87% (82%-90%)	17% (9%-29%)
dPRIMARY score	92% (85%-96%)	20% (6%-44%)	87% (85%-90%)	29% (12%-54%)
Significance*	**p<0.0001**	**p<0.05**	p>0.05	**p<0.05**

csPCa: Clinically significant prostate cancer, ISUP: International Society of Urological Pathology grade group obtained after radical prostatectomy, bISUP: ISUP GG obtained after biopsy, sPRIMARY: PRIMARY scoring for standard imaging, dPRIMARY: PRIMARY scoring for delayed imaging, NPV: Negative predictive value, PPV: Positive predictive value, CI: Confidence interval, *Statistically significant values are given bold

Additionally, inter-observer Fleiss kappa coefficients were higher in the second assessment evaluation than in the first assessment evaluation for standard and delayed images.

The mean SUV_{max} of the focal lesion, regarded as the primary tumor in the prostate gland, was 9.3±6.1 (Table 2) using standard images. The SUV_{max} significantly increased to a mean value of 11.4±7 in delayed images. The SUV_{max} was significantly higher in delayed images than in standard images ($p<0.001$, Figure 4).

Discussion

The introduction of the PRIMARY score represents a remarkable advance in the initial diagnosis of PCa using [^{68}Ga]Ga-PSMA PET/CT (4). The incorporation of the PRIMARY risk classification scheme has the potential to standardize the interpretation of lesions and allow for clearer and more objective communication between nuclear medicine physicians and clinicians (5). Nevertheless, further refinement of the PRIMARY score is required, particularly in cases of low-risk PCa (11). The purpose of PRIMARY scoring was to identify PCa in the prostate gland. However, PSMA uptake can be high under benign conditions. In such cases, PRIMARY scoring can be challenging because it is difficult to distinguish between csPCa with low PSMA expression and benign lesions with high uptake (4).

Initial studies reported that the normal prostate gland showed heterogeneous PSMA uptake and that even patients without a diagnosis of csPCa could show PSMA uptake as high as an SUV_{max} of 8.3 (17). High uptake within the prostate gland may make it difficult to distinguish csPCa with low PSMA expression. However, both early and recent studies have shown that background activity decreases in [^{68}Ga]Ga-PSMA PET/CT images taken after 2-3 hours and higher tumor/background ratios are obtained in delayed images compared with standard images (12,13,14,15). These findings may allow for better classification of benign prostate lesions and more accurate detection of masked malignant lesions. Accordingly, studies have shown that

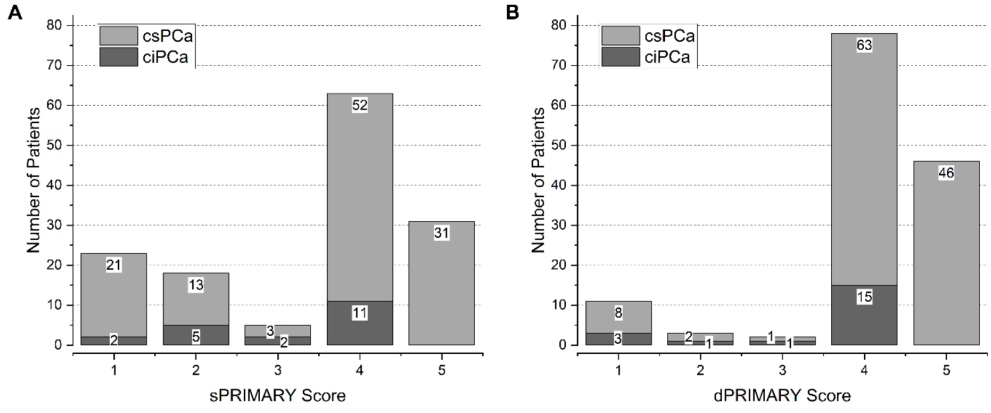

Figure 2. Distribution of ISUP groups according to primary scores obtained from standard and delayed [^{68}Ga]Ga-PSMA PET/CT
PSMA: Prostate-specific membrane antigen, PET: Positron emission tomography, CT: Computed tomography, ISUP: International Society of Urological Pathology grade group obtained after radical prostatectomy, ciPCa: Clinically insignificant prostate cancer, csPCa: Clinically significant prostate cancer

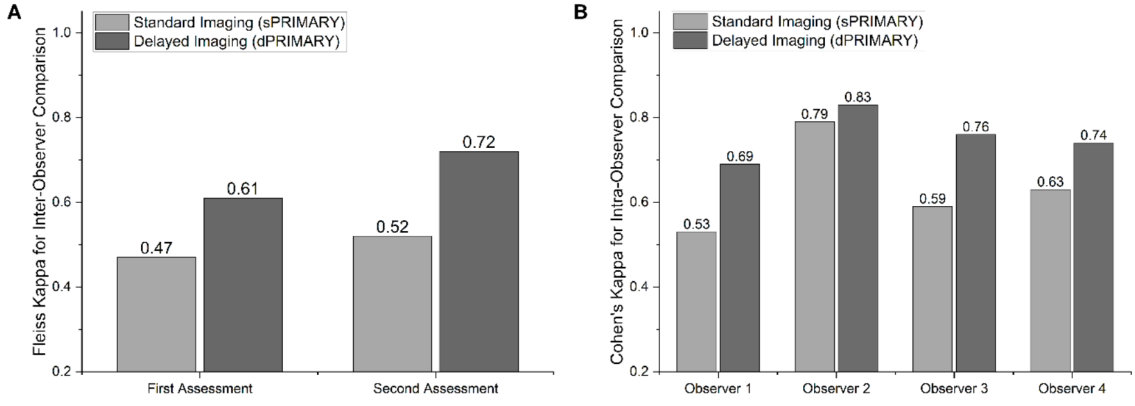

Figure 3. Intraobserver and interobserver Flesiss and Cohen's kappa analysis obtained from standard and delayed images

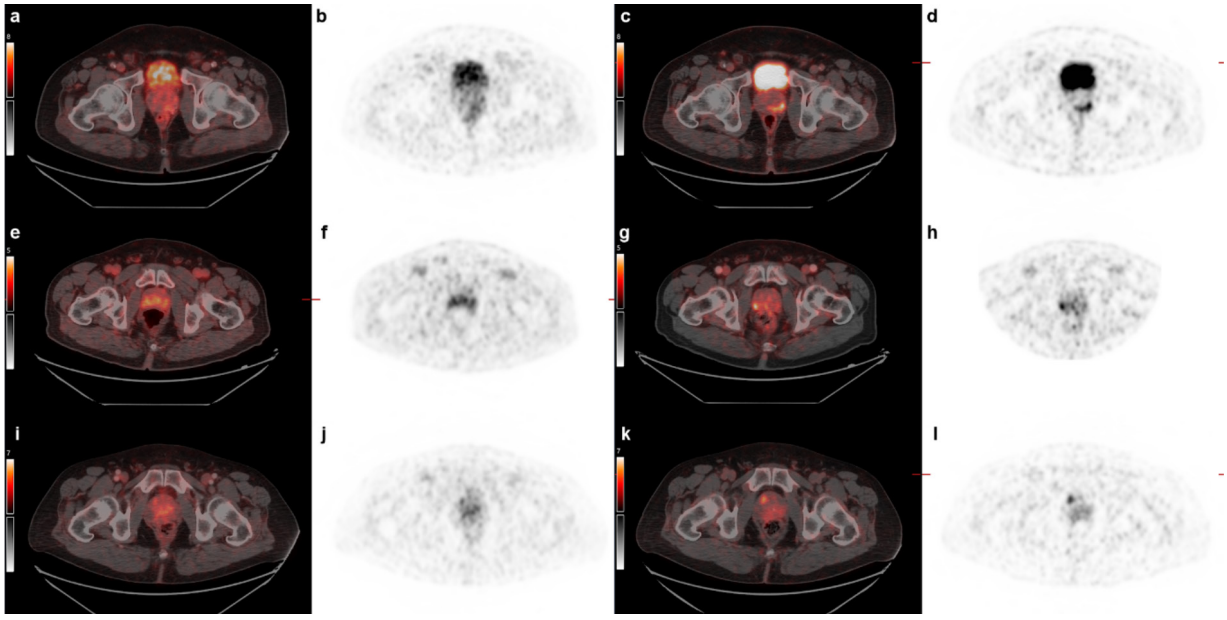

Figure 4. Standard and delayed imaging with fusion and PET/CT images of the cases. Images from different patients are presented in each line. Panels a and b display the fusion and PET images obtained during standard imaging, respectively, while panels c and d present the fusion and PET images acquired during delayed imaging. a, e, i) axial fusion images on standard images. b, f, j) axial PET images on standard images. c, g, k) axial fusion images on delayed images. d, h, l) axial PET images of delayed images.
PET/CT: Positron emission tomography/computed tomography

additional lesions that can change the stage of the disease and treatment management can be detected in up to 25% of patients in delayed images due to the higher tumor/background ratios. In our study, we observed a significant decrease in the frequency of the first two scores (from 29% to 10%) in the PRIMARY scoring on delayed images, which reflects the washout of PSMA uptake from benign lesions in delayed images ($p<0.001$). In addition, the agreement rate between two experienced nuclear medicine physicians in assigning identical PRIMARY scores during standard imaging was 66%, a rate that increased to 77% during delayed imaging ($p<0.05$).

In the aforementioned studies, it was noted that not only does the background uptake decrease in delayed images, but also the PSMA uptake of the tumor increases, resulting in enhanced visibility of the tumor (12,13,14,15). Consistent with this observation, a significant increase in SUV_{max} of the focal lesion, which is considered the primary tumor in the prostate gland, was observed in delayed [^{68}Ga]Ga-PSMA PET/CT images compared with standard [^{68}Ga]Ga-PSMA PET/CT images in our study. Decreased background activity and increased primary tumor uptake have contributed to a clearer distinction between primary tumors and benign lesions, leading to an improved identification of the primary tumor and a better assessment of its location in the peripheral zone of the prostate gland (Figure 4). Consequently, our diagnostic parameters exhibited statistically significant improvement for delayed images compared with standard images. The sensitivity of dPRIMARY scoring increased significantly from 71% to 92% compared with sPRIMARY scoring ($p<0.0001$). When comparing the AUCs of the sPRIMARY and dPRIMARY scoring in the ROC analysis, the higher AUC of the dPRIMARY score indicated superior diagnostic parameters.

For all sPRIMARY scores, Fleiss's kappa values of inter-observer reproducibility were found to be 0.47 for the first-assessment and 0.52 for the second assessment. Emmett et al. (9) found Cohen's kappa values for inter-observer reproducibility to be 0.65 for the entire sPRIMARY scoring scale. Inter-observer Fleiss's kappa values in standard images in our study were found to be lower compared to that of study by Emmett et al. (9) This difference may be explained by the presence of patients with bISUP 2 in their patient cohort and the kappa analysis with two observers instead of four. In our study, unlike the study conducted by Emmett et al. (9), PRIMARY scoring was also evaluated in delayed images. For the dPRIMARY scoring, the Fleiss's kappa coefficients were 0.61 for the first assessment and increased to 0.72 in the second assessment. The decrease in PSMA uptake in benign lesions and the increase in PSMA uptake in the primary tumor over time improved

both intra-observer and inter-observer consistency in dPRIMARY scoring. Higher consistency rates in late images were also observed for all four observers. In addition, it was consistently observed that the second assessment was better than the first assessment for both standard and delayed images. This result was considered to be related to the learning process. Even though the observers in this study were experienced in reading [^{68}Ga]Ga-PSMA PET/CT, they had not learned PRIMARY scoring before. The importance of the learning process was already emphasized by Emmett et al. (9).

In this study, as in previous studies, csPCa was detected in all patients with a PRIMARY score of 5 (4,10). Moreover, no ISUP 3-5 was detected in any of the patients with a dPRIMARY score of 1-2 after RP. This approach could have significant clinical implications and could help identify patients who should not be placed under active surveillance. he majority of patients with ISUP 1 exhibit PSMA expression and corresponding PSMA uptake; however, a subset of ISUP 2 patients lack PSMA expression and therefore show no PSMA uptake. This observation underscores the heterogeneity in prognosis among patients with ISUP 1 and 2, reflecting potential biological variability within these groups. Previously, it has been reported that the prognosis of the majority of patients with ISUP 1 is very good, 11% experience biochemical recurrence or progression, and 65% of patients with ISUP 2 do not experience recurrence (18). Additionally, it has been shown that high levels of PSMA expression may be present in some patients with ISUP 1-2 (19). The increased PSMA expression observed in patients with ISUP 1-2 may indicate poor clinical outcomes (6). Further studies on clinical outcomes are needed to clarify whether such a relationship exists or not.

The interpretation of the findings of this study requires caution due to the inherent limitations associated with retrospective studies. The patient cohort for RP introduces potential selection bias, as evidenced by the 86% incidence of csPCa, highlighting the need for careful evaluation of diagnostic parameters. However, the study focused on assessing the effectiveness of the PRIMARY SCORE in both standard and delayed images. Furthermore, the relatively elevated rate of upstaging from the bISUP might be attributable to the absence of a screening setting in the study.

Conclusion

In conclusion, when comparing standard and delayed images, a notable improvement in reliability was observed in both intra-observer and inter-observer assessments of delayed images. Furthermore, delayed images facilitated enhanced detection of csPCA patients with bISUP 1-2 that had been previously overlooked. Consequently, it can be used to distinguish individuals suitable for active surveillance in routine clinical practice.

Ethics

Ethics Committee Approval: The study was approved by the Yeditepe University Rectorate Non-Interventional Clinical Research Ethics Committee (number: E.83321821-805.02.03-377, date: 15.03.2024) and was carried out in accordance with the Declaration of Helsinki.

Informed Consent: The initial informed consent form also included consent for future retrospective analysis.

Footnotes

Authorship Contributions

Surgical and Medical Practices: O.E.Ş., R.A., E.A., Ö.E., N.A.S., A.I.D.E., Concept: L.K., Design: N.A.S., T.T., L.K., Data Collection or Processing: K.A., O.E.Ş., R.A., E.A., Ö.E., N.A.S., K.K., Analysis or Interpretation: K.A., G.B., N.A.S., L.K., Literature Search: K.A., G.B., L.K., Writing: K.A., G.B., N.A.S., T.T., L.K.

Conflict of Interest: No conflict of interest was declared by the authors.

Financial Disclosure: The authors declared that this study has received no financial support.

References

1. Hofman MS, Lawrentschuk N, Francis RJ, Tang C, Vela I, Thomas P, Rutherford N, Martin JM, Frydenberg M, Shakher R, Wong LM, Taubman K, Ting Lee S, Hsiao E, Roach P, Nottage M, Kirkwood I, Hayne D, Link E, Marusic P, Matera A, Herschtal A, Iravani A, Hicks RJ, Williams S, Murphy DG; proPSMA Study Group Collaborators. Prostate-specific membrane antigen PET-CT in patients with high-risk prostate cancer before curative-intent surgery or radiotherapy (proPSMA): a prospective, randomised, multicentre study. Lancet. 2020;395:1208-1216.
2. Gultekin MH, Demirci E, Turegun FA, Kabasakal L, Sahin OE, Ocak M, Onal B, Erozenci A. The role of 68GA-PSMA PET/CT scan in patients with prostate adenocarcinoma who underwent radical prostatectomy. Urol J. 2020;18:58-65.
3. Kabasakal L, Demirci E, Nematyazar J, Akyel R, Razavi B, Ocak M, Aygun A, Obek C, Kural AR. The role of PSMA PET/CT imaging in restaging of prostate cancer patients with low prostate-specific antigen. Nucl Med Commun. 2017;38:149-155.
4. Emmett L, Papa N, Buteau J, Ho B, Liu V, Roberts M, Thompson J, Moon D, Sheehan-Dare G, Alghazo O, Agrawal S, Murphy D, Stricker P, Hope TA, Hofman MS. The PRIMARY score: using intraprostatic 68Ga-PSMA PET/CT patterns to optimize prostate cancer diagnosis. J Nucl Med. 2022;63:1644-1650.
5. Kabasakal L, Turkay R, Onal B. Incorporating the [68Ga]Ga-PSMA PET/CT PRIMARY score into the selection criteria for prostate cancer patients eligible for active surveillance. Eur J Nucl Med Mol Imaging. 2024;51:1464-1466.
6. Hupe MC, Philippi C, Roth D, Kümpers C, Ribbat-Idel J, Becker F, Joerg V, Duensing S, Lubczyk VH, Kirfel J, Sailer V, Kuefer R, Merseburger

AS, Perner S, Offermann A. Expression of prostate-specific membrane antigen (PSMA) on biopsies is an independent risk stratifier of prostate cancer patients at time of initial diagnosis. Front Oncol. 2018;8:623.

7. Demirci E, Kabasakal L, Şahin OE, Akgün E, Gültekin MH, Doğanca T, Tuna MB, Öbek C, Kiliç M, Esen T, Kural AR. Can SUVmax values of Ga-68-PSMA PET/CT scan predict the clinically significant prostate cancer? Nucl Med Commun. 2019;40:86-91.
8. Emmett L, Buteau J, Papa N, Moon D, Thompson J, Roberts MJ, Rasiah K, Pattison DA, Yaxley J, Thomas P, Hutton AC, Agrawal S, Amin A, Blazevski A, Chalasani V, Ho B, Nguyen A, Liu V, Lee J, Sheehan-Dare G, Kooner R, Coughlin G, Chan L, Cusick T, Namdarian B, Kapoor J, Alghazo O, Woo HH, Lawrentschuk N, Murphy D, Hofman MS, Stricker P. The additive diagnostic value of prostate-specific membrane antigen positron emission tomography computed tomography to multiparametric magnetic resonance imaging triage in the diagnosis of prostate cancer (PRIMARY): a prospective multicentre study. Eur Urol. 2021;80:682-689.
9. Emmett L, Papa N, Counter W, Calais J, Barbato F, Burger I, Eiber M, Roberts MJ, Agrawal S, Franklin A, Xue A, Rasiah K, John N, Moon D, Frydenberg M, Yaxley J, Stricker P, Wong K, Coughlin G, Gianduzzo T, Kua B, Ho B, Nguyen A, Liu V, Lee J, Hsiao E, Sutherland T, Perry E, Fendler WP, Hope TA. Reproducibility and accuracy of the PRIMARY score on PSMA PET and of PI-RADS on multiparametric MRI for prostate cancer diagnosis within a real-world database. J Nucl Med. 2024;65:94-99.
10. Akcay K, Kibar A, Sahin OE, Demirbilek M, Beydagi G, Asa S, Aghazada F, Toklu T, Selcuk NA, Onal B, Kabasakal L. Prediction of clinically significant prostate cancer by [68 Ga]Ga-PSMA-11 PET/CT: a potential tool for selecting patients for active surveillance. Eur J Nucl Med Mol Imaging. 2024;51:1467-1475.
11. Zhang J, Kang F, Gao J, Jiao J, Quan Z, Ma S, Li Y, Guo S, Li Z, Jing Y, Zhang K, Yang F, Han D, Wen W, Zhang J, Ren J, Wang J, Guo H, Qin W. A prostate-specific membrane antigen PET-based approach for improved diagnosis of prostate cancer in Gleason grade group 1: a multicenter retrospective study. J Nucl Med. 2023;64:1750-1757.
12. Afshar-Oromieh A, Sattler LP, Mier W, Hadaschik BA, Debus J, Holland-Letz T, Kopka K, Haberkorn U. The clinical impact of additional late PET/CT imaging with 68Ga-PSMA-11 (HBED-CC) in the diagnosis of prostate cancer. J Nucl Med. 2017;58:750-755.
13. Herrmann K, Bluemel C, Weineisen M, Schottelius M, Wester HJ, Czernin J, Eberlein U, Beykan S, Lapa C, Riedmiller H, Krebs M, Kropf S, Schirbel A, Buck AK, Lassmann M. Biodistribution and radiation dosimetry for a probe targeting prostate-specific membrane antigen for imaging and therapy. J Nucl Med. 2015;56:855-861.
14. Afshar-Oromieh A, Malcher A, Eder M, Eisenhut M, Linhart HG, Hadaschik BA, Holland-Letz T, Giesel FL, Kratochwil C, Haufe S, Haberkorn U, Zechmann CM. PET imaging with a [68Ga]gallium-labelled PSMA ligand for the diagnosis of prostate cancer: biodistribution in humans and first evaluation of tumour lesions. Eur J Nucl Med Mol Imaging. 2013;40:486-495.
15. Yu X, Xu L, Huang G, Liu J, Chen R, Chen Y. The image quality and feasibility of solitary delayed [68 Ga]Ga-PSMA-11 PET/CT using long field-of-view scanning in patients with prostate cancer. EJNMMI Res. 2024;14:14.
16. Koole M, Armstrong I, Krizsan AK, Stromvall A, Visvikis D, Sattler B, Nekolla SG, Dickson J; EANM Physics committee. EANM guidelines for PET-CT and PET-MR routine quality control. Z Med Phys. 2023;33:103-113.
17. Demirci E, Sahin OE, Ocak M, Akovali B, Nematyazar J, Kabasakal L. Normal distribution pattern and physiological variants of 68Ga-PSMA-11 PET/CT imaging. Nucl Med Commun. 2016;37:1169-1179.
18. Offermann A, Hohensteiner S, Kuempers C, Ribbat-Idel J, Schneider F, Becker F, Hupe MC, Duensing S, Merseburger AS, Kirfel J, Reischl M, Lubczyk V, Kuefer R, Perner S. Prognostic Value of the New Prostate Cancer International Society of Urological Pathology Grade Groups. Front Med (Lausanne). 2017;29:4:157.
19. Bravaccini S, Puccetti M, Bocchini M, Ravaioli S, Celli M, Scarpi E, De Giorgi U, Tumedei MM, Raulli G, Cardinale L, Paganelli G. PSMA expression: a potential ally for the pathologist in prostate cancer diagnosis. Sci Rep. 2018;8:4254.

Original Article

Mol Imaging Radionucl Ther 2025;34:10-25 *DOI:10.4274/mirt.galenos.2024.86402*

Image Analysis as tool for Predicting Colorectal Cancer Molecular Alterations: A Scoping Review

Kolorektal Kanserdeki Moleküler Değişiklikleri Tahmin Etme Aracı Olarak Görüntü Analizi: Kapsam Derlemesi

Saman Mohammadpour[1], Hassan Emami[1], Reza Rabiei[1], Azamossadat Hosseini[1], Hamid Moghaddasi[1], Fariborz Faeghi[2], Rafat Bagherzadeh[3]

[1]Shahid Beheshti University Faculty of Medicine, Department of Health Information Technology and Management, Tehran, Iran
[2]Shahid Beheshti University Faculty of Medicine, Department of Radiology Technology, Tehran, Iran
[3]Iran University of Medical Sciences Faculty of Medicine, Department of English Language, Tehran, Iran

Abstract

Objectives: Among the most important diagnostic indicators of colorectal cancer; however, measuring molecular alterations are invasive and expensive. This study aimed to investigate the application of image processing to predict molecular alterations in colorectal cancer.

Methods: In this scoping review, we searched for relevant literature by searching the Web of Science, Scopus, and PubMed databases. The method of selecting the articles and reporting the findings was according to the guidelines of the Preferred Reporting Items for Systematic Reviews and Meta-Analyses; moreover, the Strengthening the Reporting of Observational Studies in Epidemiology checklist was used to assess the quality of the studies.

Results: Sixty seven out of 2,223 articles, 67 were relevant to the aim of the study, and finally 41 studies with sufficient quality were reviewed. The prediction of Kirsten Rat Sarcoma Viral Oncogene Homolog (KRAS), Neuroblastoma RAS Viral (NRAS), B-Raf proto-oncogene, serine/threonine kinase (BRAF), Tumor Protein 53 (TP53), Adenomatous Polyposis Coli, and microsatellite instability (MSI) with the help of image analysis has received more attention than other molecular characteristics. The studies used computed tomography (CT), magnetic resonance imaging (MRI), and ^{18}F-FDG positron emission tomography (PET)/CT with radionics and quantitative analysis to predict molecular alterations in colorectal cancer, analyzing features like texture, maximum standard uptake value, and MTV using various statistical methods. In 39 studies, there was a significant relationship between the features extracted from these images and molecular alterations. Different modalities were used to measure the area under the receiver operating characteristic curve for predicting the alterations in KRAS, MSI, BRAF, and TP53, with an average of 78, 81, 80 and 71%, respectively.

Conclusion: This scoping review underscores the potential of radiogenomics in predicting molecular alterations in colorectal cancer through non-invasive imaging modalities, like CT, MRI, and ^{18}F-FDG PET/CT. The analysis of 41 studies showed the appropriate prediction of key alterations, such as KRAS, NRAS, BRAF, TP53, and MSI, highlighting the promise of radionics and texture features in enhancing predictive accuracy.

Keywords: Radiogenomics, colorectal cancer, molecular alterations, image processing

Address for Correspondence: Reza Rabiei, Shahid Beheshti University Faculty of Medicine, Department of Health Information Technology and Management, Tehran, Iran
E-mail: Rabiei_rf@yahoo.com **ORCID ID:** orcid.org/0000-0003-0771-7306
Received: 06.05.2024 **Accepted:** 25.08.2024 **Publication Date:** 07.02.2025

Cite this article as: Mohammadpour S, Emami H, Rabiei R, Hosseini A, Moghaddasi H, Faeghi F, Bagherzadeh R. Image analysis as tool for predicting colorectal cancer molecular alterations: a scoping review. Mol Imaging Radionucl Ther. 2025;34:10-25.

Öz

Amaç: Kolorektal kanserin en önemli tanı göstergelerinden biri olsa da moleküler değişikliklerin ölçümü invaziv ve pahalıdır. Bu çalışmada, kolorektal kanserdeki moleküler değişiklikleri tahmin etmede görüntü işleme uygulamasını araştırmak amaçlanmıştır.

Yöntem: Bu kapsam derlemesinde, Web of Science, Scopus ve PubMed veri tabanlarını tarayarak ilgili literatürü inceledik. Makaleleri seçme ve bulguları raporlama sistematik derlemeler ve meta-analizler için tercih edilen raporlama öğeleri yönergelerine göre yapıldı; ayrıca, çalışmaların kalitesini değerlendirmek için Epidemiyolojide Gözlemsel Çalışmaların Raporlanmasını Güçlendirme kontrol listesi kullanıldı.

Bulgular: İki bin iki yüz yirmi üç makaleden 67'si çalışmanın amacıyla ilgiliydi ve son olarak yeterli kaliteye sahip 41 çalışma incelendi. Kirsten Rat Sarcoma Viral Oncogene Homolog (KRAS), Neuroblastoma RAS Viral (NRAS), B-Raf proto-oncogene, serin/treonin kinaz (BRAF), Tümör Protein 53 (TP53), Adenomatous Polyposis Coli ve Mikrosatellite instabilitesinin (MSI) görüntü analizi yardımıyla tahmini diğer moleküler özelliklerden daha fazla ilgi görmüştür. Çalışmalarda radyonik ve kantitatif analizle birlikte bilgisayarlı tomografi (BT), manyetik rezonans görüntüleme (MRG) ve ^{18}F-FDG pozitron emisyon tomografisi (PET)/BT kullanılarak kolorektal kanserdeki moleküler değişiklikleri tahmin etmek için doku, maksimum standart tutulum değeri ve MTV gibi özellikler çeşitli istatistiksel yöntemler kullanılarak analiz edilmiştir. Otuz dokuz çalışmada bu görüntülerden çıkarılan özellikler ile moleküler değişiklikler arasında anlamlı bir ilişki bulunmuştur. KRAS, MSI, BRAF ve TP53'teki değişiklikleri tahmin etmek için alıcı çalışma karakteristiği eğrisinin altındaki alanı ölçmek için farklı yöntemler kullanıldı ve sırasıyla ortalama %78, %81, %80 ve %71'lik sonuçlar elde edildi.

Sonuç: Bu kapsam derlemesi, BT, MRG ve ^{18}F-FDG PET/BT gibi invaziv olmayan görüntüleme yöntemleri aracılığıyla kolorektal kanserdeki moleküler değişiklikleri tahmin etmede radyogenomiğin potansiyelini vurgulamaktadır. Kırk bir çalışmanın analizi, KRAS, NRAS, BRAF, TP53 ve MSI gibi temel değişikliklerin uygun şekilde tahmin edildiğini göstererek, tahmin doğruluğunu artırmada radyonik ve doku özelliklerinin potansiyelini vurgulamaktadır.

Anahtar kelimeler: Radyogenom, kolorektal kanser, moleküler değişiklikler, görüntü işleme

Introduction

Colorectal cancer is the third most common cancer in the world; it ranks second in men and third in women in terms of cancer-related deaths (1,2). In 2022, a total of 1,926,118 new cancer cases and 903,859 deaths were reported (3). Although the incidence of cancer has decreased in high-income countries because of continuous screenings in the elderly and changes in risk factors (1,4), it is still increasing in low-income countries (5,6).

Colorectal cancer, which is caused by the accumulation of genetic and epigenetic changes in the colon epithelium, is a complex heterogeneous disease with different histopathology, (7). These changes lead to the activation of oncogenes, inactivation of tumor suppressor genes, and disturbance in the regulation of signaling pathways involved in cell proliferation, differentiation, and apoptosis (8). As a result of different histopathology and heterogeneity, the progress of colorectal cancer is very different in different people. Therefore, it is very important to predict disease progression to determine the appropriate treatment (7). To date, many efforts have been made to identify factors affecting disease progression, such as the "Tumor", "Nodes", "Metastases" (TNM) classification which, from histopathology point of view, classifies cancer into four groups with different rates of disease progression (9,10). However, the rate of disease progression in the TNM groups differed due to the molecular differentiation and heterogeneity within the tumor (11).

One-way to predict disease progression is to pay attention to molecular alterations, such as Kirsten Rat Sarcoma Viral Oncogene Homolog (KRAS), Neuroblastoma RAS Viral (NRAS), B-Raf proto-oncogene, serine/threonine kinase (BRAF), Tumor Protein 53 (TP53), microsatellite instability (MSI) and PIK3CA (9). Current methods for measuring these factors in colorectal cancer, such as DNA sequence analysis, are costly, time-consuming, and invasive (12). In addition, sampling from one point of the tumor to perform genetic tests and heterogeneity in different parts of the tumor, this method may not accurately reflect the molecular alterations of colorectal cancer (13). The problems of measuring molecular alterations can be overcome by predicting their values through analyzing medical images, such as computed tomography (CT) scan, magnetic resonance imaging (MRI), and ^{18}F-FDG PET/CT, which have recently attracted the attention of researchers (12). Radiogenomics, a new concept introduced in recent years, examines the relationship between molecular alterations (especially genetic alterations) of cells and images (9). Non-invasive imaging provides information on tumor morphology and metabolism to some extent and can be used to identify potential biomarkers and molecular alterations in colorectal cancer (12). Several studies have shown that CT scanning can predict the KRAS mutation status in colorectal cancer patients (14,15).

However, the use of image processing to predict MC molecular alterations is still in its early stages (12,16). Therefore, this study aimed to investigate the use of image processing to predict molecular alterations in colorectal cancer. The research questions of this study are as follows:

1. Which molecular alterations have received more attention in the field of radiogenomics?

2. Which imaging modalities are used to predict molecular alterations?

3. What is the performances of the modalities in the prediction of various molecular alterations?

Materials and Methods

In this scoping review conducted in 2024, the reporting process was based on the Preferred Reporting Items for Systematic Reviews and Meta-Analysis (PRISMA) (17). All original articles published from January 01, 2013 to April 31, 2024 and indexed in Scopus, PubMed, and Web of Science databases were extracted. The inclusion criteria were original research articles in colorectal cancer. The exclusion criteria were review studies, non-English articles, studies beyond the scope of colorectal cancer, and articles with limited access.

The standard keywords and their synonyms for the three terms "molecular alterations", "medical image" and "colorectal cancer" were determined according to medical subject headings, and a search strategy was determined for each database (Table 1).

After searching and retrieving sources based on the search strategies, duplicate articles were removed using EndNote software. Then, the titles and abstracts of the articles were checked, and irrelevant articles were removed. This screening was performed by two experts in the field of Medical Informatics, and any disagreement was resolved by consensus with a third expert. In the next step, the full texts of the articles were reviewed. Finally, articles that were in line with the purpose of the study were selected. The quality of the selected articles was measured using the Strengthening the Reporting of Observational Studies in Epidemiology checklist, and articles with insufficient quality were excluded from the study (18).

The data collection tool consisted of a data extraction form including the type of study, first author's name, country and year of publication, purpose of the study, sample size, molecular factors, type of modality, image characteristics, statistical method for prediction, and summary of findings. Furthermore, a narrative synthesis method was used for data analysis.

Statistical Analysis

In this study, basic descriptive statistics, including the sum and mean, were used to analyze the results. Additionally, when the area under the ROC curve was calculated to predict molecular alterations in the studies, the weighted average was computed based on the molecular alterations and modality.

Patient Consent Information

This systematic review was based on data from previously published studies, and new patient data were not collected. Therefore, patient consent was not required.

Table 1. Search strategy by database

Data base	Search strategy
PubMed	((((Gene[mesh] OR Genom*[Title/Abstract] OR "molecular alterations"[Title/Abstract] OR "Genes, APC"[mesh] OR "Genes, ras"[mesh] OR "Proto-Oncogene Proteins B-raf"[mesh] OR TP53 [Title/Abstract] OR "microsatellite instability"[mesh] OR MSI[Title/Abstract]) AND ("Tomography, X-Ray Computed" [mesh] OR "Positron emission tomography" [mesh] OR "Magnetic resonance imaging" [mesh] OR "Diagnostic imaging" [mesh] OR Radiomics [mesh])) OR "radio-genomics" [Title/Abstract] OR radiogenomics [Title/Abstract] OR "imaging genomics" [Title/Abstract] OR "radiation genomics" [Title/Abstract]) AND (Colorectal Neoplasms [mesh] OR CRC[Title/Abstract])) AND 2013/01/01: 2024/04/28 [dp]
Web of Science	((((TS=(Gene) OR TS=(Genom*)OR TS =(" molecular alterations")OR TS=(Cistron*)OR TS=(Genetic)OR TS=("Genes, APC") OR TS=("Genes, ras") OR TS=(RAS) OR TS=(APC) OR TS=(APC) OR TS=("Proto-Oncogene Proteins B-raf") OR TS=(BRAF) OR TS=(BRAF) OR TS=("tumor protein p53") OR TS=(TP53) OR TS=("microsatellite instability") OR TS=(MSI)) AND (TS=("Diagnostic imaging") OR TS=("CT scan") OR TS=(MRI) OR TS=("18F-FDG PET/CT") OR TS=("computerized tomography") OR TS=("Positron emission tomography") OR TS=("Magnetic resonance imaging") OR TS=(Radiomics))) OR (TS=("radio-genomics") OR TS=(radiogenomics) OR TS=("imaging genomics") OR TS=("radiation genomics")))AND (TS=("Colorectal Neoplasms") OR TS=("Colorectal cancer") OR TS=(CRC))) AND PY=(2013-2024)
Scopus	(((TITLE-ABS-KEY(Gene) OR TITLE-ABS-KEY(Cistron*) OR TITLE-ABS-KEY("molecular alterations") OR TITLE-ABS-KEY(Genetic) OR TITLE-ABS-KEY(genom*) OR TITLE-ABS-KEY("Genes, APC") OR TITLE-ABS-KEY(APC) OR TITLE-ABS-KEY("Genes, ras") OR TITLE-ABS-KEY(RAS) OR TITLE-ABS-KEY(BRAF) OR TITLE-ABS-KEY("Proto-Oncogene Proteins B-raf") OR TITLE-ABS-KEY("tumor protein p53") OR TITLE-ABS-KEY(TP53) OR TITLE-ABS-KEY("microsatellite instability") OR TITLE-ABS-KEY(MSI)) AND (TITLE-ABS-KEY("Diagnostic imaging") OR TITLE-ABS-KEY("CT scan") OR TITLE-ABS-KEY(MRI) OR TITLE-ABS-KEY("18F-FDG PET/CT") OR TITLE-ABS-KEY("computerized tomography") OR TITLE-ABS-KEY("Magnetic resonance imaging") OR TITLE-ABS-KEY("Positron emission tomography") OR TITLE-ABS-KEY(Radiomics))) OR (TITLE-ABS-KEY(radiogenomics) OR TITLE-ABS-KEY("radio-genomics") OR TITLE-ABS-KEY("imaging genomics") OR TITLE-ABS-KEY("radiation genomics"))) AND (TITLE-ABS-KEY("Colorectal Neoplasms") OR TITLE-ABS-KEY("Colorectal cancer") OR TITLE-ABS-KEY(CRC))) AND (PUBYEAR > 2013 AND PUBYEAR < 2024)

Results

A summary of the study review process based on the PRISMA guidelines is presented in Figure 1.

Molecular Factors

Research has shown that many molecular factors contribute to the treatment of colorectal cancer. Some of the key molecular factors (genes/oncogene/suppressor) in colorectal cancer are KRAS, BRAF, NRAS, PIK3CA, and TP53 (9). Various molecular factors were predicted in the selected studies; however, in 68% of them, KRAS changes were investigated. The frequency of the investigated molecular factors is shown in Figure 2.

Modalities

Recently, different imaging modalities have been used for predicting molecular factors in colorectal cancer. The most important modalities are MRI, CT, and positron emission tomography (PET) (9). The frequency of modalities used in the included studies is presented in Figure 3.

Analyzing Technics

The reviewed studies employed various imaging modalities, such as CT, MRI, and ^{18}F-FDG PET/CT, and utilized radionics and quantitative analysis techniques to predict molecular alterations in colorectal cancer. Key features analyzed included texture features, maximum standardized uptake value (SUV_{max}), SUV_{mean}, metabolic tumor volume, total lesion glycolysis, and various radionics features derived from intensity, shape, and texture matrices like GLCM, GLRLM, GLSZM, and NGLDM. The statistical methods varied, including Spearman correlation, Mann-Whitney U test, logistic regression, and machine learning models like random forest and SVM.

Area Under the Receiver Operating Characteristic (ROC) Curve for Predicting Molecular Factors Based on Image

In 20 studies, the area under the ROC curve (AUC) was reported for predicting KRAS (n=13), MSI (n=4), BRAF (n=2), and TP53 (n=1) changes. The weighted average of this index (relative to the number of samples) for each molecular factor is presented in Table 3. Table 4 presents the relationships among the three modalities used in studies on molecular factors.

Discussion

In this systematic review, 41 studies related to the use of radiogenomics in colorectal cancer for predicting molecular factors were examined. According to the results, 42% of the studies were conducted in China, and 71% of the studies were conducted between 2019 and 2022. According to recent progress in understanding the relationship between molecular factors and response to drugs, the emergence of the concept of radiogenomics, and the increase in the

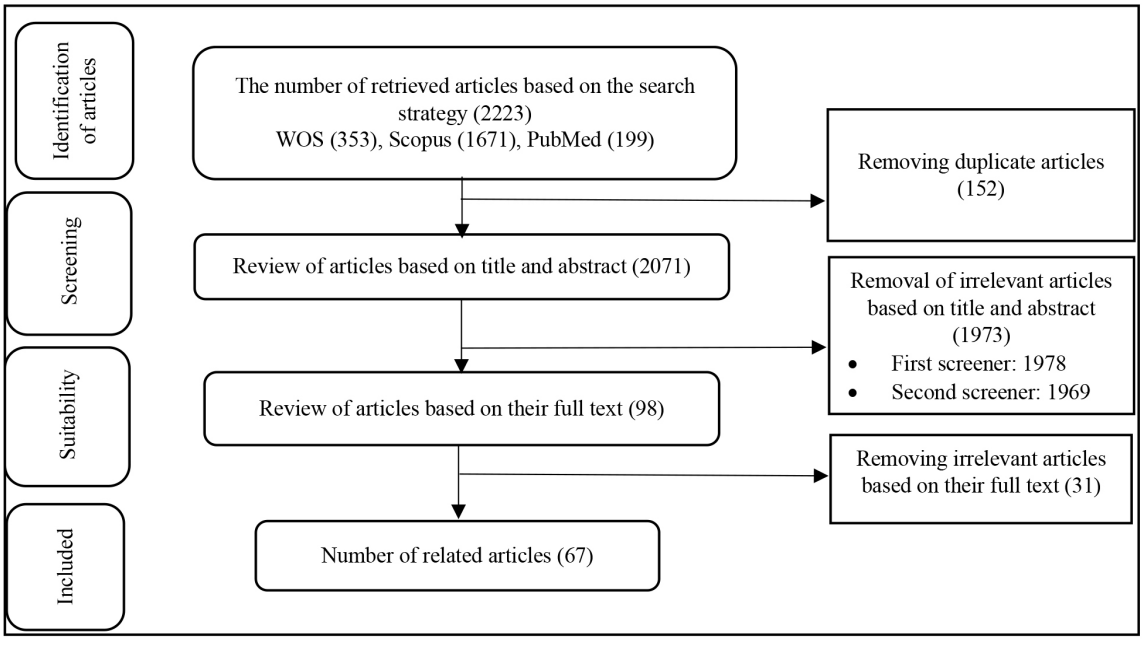

Figure 1. The study selection process

quality of different modalities in recent years, such studies have received much attention from researchers (9).

Furthermore, most studies have investigated the association between medical images and RAS (KRAS, NRAS), BRAF, TP53, activated protein C (APC), and MSI alterations with a frequency of 35, 28, 8, 7, 5, 4, and 4, in that order. RAS mutations (KRAS/NRAS) are common in colorectal cancer and can affect treatment outcomes. These mutations are associated with resistance to anti-epidermal growth factor receptor monoclonal antibodies and limit their efficacy. Targeted therapies that specifically inhibit mutant KRAS are

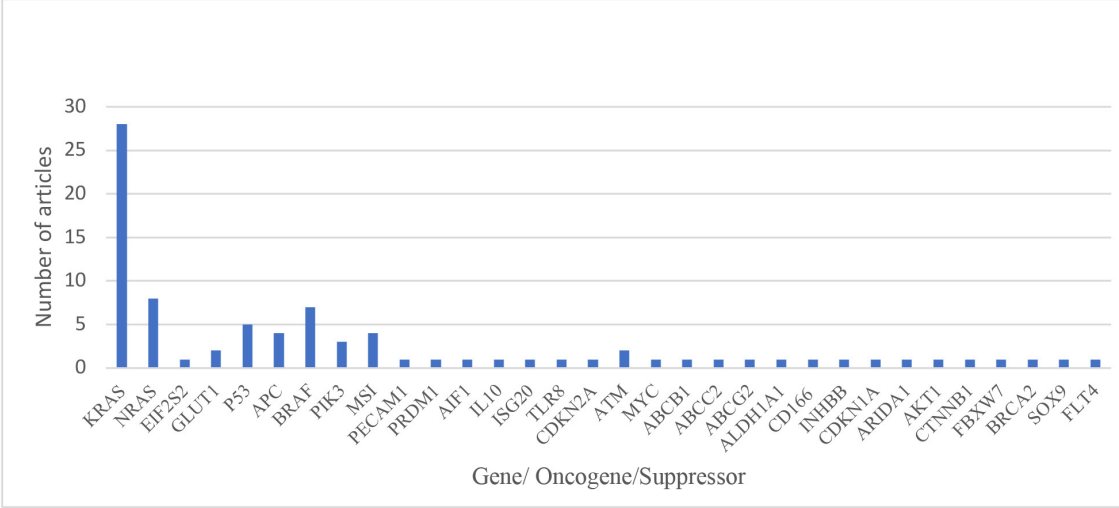

Figure 2. Frequency of the predicted molecular factors
KRAS: Kirsten Rat Sarcoma Viral Oncogene Homolog, NRAS: Neuroblastoma RAS Viral, EIF2S2: Eukaryotic Translation Initiation Factor 2 Subunit 2 GLUTI: Glucose Box 1, BRAF: B-Raf proto-onkogen, MSI: Microsatellite Instability, PECAMI: Platelet Endothelial Cell Adhesion Molecule 1, AIFI: Activated Inducible Family of Immune receptors, ISG20: Interferon-Stimulated Gene 20, TLR8: Toll-like Receptor 8, CDKN2A: Cyclin-Dependent Kinase Inhibitor 2A, ATM: Ataxia-Telangiectasia Mutated, ABCG2: ATP Binding Cassette Subfamily G Member 2, ABCB1: ATP Binding Cassette Subfamily B Member 1, AMCC2: Armadillo Motif Containing 2, ABCG2: ATP Binding Cassette Subfamily G Member 2, ALDHIA1: Aldehyde Dehydrogenase 1 Family Member A1, CD166: Cluster of Differentiation 166, INHBB: Inhibin Beta B, CDKNIA: Cyclin-Dependent Kinase Inhibitor 1A, ARIDA1: AT-rich interaction domain 1A, CTNNBI: Catenin Beta 1, FBXW7: F-box and WD-40 domain protein 7, BRAC2: Breast Cancer 2, FLT: Fms-like Tyrosine Kinase

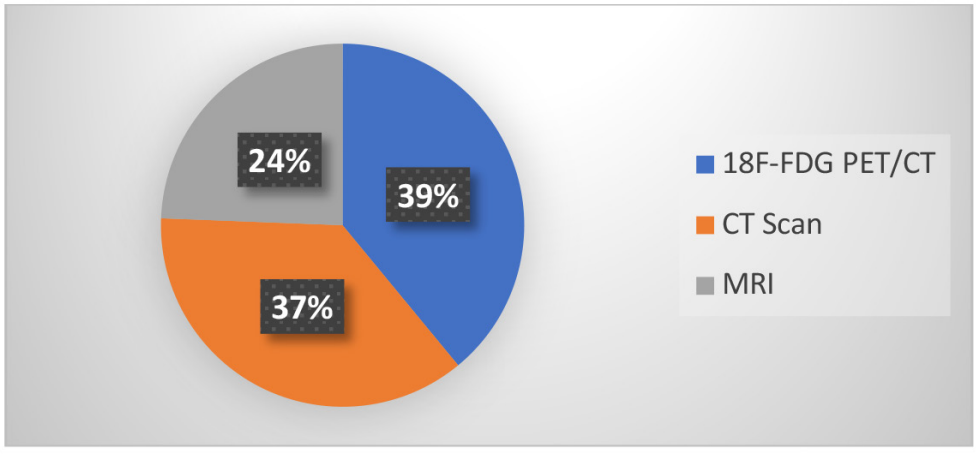

Figure 3. Frequency of modalities used in the included studies
PET/CT: Positron emission tomography/computed tomography, MRI: Magnetic resonance imaging

Table 2. Characteristics of reviewed studies

Studies			Participants		Molecular factors	Image		Statistics
Author	Type	Country/Year	Participants	Aim	Gene Oncogene/ Suppressor	Modality	Analyzing techniques (features)	Technique
Lovinfosse et al. (19)	Retrospective study	Belgium/2016	151	Predicting RAS mutation as an indicator of treatment	KRAS NRAS RAS	^{18}F-FDG PET/CT	Radiomics (texture features)	Spearman correlation coefficient
Yang et al. (20)	Retrospective study	China\ 2021	42	Investigating the association between EIF2S2 and ^{18}F-FDG PET/CT	EIF2S2 GLUT1	^{18}F-FDG PET/CT	Radiomics [SUV_{max}, SUV_{mean}, total lesion glycolysis (TLG), and metabolic tumor volume (MTV)]	Spearman's correlation coefficient
Huang et al. (21)	Cohort study	Taiwan \ 2022	71	Finding therapeutic targets using radiomic features	PECAM1 PRDM1 AIF1 IL10 ISG20 TLR8	CT scan	Radiomics (1,037 radiomic feature)	Heatmap visualization and correlation coefficient
Jo and Kim. (22)	Retrospective study	South Korea \ 2018	75	Investigating the association between KRAS mutations and MRI-based radiologic findings	KRAS	MRI	Axial to longitudinal tumor length (ATL/LTL)	The Mann-Whitney U test
Yang et al. (23)	Retrospective study	China \ 2017	61	Prediction of KRAS/NRAS/BRAF mutations	KRAS NRAS BRAF	CT scan	Radiomics [shape features, gray-level histogram features, gray-level co-occurrence matrix (GLCM) features, gray-level run-length matrix (GLRLM) features]	t-test or the Mann-Whitney U test for continuous variables and the chi-square test for categorical variables
Xu et al. (24)	Retrospective study	China \ 2019	158	Prediction of KRAS mutation as a therapeutic indicator	KRAS	MRI	Radiomics (texture features)	Mann–Whitney U test The chi-square test or Fisher exact test.
Li et al. (25)	Retrospective study	China \ 2021	368	Prediction of the microsatellite instability (MSI) status	MLH1 MSH2 MSH6 PMS2	CT scan	Radiomics (intensity histogram, gray level co-occurrence matrix, gray level run length matrix, neighbor intensity difference, and shape)	Logistic regression, Support vector machine (SVM), Random forest, Gradient boosting machine (GBM), Naive Bayes
Crimì et al. (26)	Retrospective study	Italy \ 2022	47	Prediction of the presence of specific genetic mutations associated with CRC	MSI	CT scan	Radiomics [derived from histogram, run length matrix (RLM), gray-level co-occurrence matrix (GLCM), gray-level run length matrix (GLRLM), and neighboring gray-level dependence matrix (NGLDM)]	Mann-Whitney U test and Bonferroni correction

Table 2. continued

Studies			Participants		molecular factors	Image		Statistics
Cho et al. (27)	Retrospective study	Republic of Korea \ 2017	93	Prediction of KRAS mutations	KRAS	^{18}F-FDG PET/CT	Quantitative Analysis (SUV_{max}, SUV_{mean}, MTV, and TLG)	the χ^2 test or Mann-Whitney U test
Chen et al. (28)	Retrospective study	Taiwan \ 2013	121	Prediction of KRAS mutations	KRAS	^{18}F-FDG PET/CT	SUV_{max}, SUV_{mean}, MTV	using a Mann-Whitney U test and logistic regression analysis
Yeo et al. (29)	Retrospective study	Republic of Korea \ 2015	46	Whether DCE-MRI correlates with angiogenesis and the biological aggressiveness of rectal cancer	EGFR	MRI	Quantitative Analysis(K^{trans}, k_{ep}, v_e, and iAUC)	Student's t-test and analysis of variance (ANOVA)
Mao et al. (30)	Retrospective study	China\ 2019	49	Prediction of KRAS mutations	KRAS	^{18}F-FDG PET/CT	Quantitative Analysis(SUVearly, SUVdelayed, ΔSUV_{max})	Chi-square test or Mann–Whitney U test
Taguchi et al. (31)	Retrospective study	Japan \ 2019	40	Prediction of KRAS mutations	KRAS	CT scan	Quantitative Analysis [CT texture parameters (Skewness, Kurtosis, Entropy, Energy, Homogeneity,..) and ^{18}F-FDG PET parameter) SUV_{max})]	two-tailed independent t-test and the Mann-Whitney U test
Zhong et al. (32)	Retrospective study	China \ 2022	1601	Prognostic prediction model for colorectal cancer	KRAS	CT scan	Radiomics (radiomics features)	Unsupervised deconvolution analysis
Wu et al. (33)	Cohort study	China \ 2019	279	Predicting KRAS status in patients with colorectal cancer (CRC)	KRAS	CT scan	Radiomics and deep learningn (hand-crafted features and deep learning features)	using multivariable logistic regression analysis
Seth et al. (34)	Retrospective study	Canada \ 2021	20	Investigating the association between TTE and genetic mutations	APC ARIDA1 TP53 AKT1 ATM BRAF CTNNB1 EGFR FBXW7 KRAS NRAS PIK3 CAPTENSMAD	MRI	Quantitative Analysis [target tumor enhancement (weak and strong TTE)]	Kruskal-Wallis test and Mann-Whitney and/or t-test
Cui et al. (35)	Retrospective study	China \ 2020	304	prediction of KRAS mutation	KRAS	MRI	Radiomics (radiomics feature)	mainly consist of univariate statistical tests

Table 2. continued

Studies			Participants		molecular factors	Image		Statistics
Cao et al. (36)	Retrospective study	China\ 2020	124	prediction of KRAS mutation	KRAS	CT scan	Quantitative analysis(DESCT parameters Including the monochromatic CT value, iodine, water, and effective atomic number	logistic regression analysis
Cui et al. (37)	Retrospective study	China \ 2019	148	prediction of KRAS mutations	KRAS	MRI	Quantitative analysis (DKI and ADC)	Student's t-test or Mann-Whitney U test and receiver operating characteristic (ROC) curve analysis
Granata et al. (38)	Retrospective study	Italy \ 2020	106	Identification of RAS mutation in colorectal liver metastasis	KRAS NRAS	MRI	Quantitative analysis (ADC-, IVIM- and DKI)	Wilcoxon-Mann-Whitney U tests for receiver operating characteristic (ROC) analyses
Chen et al. (39)	Retrospective study	Taiwan \ 2015	103	Investigating the association between genetic mutations and ^{18}F-FDG PET in colorectal cancer (CRC).	TP53 KRAS APC BRAF PIK3CA	^{18}F-FDG PET/CT	Quantitative analysis (SUV_{max}, SUV_{mean}, MTV, and TLG)	Mann-Whitney U test and logistic regression analysis
Promsorn et al. (40)	Retrospective study	Thailand \ 2021	113	prediction of KRAS mutation status	KRAS	CT scan	Qualitative and quantitative analyses (ATL, LTL, ATL/LTL, tumor location, gross tumor patterns, tumor margins, tumor enhancement patterns, T staging, regional lymph node metastasis, distant lymph node metastasis, or distal organ metastasis)	t test Mann-Whitney U test
Liu et al. (41)	Retrospective study	China \ 2021	134	Prediction of metastasis in colorectal cancer	ABCB1 TP53 ATM MYC	CT scan	Radiomics (radiomics feature)	Multivariable logistic regression analyses
Popovic et al. (42)	Retrospective study	USA \ 2020	37	Explore the predictive value of 2-[^{18}F]FDG uptake according to KRAS mutation status	KRAS mutation	2-[^{18}F]FDG PET/C	quantitative analysis(SUV (HERMES), SUV (MIM), PVEC)	Student's t test Wilcoxon rank-sum test Logistic regression and receiver operating characteristics (ROC)
Krikelis et al. (43)	Retrospective study	Greece \ 2014	44	prediction of KRAS mutation status	GLUT1 KRAS	^{18}F-FDG PET/CT	quantitative analyses (SUV_{max})	t-test Kruskal–Wallis test Fisher's exact test of Spearman's Rho

Table 2. continued

Studies			Participants		molecular factors	Image		Statistics
Chen et al. (44)	Retrospective study	Taiwan \ 2019	74	Investigating the association between genetic mutations and radionics in ^{18}F-FDG PET/CT In colorectal cancer (CRC)	KRAS TP53 APC	^{18}F-FDG PET/CT	quantitative analyses (SUV_{max}, MTV)	Receiver- operating characteristic (ROC) Mann-Whitney U test Spearman's rank correlation coefficient
Zhang et al. (45)	Retrospective study	China \ 2021	83	Analyzing the association between MRI radiomic features and KRAS status in LARC patients.	KRAS NRAS BRAF	MRI	Radiomics (radiomics feature)	The least absolute shrinkage and selection operator (LASSO) regression
Miles et al. (46)	prospective study	United Kingdom \ 2014	33	Exploring the potential of multifunctional imaging in providing a KRAS signature	KRAS	PET/CT	quantitative analysis[^{18}F-FDG uptake (^{18}F-FDG maximum standardized uptake value (SUV_{max})], CT texture (expressed as mean of positive pixels (MPP)]	CT Texture Analyses (CT TA) CT TA was performed using the following parameters: TexRAD Recursive decision tree Monte Carlo analysis
He et al. (47)	Retrospective study	China \ 2020	157	prediction of KRAS mutation status	KRAS	CT scan	Radiomics (radiomics feature)	LASSO regression-radiomics model using a random forest classifier (RFC)
Shi et al. (48)	Retrospective study	China\ 2020	159	predicting the RAS(KRAS and NRAS) and BRAF gene mutation statuses	KRAS NRAS BRAF	CT scan	Radiomics(Gray Level Co-occurrence Matrix (GLCM), gray level size zone matrix (GLSZM), Gray Level Run Length Matrix (GLRLM), neighboring Gray Tone Difference Matrix (NGTDM), and gray level dependence matrix (GLDM))	Fisher's exact test
He et al. (49)	Retrospective study	China \ 2021	85	association between KRAS/NRAS / BRAF mutations and metabolic parameters of pretreatment ^{18}FFDG-PET/CT in colorectal cancer	KRAS NRAS BRAF	^{18}F-FDG PET/CT	quantitative analyses (SUV_{max})	Mann–Whitney U test.

Table 2. continued

Studies		Participants		molecular factors	Image		Statistics
Sh et al. (50)	prospective study	Egypt\ 2021	38	correlation between 18F-FDG PET/CT imaging and KRAS expression in mCRC	KRAS mutational	^{18}F-FDG PET/CT	quantitative analysis (maximum standardized uptake value (SUV_{max}), total lesion glycolysis (TLG) and metabolic tumor volume (MTV))	independent samples t-test Mann-Whitney U test)
Li et al. (51)	Retrospective study	China\ 2021	173	Prediction of Microsatellite instability in colorectal tissue Cancer	MSI-H MSS	^{18}F-FDG PET/CT	Radiomics (radiomics feature)	multivariate random forest selection and univariate relevancy tests Balanced Bagging the area under The curve (AUC)
Horvat et al. (52)	Retrospective study	USA\ 2019	65	To investigate associations between genetic mutations and qualitative and quantitative features on magnetic resonance imaging (MRI) in rectal adenocarcinoma	APC TP53 KRAS PIK3CA BRCA2 ATM SOX9 FLT4	MRI	Quantitative and qualitative analyses [Tumor Localization, Tumor Length (cm), Mucin Content, CRM distance (mm), CRM status, DWI restriction, Early perfusion on DCE, Metastatic lymph nodes]	Fisher's exact test and Wilcoxon rank sum test
Badic et al. (53)	Retrospective study	Franche\ 2019	64	the relationship between imaging radiomic features and gene expression changes	ABCB1 ABCC2 ABCG2 ALDH1A1 CD166 (ALCAM) CDKN1A INHBB	CT scan	Radiomics [Flatness, Sum entropy (SENTR), entropy from Gray-level-co-occurrence-matrix (EntropyGLCM E), Gray-level non-uniformity (GLNUL)]	Kruskal-Wallis test
Ma et al. (54)	Retrospective study	USA\ 2022	230	explore whether the preoperative CT radionics can predict Status of microsatellite instability (MSI) in colorectal cancer (CRC)	LH1, MSH2 MSH6 PMS2	CT scan	Radiomics (first-order statistics, shape, gray-level co-occurrence matrix (GLCM), gray-level dependence matrix (GLDM), gray-level size zone matrix (GLSZM), gray-level run length matrix (GLRLM), and neighboring gray-level tone difference matrix (NGTDM))	inter-class correlation coefficient intraclass correlation coefficient
Negreros-Osuna et al. (55)	Retrospective study	Mexico\ 2020	145	To explore the potential of radionics texture features as biomarkers of BRAF mutation	BRAF	CT scan	Radiomics (texture features: mean, SD, mean value of positive pixels (MPP), skewness, kurtosis, and entropy)	Laplacian-of-Gaussian filters Wilcoxon rank sum

Table 2. continued

Studies			Participants		molecular factors	Image		Statistics
Granata et al. (56)	Retrospective study	Italy\ 2021	52	Investigating the association between RAS mutation status and radiomics-derived data using contrast-enhanced magnetic resonance imaging (CE-MRI) in liver metastases	KRAS NRAS	MRI	Radiomics (texture features)	Wilcoxon-Mann-Whitney U Test Receiver Operating Characteristic (ROC)
Kawada et al. (57)	Retrospective study	Japan\ 2015	55	to investigate whether KRAS status is associated with 18F-FDG accumulation in metastatic CRC. and whether 18F-FDG PET/CT can be used to predict KRAS status of metastatic CRC.	KRAS	^{18}F-FDG PET/CT	quantitative analysis(SUV_{max})	Mann–Whitney U test
Mao et al. (30)	Retrospective study	China\ 2018	49	To investigate the association between meta-Bolic parameters of dual time point 18 F-FDG PET/CT and KRAS mutation status in colorectal liver metastases (CRLM).	KRAS	^{18}F-FDG PET/CT	quantitative analysis (SUVearly, SUVdelayed, ΔSUV_{max} and RI)	Uni-variate multi-variate analyses
Arslan et al. (58)	Retrospective study	Turkey\ 2020	83	Investigating the association between FDG uptake patterns and 18 F-FDG PET/CT imaging and KRAS mutation	KRAS	^{18}F-FDG PET/CT	quantitative analyses (SUV_{max})	Mann-Whitney U Kruskal-Wallis tests Pearson's test.

KRAS: Kirsten Rat Sarcoma Viral Oncogene Homolog, NRAS: Neuroblastoma RAS Viral, EIF2S2: Eukaryotic Translation Initiation Factor 2 Subunit 2 GLUTI: Glucose Box 1, BRAF: B-Raf proto-onkogen, MSI: Microsatellite Instability, PECAMI: Platelet Endothelial Cell Adhesion Molecule 1, AIFI: Activated Inducible Family of Immune receptors, ISG20: Interferon-Stimulated Gene 20, TLR8: Toll-like Receptor 8, CDKN2A: Cyclin-Dependent Kinase Inhibitor 2A, ATM: Ataxia-Telangiectasia Mutated, ABCG2: ATP Binding Cassette Subfamily G Member 2, ABCB1: ATP Binding Cassette Subfamily B Member 1, AMCC2: Armadillo Motif Containing 2, ABCG2: ATP Binding Cassette Subfamily G Member 2, ALDHIA1: Aldehyde Dehydrogenase 1 Family Member A1, CD166: Cluster of Differentiation 166, INHBB: Inhibin Beta B, CDKNIA: Cyclin-Dependent Kinase Inhibitor 1A, ARIDA1: AT-rich interaction domain 1A, CTNNBI: Catenin Beta 1, FBXW7: F-box and WD-40 domain protein 7, BRAC2: Breast Cancer 2, FLT: Fms-like Tyrosine Kinase

Table 3. Area under the receiver operating characteristic curve of different modalities for predicting molecular factors

Molecular factors	Modality	Number of articles	Average sample size (SD of sample size)	AUC mean*
KRAS	MRI	5	153.6 (82.2)	0.77
	CT scan	4	120 (48.23)	0.82
	PET/CT	4	82.5 (48.9)	0.73
	ALL	13	121.4 (68.5)	0.78
MSI	MRI	0	0 (0)	0
	CT scan	3	215 (131)	0.80
	PET/CT	1	173 (0)	0.83
	ALL	4	194 (115.4)	0.81
BRAF	MRI	1	159 (0)	0.79
	CT scan	1	61 (0)	0.83
	PET/CT	0	0 (0)	0
	ALL	2	110 (0)	0.80
TP53	MRI	0	0 (0)	0
	CT scan	0	0 (0)	0
	PET/CT	1	74 (0)	0.71
	ALL	1	74 (0)	0.71

*AUC mean, SD: Standard deviation, AUC: Area under the curve, MRI: Magnetic resonance imaging, CT: Computed tomography, PET: Positron emission tomography, ALL: Acute lymphoblastic leukemia, MSI: Mikrosatellit Instabilitesi, BRAF: B-Raf proto-oncogene, serine/threonine kinase, TP53: Tumor Protein 53

being developed to overcome this resistance (59,61). RAS mutations have been investigated in 35 studies, and the relationship between image characteristics and molecular factors was significant in 33 studies. Moreover, 13 studies used image analysis to report the area under the ROC curve for predicting KRAS whose weighted average, relative to the number of samples, was 78%, which is in contrast with the result of the study by Kim et al. (2), where the same value for 9 studies was 69%. This difference can be attributed to the research period. Additionally, regarding recent advances in imaging and image-analyzing methods, the higher level under the ROC curve in the present study can be justified.

BRAF mutations, particularly V600E mutation, are found in a subset of colon cancers and are associated with poor prognosis. In recent years, BRAF inhibitors have shown promise in the treatment of colorectal cancer (with BRAF mutation), either alone or in combination with other drugs (61). BRAF mutation has been examined in 7 studies, and the relationship between image features and BRAF mutation was significant in 6 studies. In 2 studies image analyzing was used to report the area under the ROC curve for predicting BRAF whose weighted average, in relation to the number of samples, was 80%. In their study, Santhanam et al. (62) identified 7 studies on the relationship between ^{18}F-FDG PET/CT characteristics and BRAF mutation in thyroid cancer, and the results indicated a significant relationship between them.

TP53 is a tumor suppressor that plays an important role in maintaining genomic stability. TP53 mutations are frequently found in colorectal cancer, and they are associated with worse prognosis and resistance to therapy. New therapies targeting TP53 mutations (such as gene therapies and small molecule inhibitors) are being investigated to overcome these challenges (63). The TP53 mutation has been investigated in 5 studies where the relationship between image characteristics and TP53 mutation was significant. In another study, image analysis was used, and the area under the receiver operating characteristic curve for predicting TP53 was 71%. In their review study, Seow et al. (64) investigated the relationship between radiomic features and molecular factors and found a correlation between TP53 mutation and radiomic features.

MSI is observed in approximately 15% of colorectal cancers. From the treatment point of view, high MSI colorectal cancers exhibit particular responses to immunotherapy; they respond better to immune checkpoint inhibitors (65). Image analysis was used in 4 studies to report the area under the receiver operating characteristic curve for MSI, with an average of 81%. Similarly, Le et al. (66) identified 8 studies related to the use of radionics for the prediction of MSI, and the average area under the ROC curve was 83%.

As a suppressor, APC plays an important role in the development of colon cancer and is used to identify people

Table 4. Relationship between molecular alterations and image quality by modality

Modality	Gene	Positive*		Negative**		Total
		Number of articles	Average sample size (SD of sample size)	Number of articles	Average of sample size (SD of sample size)	Number of articles
^{18}F-FDG PET/CT	KRAS	12	78.17 (34.24)	1	44 (0)	13
	NRAS	2	118 (33)	0	0 (0)	1
	EIF2S2	1	42 (0)	0	0 (0)	2
	GLUT1	1	42 (0)	1	44 (0)	2
	TP53	2	88.5 (14.5)	0	0 (0)	2
	APC	1	74 (0)	1	103 (0)	2
	BRAF	1	85 (0)	1	103 (0)	1
	PIK3CA	0	0 (0)	1	103 (0)	1
	MSI	1	173 (0)	0	0 (0)	1
CT scan	PECAM1	1	71 (0)	0	0 (0)	1
	PRDM1	1	71 (0)	0	0 (0)	1
	AIF1	1	71 (0)	0	0 (0)	1
	IL10	1	71 (0)	0	0 (0)	1
	ISG20	1	71 (0)	0	0 (0)	1
	TLR8	1	71 (0)	0	0 (0)	6
	KRAS	6	109 (43.1)	0	0 (0)	2
	NRAS	2	110 (49)	0	0 (0)	3
	BRAF	3	121.6 (43.33)	0	0 (0)	3
	MSI	3	215 (131)	0	0 (0)	1
	CDKN2A	1	134 (0)	0	0 (0)	1
	TP53	1	134 (0)	0	0 (0)	1
	ATM	1	134 (0)	0	0 (0)	1
	MYC	1	134 (0)	0	0 (0)	1
	ABCB1	1	64 (0)	0	0 (0)	1
	ABCC2	1	64 (0)	0	0 (0)	1
	ABCG2	1	64 (0)	0	0 (0)	1
	ALDH1A1	1	64 (0)	0	0 (0)	1
	CD166	1	64 (0)	0	0 (0)	1
	INHBB	1	64 (0)	0	0 (0)	1
	CDKN1A	1	64 (0)	0	0 (0)	1
MRI	KRAS	8	118.2 (86.8)	1	65 (0)	9
	EGFR	2	33 (13.2)	0	0 (0)	2
	APC	1	20 (0)	1	65 (0)	2
	ARIDA1	1	20 (0)	0	0 (0)	1
	TP53	2	42.5 (22.5)	0	0 (0)	2
	AKT1	1	20 (0)	0	0 (0)	1
	ATM	2	42.5 (22.5)	0	0 (0)	2
	BRAF	1	20 (0)	1	83 (0)	2
	CTNNB1	1	20 (0)	0	0 (0)	1
	FBXW7	1	20 (0)	0	0 (0)	1
	NRAS	3	65.4 (36.3)	1	65 (0)	4
	PIK3	1	20 (0)	1	65 (0)	2
	BRCA2	0	0 (0)	1	65 (0)	1
	SOX9	0	0 (0)	1	65 (0)	1
	FLT4	0	0 (0)	1	65 (0)	1

*Positive=There is a correlation between image features and molecular alterations, **Negetive=There is no correlation/relationship between image features and molecular alterations, KRAS: Kirsten Rat Sarcoma Viral Oncogene Homolog, NRAS: Neuroblastoma RAS Viral, EIF2S2: Eukaryotic Translation Initiation Factor 2 Subunit 2 GLUTI: Glucose Box 1, BRAF: B-Raf proto-onkogen, MSI: Microsatellite Instability, PECAMI: Platelet Endothelial Cell Adhesion Molecule 1, AIFI: Activated Inducible Family of Immune receptors, ISG20: Interferon-Stimulated Gene 20, TLR8: Toll-like Receptor 8, CDKN2A: Cyclin-Dependent Kinase Inhibitor 2A, ATM: Ataxia-Telangiectasia Mutated, ABCG2: ATP Binding Cassette Subfamily G Member 2, ABCB1: ATP Binding Cassette Subfamily B Member 1, AMCC2: Armadillo Motif Containing 2, ABCG2: ATP Binding Cassette Subfamily G Member 2, ALDHIA1: Aldehyde Dehydrogenase 1 Family Member A1, CD166: Cluster of Differentiation 166, INHBB: Inhibin Beta B, CDKNIA: Cyclin-Dependent Kinase Inhibitor 1A, ARIDA1: AT-rich interaction domain 1A, CTNNBI: Catenin Beta 1, FBXW7: F-box and WD-40 domain protein 7, BRAC2: Breast Cancer 2, FLT: Fms-like Tyrosine Kinase

at risk or diagnose the disease. In addition, Wnt pathway inhibitors therapies may be appropriate for APC-mutated colorectal cancer (67). APC mutation has been examined in 4 studies in which the relationship between image feature and APC changes was significant. A review study by Aghabozorgi et al. (68), on the relationship between radionics features and histopathological changes indicated a relationship between APC mutation and radionics features.

MRI, CT scanning, and ^{18}F-FDG PET/CT were used in 10, 15, and 16 studies, respectively. MRI is a non-invasive imaging technique that provides high-resolution anatomical images. It provides good soft-tissue contrast and is useful for evaluating colorectal tumor characteristics, such as size, location, and invasion depth (9,69). According to the performance of MRI, this modality is mostly used for predicting RAS (KRAS/NRAS).

There was also a significant relationship between MRI and molecular factors in all selected studies, except for Horvat et al. (52) study in which qualitative characteristics of images were related to molecular factors; however, no significant relationship was found between quantitative characteristics and molecular factors due to the limitations presented in the study.

The analysis of radionics and quantitative features across various imaging modalities, such as CT, MRI, and ^{18}F-FDG PET/CT, revealed the potential for predicting molecular alterations in colorectal cancer. Radiomics features, including texture and intensity metrics, can help improve the prediction accuracy. Techniques like GLCM, GLRLM, and GLSZM combined with statistical methods such as logistic regression and machine learning models demonstrate varying degrees of success in identifying key genetic mutations such as KRAS, NRAS, BRAF, TP53, and MSI. However, the heterogeneity in methodologies and sample sizes across studies underscores the need for standardized imaging protocols and radiomic analysis techniques.

Study Limitations

Because the studies were conducted considering a small sample size and were still in their early stages, multi-center prospective studies with a larger number of participants should be conducted.

Conclusion

This scoping review highlights the promising potential of radiogenomics in predicting molecular alterations in colorectal cancer through noninvasive imaging modalities. Our comprehensive analysis of 41 high-quality studies revealed that various imaging techniques, including CT scanning, MRI, and 18F-FDG PET/CT, can effectively predict key molecular changes, such as KRAS, NRAS, BRAF, TP53, and MSI. The primary focus has been on CT scanning and MRI, with texture features and radionics playing critical roles in enhancing predictive accuracy. Despite these advancements, the field is still in its nascent stages, with varying levels of predictive performance and sample sizes. The heterogeneity of methodologies and the need for larger, more diverse cohorts underscore the need for further research. Standardization of imaging protocols and radiomic analysis, along with cross-institutional collaborations, will be crucial for validating and refining these predictive models. In conclusion, radiogenomics has significant potential to revolutionize the prediction of molecular alterations in colorectal cancer, facilitating personalized treatment approaches. Continued research and technological advancements are essential for fully realizing its clinical implications and improving patient outcomes.

Ethics

Ethics Committee Approval: This study did not require ethical approval as it did not involve interaction with patients or human subjects.

Informed Consent: This systematic review was based on data from previously published studies, and new patient data were not collected. Therefore, patient consent was not required.

Footnotes

Authorship Contributions

Concept: S.M., H. E., R.R., Design: S.M., H. E., R.R., Data Collection or Processing: S.M., H.M., F.F., Analysis or Interpretation: S.M., H. E., A.H., Literature Search: S.M., A.H., H.M., F.F., R.B., Writing: S.M., H. E., R.R., R.B.

Conflict of Interest: No conflict of interest was declared by the authors.

Financial Disclosure: The authors declared that this study has received no financial support.

References

1. Patel SG, Karlitz JJ, Yen T, Lieu CH, Boland CR. The rising tide of early-onset colorectal cancer: a comprehensive review of epidemiology, clinical features, biology, risk factors, prevention, and early detection. Lancet Gastroenterol Hepatol. 2022;7:262-274.
2. Kim SJ, Pak K, Kim K. Diagnostic performance of F-18 FDG PET/CT for prediction of KRAS mutation in colorectal cancer patients: a systematic review and meta-analysis. Abdom Radiol. 2019;44:1703-1711.
3. Bray F, Laversanne M, Sung H, Ferlay J, Siegel RL, Soerjomataram I, Jemal A. Global cancer statistics 2022: GLOBOCAN estimates of incidence and mortality worldwide for 36 cancers in 185 countries. CA Cancer J Clin. 2024;74:229-263.

4. Rabiei R, Ayyoubzadeh SM, Sohrabei S, Esmaeili M, Atashi A. Prediction of breast cancer using machine learning approaches. J Biomed Phys Eng. 2022;12:297-308.
5. Awedew AF, Asefa Z, Belay WB. Burden and trend of colorectal cancer in 54 countries of Africa 2010-2019: a systematic examination for Global Burden of Disease. BMC Gastroenterol. 2022;22:204.
6. Mehdizadeh H, Asadi F, Mehrvar A, Nazemi E, Emami H. Smartphone apps to help children and adolescents with cancer and their families: a scoping review. Acta Oncol. 2019;58:1003-1014.
7. Sveen A, Kopetz S, Lothe RA. Biomarker-guided therapy for colorectal cancer: strength in complexity. Nat Rev Clin Oncol. 2020;17(1):11-32.
8. Vogelstein B, Papadopoulos N, Velculescu VE, Zhou S, Diaz Jr LA, Kinzler KW. Cancer genome landscapes. Science. 2013;339:1546-1558.
9. Badic B, Tixier F, Cheze Le Rest C, Hatt M, Visvikis D. Radiogenomics in colorectal cancer. Cancers. 2021;13:973.
10. Siegel RL, Miller KD, Goding Sauer A, Fedewa SA, Butterly LF, Anderson JC, Cercek A, Smith RA, Jemal A. Colorectal cancer statistics, 2020. CA Cancer J Clin. 2020;70:145-164.
11. Dagogo-Jack I, Shaw AT. Tumour heterogeneity and resistance to cancer therapies. Nat Rev Clin Oncol. 2018;15:81-94.
12. Liu Z, Zhang XY, Shi YJ, Wang L, Zhu HT, Tang Z, Wang S, Li XT, Tian J, Sun YS. Radiomics analysis for evaluation of pathological complete response to neoadjuvant chemoradiotherapy in locally advanced rectal cancer. Clin Cancer Res. 2017;23:7253-7262.
13. Burrell RA, Swanton C. Tumour heterogeneity and the evolution of polyclonal drug resistance. Mol Oncol. 2014;8:1095-1111.
14. Li M, Zhang J, Dan Y, Yao Y, Dai W, Cai G, Yang G, Tong T. A clinical-radiomics nomogram for the preoperative prediction of lymph node metastasis in colorectal cancer. J Transl Med. 2020;18:46.
15. Liu S, Pan X, Liu R, Zheng H, Chen L, Guan W, Wang H, Sun Y, Tang L, Guan Y, Ge Y, He J, Zhou Z. Texture analysis of CT images in predicting malignancy risk of gastrointestinal stromal tumours. Clin Radiol. 2018;73:266-274.
16. de la Pinta C, Castillo ME, Collado M, Galindo-Pumariño C, Peña C. Radiogenomics: hunting down liver metastasis in colorectal cancer patients. Cancers. 2021;13:5547.
17. Page MJ, McKenzie JE, Bossuyt PM, Boutron I, Hoffmann TC, Mulrow CD, Shamseer L, Tetzlaff JM, Akl EA, Brennan SE, Chou R, Glanville J, Grimshaw JM, Hróbjartsson A, Lalu MM, Li T, Loder EW, Mayo-Wilson E, McDonald S, McGuinness LA, Stewart LA, Thomas J, Tricco AC, Welch VA, Whiting P, Moher D. The PRISMA 2020 statement: an updated guideline for reporting systematic reviews. Int J Surg. 2021;88:105906.
18. Darvish L, Bahreyni-Toossi M-T, Roozbeh N, Azimian H. The role of radiogenomics in the diagnosis of breast cancer: a systematic review. Egypt J Med Hum Genet. 2022;23:1-16.
19. Lovinfosse P, Koopmansch B, Lambert F, Jodogne S, Kustermans G, Hatt M, Visvikis D, Seidel L, Polus M, Albert A, Delvenne P, Hustinx R. 18F-FDG PET/CT imaging in rectal cancer: relationship with the RAS mutational status. Br J Radiol. 2016;89:20160212.
20. Yang JW, Yuan LL, Gao Y, Liu XS, Wang YJ, Zhou LM, Kui XY, Li XH, Ke CB, Pei ZJ. 18F-FDG PET/CT metabolic parameters correlate with EIF2S2 expression status in colorectal cancer. J Cancer. 2021;12:5838-5847.
21. Huang YC, Tsai YS, Li CI, Chan RH, Yeh YM, Chen PC, Shen MR, Lin PC. Adjusted CT image-based radiomic features combined with immune genomic expression achieve accurate prognostic classification and identification of therapeutic targets in stage III colorectal cancer. 2022;14:1895.
22. Jo SJ, Kim SH. Association between oncogenic RAS mutation and radiologic-pathologic findings in patients with primary rectal cancer. Quant Imaging Med Surg. 2019;9:238-246.
23. Yang L, Dong D, Fang M, Zhu Y, Zang Y, Liu Z, Zhang H, Ying J, Zhao X, Tian J. Can CT-based radiomics signature predict KRAS/NRAS/BRAF mutations in colorectal cancer? Eur Radiol. 2018;28:2058-2067.
24. Xu Y, Xu Q, Ma Y, Duan J, Zhang H, Liu T, Li L, Sun H, Shi K, Xie S, Wang W. Characterizing MRI features of rectal cancers with different KRAS status. BMC cancer. 2019;19:1111.
25. Li Z, Zhong Q, Zhang L, Wang M, Xiao W, Cui F, Yu F, Huang C, Feng Z. Computed tomography-based radiomics model to preoperatively predict microsatellite instability status in colorectal cancer: a multicenter study. Front Oncol. 2021;11:666786.
26. Crimì F, Zanon C, Cabrelle G, Luong KD, Albertoni L, Bao QR, Borsetto M, Baratella E, Capelli G, Spolverato G, Fassan M, Pucciarelli S, Quaia E. Contrast-enhanced CT texture analysis in colon cancer: correlation with genetic markers. Tomography. 2022;8:2193-2201.
27. Cho A, Jo K, Hwang SH, Lee N, Jung M, Yun M, Hwang HS. Correlation between KRAS mutation and 18 F-FDG uptake in stage IV colorectal cancer. Abdom Radiol. 2017;42:1621-1626.
28. Chen SW, Chiang HC, Chen WT, Hsieh TC, Yen KY, Chiang SF, Kao CH. Correlation between PET/CT parameters and KRAS expression in colorectal cancer. Clin Nucl Med. 2014;39:685-689.
29. Yeo DM, Oh SN, Jung CK, Lee MA, Oh ST, Rha SE, Jung SE, Byun JY, Gall P, Son Y. Correlation of dynamic contrast enhanced MRI perfusion parameters with angiogenesis and biologic aggressiveness of rectal cancer: preliminary results. J Magn Reson Imaging. 2015;41:474-480.
30. Mao W, Zhou J, Zhang H, Qiu L, Tan H, Hu Y, Shi H. Relationship between KRAS mutations and dual time point 18 F-FDG PET/CT imaging in colorectal liver metastases. Abdominal Radiology. 2019;44:2059-2066.
31. Taguchi N, Oda S, Yokota Y, Yamamura S, Imuta M, Tsuchigame T, Nagayama Y, Kidoh M, Nakaura T, Shiraishi S, Funama Y, Shinriki S, Miyamoto Y, Baba H, Yamashita Y. CT texture analysis for the prediction of KRAS mutation status in colorectal cancer via a machine learning approach. Eur J Radiol. 2019;118:38-43.
32. Zhong ME, Duan X, Ni-Jia-Ti MY, Qi H, Xu D, Cai D, Li C, Huang Z, Zhu Q, Gao F, Wu X. CT-based radiogenomic analysis dissects intratumor heterogeneity and predicts prognosis of colorectal cancer: a multi-institutional retrospective study. J Transl Med. 2022;20:574.
33. Wu X, Li Y, Chen X, Huang Y, He L, Zhao K, Huang X, Zhang W, Huang Y, Li Y, Dong M, Huang J, Xia T, Liang C, Liu Z. Deep learning features improve the performance of a radiomics signature for predicting KRAS status in patients with colorectal cancer. Acad Radiol. 2020;27:254-262.
34. Seth A, Amemiya Y, Cheung H, Hsieh E, Law C, Milot L. Delayed MRI enhancement of colorectal cancer liver metastases is associated with metastatic mutational profile. Cancer Genomics Proteomics. 2021;18:627-635.
35. Cui Y, Liu H, Ren J, Du X, Xin L, Li D, Yang X, Wang D. Development and validation of a MRI-based radiomics signature for prediction of KRAS mutation in rectal cancer. Eur Radiol. 2020;30:1948-1958.
36. Cao Y, Zhang G, Bao H, Zhang S, Zhang J, Zhao Z, Zhang W, Li W, Yan X, Zhou J. Development of a dual-energy spectral CT based nomogram for the preoperative discrimination of mutated and wild-type KRAS in patients with colorectal cancer. Clin Imaging. 2021;69:205-212.
37. Cui Y, Cui X, Yang X, Zhuo Z, Du X, Xin L, Yang Z, Cheng X. Diffusion kurtosis imaging-derived histogram metrics for prediction of KRAS mutation in rectal adenocarcinoma: Preliminary findings. J Magn Reson Imaging. 2019;50:930-939.
38. Granata V, Fusco R, Risi C, Ottaiano A, Avallone A, De Stefano A, Grimm R, Grassi R, Brunese L, Izzo F, Petrillo A. Diffusion-weighted MRI and diffusion kurtosis imaging to detect RAS mutation in colorectal liver metastasis. Cancers. 2020;12:2420.
39. Chen SW, Lin CY, Ho CM, Chang YS, Yang SF, Kao CH, Chang JG. Genetic alterations in colorectal cancer have different patterns on 18F-FDG PET/CT. Clin Nucl Med. 2015;40:621-626.
40. Promsorn J, Chadbunchachai P, Somsap K, Paonariang K, Sa-ngaimwibool P, Apivatanasiri C, et al. Imaging features associated with survival outcomes among colorectal cancer patients with and without KRAS mutation. Egypt J Radiol Nucl Med. 2021;52:1-10.

41. Liu Q, Li J, Xu L, Wang J, Zeng Z, Fu J, Huang X, Chu Y, Wang J, Zhang HY, Zeng F. Individualized prediction of colorectal cancer metastasis using a radiogenomics approach. Front Oncol. 2021;11:620945.
42. Popovic M, Talarico O, van den Hoff J, Kunin H, Zhang Z, Lafontaine D, Dogan S, Leung J, Kaye E, Czmielewski C, Mayerhoefer ME, Zanzonico P, Yaeger R, Schöder H, Humm JL, Solomon SB, Sofocleous CT, Kirov AS. KRAS mutation effects on the 2-[18F] FDG PET uptake of colorectal adenocarcinoma metastases in the liver. EJNMMI Res. 2020;10:142.
43. Krikelis D, Skoura E, Kotoula V, Rondogianni P, Pianou N, Samartzis A, Xanthakis I, Fountzilas G, Datseris IE. Lack of association between KRAS mutations and 18F-FDG PET/CT in Caucasian metastatic colorectal cancer patients. Anticancer Res. 2014;34:2571-2579.
44. Chen SW, Shen WC, Chen WT, Hsieh TC, Yen KY, Chang JG, Kao CH. Metabolic imaging phenotype using radiomics of [18 F] FDG PET/CT associated with genetic alterations of colorectal cancer. Mol Imaging Biol. 2019;21:183-190.
45. Zhang Z, Shen L, Wang Y, Wang J, Zhang H, Xia F, et al. MRI radiomics signature as a potential biomarker for predicting KRAS status in locally advanced rectal cancer patients. Front Oncol. 2021;11:614052.
46. Miles KA, Ganeshan B, Rodriguez-Justo M, Goh VJ, Ziauddin Z, Engledow A, Meagher M, Endozo R, Taylor SA, Halligan S, Ell PJ, Groves AM. Multifunctional imaging signature for V-Kl-RAS2 Kirsten rat sarcoma viral oncogene homolog (KRAS) mutations in colorectal cancer. J Nucl Med. 2014;55:386-391.
47. He K, Liu X, Li M, Li X, Yang H, Zhang H. Noninvasive KRAS mutation estimation in colorectal cancer using a deep learning method based on CT imaging. BMC Med Imaging. 2020;20:59.
48. Shi R, Chen W, Yang B, Qu J, Cheng Y, Zhu Z, Gao Y, Wang Q, Liu Y, Li Z, Qu X. Prediction of KRAS, NRAS and BRAF status in colorectal cancer patients with liver metastasis using a deep artificial neural network based on radiomics and semantic features. Am J Cancer Res. 2020;10:4513-4526.
49. He P, Zou Y, Qiu J, Yang T, Peng L, Zhang X. Pretreatment 18F-FDG PET/CT imaging predicts the KRAS/NRAS/BRAF gene mutational status in colorectal cancer. J Oncol. 2021;2021:6687291.
50. Sh M, NM M. 18F-FDG PET/CT based quantitative parameters as predictive biomarkers for kras mutations in metastatic colorectal cancer. egyptian journal nuclear medicine. 2021;23:74-90.
51. Li J, Yang Z, Xin B, Hao Y, Wang L, Song S, Xu J, Wang X. Quantitative prediction of microsatellite instability in colorectal cancer with preoperative PET/CT-based radiomics. Front Oncol. 2021;11:702055.
52. Horvat N, Veeraraghavan H, Pelossof RA, Fernandes MC, Arora A, Khan M, Marco M, Cheng CT, Gonen M, Golia Pernicka JS, Gollub MJ, Garcia-Aguillar J, Petkovska I. Radiogenomics of rectal adenocarcinoma in the era of precision medicine: a pilot study of associations between qualitative and quantitative MRI imaging features and genetic mutations. Eur J Radiol. 2019;113:174-181.
53. Badic B, Hatt M, Durand S, Jossic-Corcos CL, Simon B, Visvikis D, Corcos L. Radiogenomics-based cancer prognosis in colorectal cancer. Sci Rep. 2019;9:9743.
54. Ma Y, Lin C, Liu S, Wei Y, Ji C, Shi F, Lin F, Zhou Z. Radiomics features based on internal and marginal areas of the tumor for the preoperative prediction of microsatellite instability status in colorectal cancer. Front Oncol. 2022;12:1020349.
55. Negreros-Osuna AA, Parakh A, Corcoran RB, Pourvaziri A, Kambadakone A, Ryan DP, Sahani DV. Radiomics texture features in advanced colorectal cancer: correlation with BRAF mutation and 5-year overall survival. Radiol Imaging Cancer. 2020;2:190084.
56. Granata V, Fusco R, Avallone A, De Stefano A, Ottaiano A, Sbordone C, Brunese L, Izzo F, Petrillo A. Radiomics-derived data by contrast enhanced magnetic resonance in RAS mutations detection in colorectal liver metastases. Cancers. 2021;13:453.
57. Kawada K, Toda K, Nakamoto Y, Iwamoto M, Hatano E, Chen F, Hasegawa S, Togashi K, Date H, Uemoto S, Sakai Y. Relationship between 18F-FDG PET/CT scans and KRAS mutations in metastatic colorectal cancer. J Nucl Med. 2015;56:1322-1327.
58. Arslan E, Aksoy T, Gürsu RU, Dursun N, Çakar E, Çermik TF. The prognostic value of 18F-FDG PET/CT and KRAS mutation in colorectal cancers. Molecular Imaging and Radionuclide Therapy. 2020;29:17-24.
59. Huang L, Guo Z, Wang F, Fu L. KRAS mutation: from undruggable to druggable in cancer. Signal Transduct Target Ther. 2021;6:386.
60. Uhlyarik A, Piurko V, Vizkeleti L, Pápai Z, Rásó E, Lahm E, Kiss E, Sikter M, Vachaja J, Kenessey I, Tímár J. EGFR protein expression of KRAS wild-type colorectal cancer: predictive value of the sidedness for efficacy of anti-EGFR Therapy. Pathol Oncol Res. 2020;26:1429-1434.
61. Kopetz S, Desai J, Chan E, Hecht JR, O'Dwyer PJ, Maru D, Morris V, Janku F, Dasari A, Chung W, Issa JP, Gibbs P, James B, Powis G, Nolop KB, Bhattacharya S, Saltz L. Phase II pilot study of vemurafenib in patients with metastatic BRAF-mutated colorectal cancer. J Clin Oncol. 2015;33:4032-4038.
62. Santhanam P, Khthir R, Solnes LB, Ladenson PW. The relationship of BRAFV600E mutation status to FDG PET/CT avidity in thyroid cancer: a review and meta-analysis. Endocr Pract. 2018;24:21-26.
63. Liebl MC, Hofmann TG. The role of p53 signaling in colorectal cancer. Cancers. 2021;13:2125.
64. Seow P, Wong JH, Ahmad-Annuar A, Mahajan A, Abdullah NA, Ramli N. Quantitative magnetic resonance imaging and radiogenomic biomarkers for glioma characterisation: a systematic review. Br J Radiol. 2018;91:20170930.
65. Moosavi B, Flood TA, Al-Dandan O, Breau RH, Cagiannos I, Morash C, Malone SC, Schieda N. Multiparametric MRI of the anterior prostate gland: clinical-radiological-histopathological correlation. Clin Radiol. 2016;71:405-417.
66. Le DT, Durham JN, Smith KN, Wang H, Bartlett BR, Aulakh LK, Lu S, Kemberling H, Wilt C, Luber BS, Wong F, Azad NS, Rucki AA, Laheru D, Donehower R, Zaheer A, Fisher GA, Crocenzi TS, Lee JJ, Greten TF, Duffy AG, Ciombor KK, Eyring AD, Lam BH, Joe A, Kang SP, Holdhoff M, Danilova L, Cope L, Meyer C, Zhou S, Goldberg RM, Armstrong DK, Bever KM, Fader AN, Taube J, Housseau F, Spetzler D, Xiao N, Pardoll DM, Papadopoulos N, Kinzler KW, Eshleman JR, Vogelstein B, Anders RA, Diaz LA Jr. Mismatch repair deficiency predicts response of solid tumors to PD-1 blockade. Science. 2017;357:409-413.
67. Wang Q, Xu J, Wang A, Chen Y, Wang T, Chen D, Zhang J, Brismar TB. Systematic review of machine learning-based radiomics approach for predicting microsatellite instability status in colorectal cancer. Radiol Med. 2023;128:136-148.
68. Aghabozorgi AS, Bahreyni A, Soleimani A, Bahrami A, Khazaei M, Ferns GA, Avan A, Hassanian SM. Role of adenomatous polyposis coli (APC) gene mutations in the pathogenesis of colorectal cancer; current status and perspectives. Biochimie. 2019;157:64-71.
69. Coppola F, Giannini V, Gabelloni M, Panic J, Defeudis A, Lo Monaco S, Cattabriga A, Cocozza MA, Pastore LV, Polici M, Caruso D, Laghi A, Regge D, Neri E, Golfieri R, Faggioni L. Radiomics and magnetic resonance imaging of rectal cancer: from engineering to clinical practice. Diagnostics. 2021;11:756.

Original Article

Mol Imaging Radionucl Ther 2025;34:26-30 *DOI:10.4274/mirt.galenos.2024.78557*

Relationship of Plasma Cell Infiltration Rates with ^{18}F-FDG PET/CT Data and Hematological Parameters in Multiple Myeloma

Multipl Myelomda Plazma Hücre İnfiltrasyon Oranlarının ve Hematolojik Parametrelerin ^{18}F-FDG PET/CT Verileri Arasındaki İlişki

Özge Ulaş Babacan[1], Zekiye Hasbek[2], Hatice Terzi[3]

[1]*Tokat Gaziosmanpaşa University Faculty of Medicine, Department of Nuclear Medicine, Tokat, Türkiye*
[2]*Sivas Cumhuriyet University Faculty of Medicine, Department of Nuclear Medicine, Sivas, Türkiye*
[3]*Sivas Cumhuriyet University Faculty of Medicine, Department of Hematology, Sivas, Türkiye*

Abstract

Objectives: This study aimed to evaluate the relationship between the degree of bone marrow involvement, hematological parameters, and ^{18}F-fluorodeoxyglucose (^{18}F-FDG)-positron emission tomography/computed tomography (PET/CT) data in patients diagnosed with multiple myeloma.

Methods: A total of 71 patients [19 females, 52 males, mean age 67 (36-83) years] who were diagnosed with multiple myeloma between 2014 and 2021, had not received any treatment yet, and underwent ^{18}F-FDG-PET/CT for staging were included in the study.

Results: No significant correlation was observed between bone marrow standardized uptake value $(SUV)_{max}$ and plasma cell infiltration (p=0.07). However, we found that patients with visually increased bone marrow counts also had higher plasma cell infiltration rates (p=0.037). No significant correlation was found between plasma cell infiltration rates and bone marrow SUV_{max} and systemic inflammatory index (SII) (p=0.187 and p=0.446, respectively). However, there was a significant correlation between the SUV_{max} of lytic lesions showing increased ^{18}F-FDG uptake in bone and SII (p=0.025, r=0.330).

Conclusion: We believe that ^{18}F-FDG PET/CT may be an advantage over bone marrow biopsy in the diagnosis and evaluation of multiple myeloma recurrence and may prevent repeated bone marrow biopsies.

Keywords: Multiple myeloma, ^{18}F-FDG PET/CT, plasma cell infiltration rate, systemic immune-inflammatory index

Öz

Amaç: Bu çalışmada multipl myelom tanısı alan hastalardaki kemik iliği plazma hücre infiltrasyonu ve hematolojik parametreler ile ^{18}F-florodeoksiglukoz (^{18}F-FDG)-pozitron emisyon tomografisi/bilgisayarlı tomografinin (PET/BT) verileri arasındaki ilişkinin değerlendirilmesi amaçlandı.

Yöntem: 2014-2021 yılları arasında multipl myelom tanısı alan, henüz tedavi almayan ve evreleme amaçlı ^{18}F-FDG- PET/BT uygulanan toplam 71 hasta [19'u kadın, 52'si erkek, ortalama yaş 67 (36-83)] çalışmaya dahil edildi.

Bulgular: Kemik iliği standartlaştırılmış alım değeri $(SUV)_{maks}$ değerleri ile plazma hücre infiltrasyonu arasında anlamlı bir ilişki bulunamadı (p=0,07). Ancak görsel olarak kemik iliği artışı olan hastalarda plazma hücre infiltrasyon oranlarının da daha yüksek olduğunu bulduk (p=0,037). Plazma hücre infiltrasyon oranları ile kemik iliği SUV_{maks} değeri ve sistemik inflamatuar indeks (SII) arasında anlamlı bir korelasyon bulunamadı (sırasıyla

Address for Correspondence: Özge Ulaş Babacan, Tokat Gaziosmanpaşa University Faculty of Medicine, Department Of Nuclear Medicine, Tokat, Türkiye
E-mail: ozgeulas23@gmail.com **ORCID ID:** orcid.org/0000-0002-8687-5769
Received: 14.06.2024 **Accepted:** 19.09.2024 **Publication Date:** 07.02.2025

Cite this article as: Babacan ÖU, Hasbek Z, Terzi H. Relationship of plasma cell infiltration rates with ^{18}F-FDG PET/CT data and hematological parameters in multiple myeloma. Mol Imaging Radionucl Ther. 2025;34:26-30.

p=0,187 ve p=0,446). Ancak kemikte artmış ^{18}F-FDG tutulumu gösteren litik lezyonların SUV_{maks} değeri ile SII arasında anlamlı bir korelasyon vardı (p=0,025, r=0,330).

Sonuç: Sonuç olarak multipl myelom nükslerinin tanı ve değerlendirilmesinde ^{18}F-FDG PET/BT'nin kemik iliği biyopsisine avantaj sağlayabileceğini ve tekrarlanan kemik iliği biyopsilerini önleyebileceğini düşünüyoruz.

Anahtar kelimeler: Multipl myelom, ^{18}F-FDG PET/BT, plazma hücre infiltrasyon oranı, sistemik immün-inflamatuar indeks

Introduction

Multiple myeloma constitutes 1% of all cancers and ~13% of hematological malignancies (1,2). In addition, it has been the focus of studies because it is the 2nd most common cancer type after non-Hodgkin lymphoma in hematological malignancies, and its incidence has increased by 126% from 1991 to 2016 (1,3). Multiple myeloma is a malignancy characterized by the uncontrolled proliferation of clonal plasma cells in bone marrow and by the secretion of monoclonal immunoglobulin protein (M protein) (2,3,4).

The National Comprehensive Cancer Network recommendations for staging patients with multiple myeloma at diagnosis are positron emission tomography/computed tomography (PET/CT) or whole-body low-dose CT (5).

As in many other cancers, ^{18}F-fluorodeoxyglucose (^{18}F-FDG)-PET/CT is an imaging system used in staging and treatment diagnosis evaluation of hematological malignancies (6,7). ^{18}F-FDG-PET/CT is an effective method for detecting skeletal and extramedullary lesions in multiple myeloma patients (8).

We aimed to investigate the potential distribution of bone marrow plasma cell infiltration rates, PET/CT data, and hematological parameters in multiple myeloma. Thus, we aimed to determine whether ^{18}F-FDG-PET/CT can be used instead of repeated invasive bone marrow biopsy when investigating the diagnosis and recurrence of patients.

Materials and Methods

A total of 71 patients [19 females, 52 males, mean age 67 (36-83) years] diagnosed with multiple myeloma between 2014 and 2021, who had not received any treatment yet, and who underwent ^{18}F-FDG-PET/CT for staging purposes were included in the study. Our study was retrospective, and informed consent was obtained from all patients.

No patient diagnosed outside Sivas Cumhuriyet University and/or who underwent ^{18}F-FDG PET/CT at an external center were included in the study. Patients who received treatment after diagnosis or for other malignancies were also excluded.

Bone marrow aspiration results and creatinine, albumin, calcium, neutrophil, lymphocyte, beta-2 microglobulin, and platelet values were recorded from blood samples obtained within 2 weeks after the diagnosis of ^{18}F-FDG-PET/CT. The systemic inflammatory index (SII) of the patients was calculated using the neutrophil x lymphocyte/platelet formula.

Standardized uptake value maxima (SUV_{max}) values, which were calculated with ^{18}F-FDG PET/CT software in the Department of Nuclear Medicine, and the presence/absence of metastases detected by ^{18}F-FDG PET/CT were recorded.

In PET/CT image analysis, when bone lesions were evaluated, uptake greater than background bone marrow activity was considered positive. A bone marrow SUV_{max} > hepatic SUV_{max} was considered positive for diffuse bone marrow infiltration.

Approval for this study was obtained from the Sivas Cumhuriyet University Non-Invasive Clinical Research Ethics Committee (decision no: 2022-01/21, date: 13.01.2022).

^{18}F-FDG PET/CT Imaging Protocol

Blood sugar levels of patients who remained open for a minimum of 4-6 hours were measured before the ^{18}F-FDG injection. Injection was allowed for patients whose blood sugar was below <200 mg/dL. 0.1 mCi ^{18}F-FDG per kilogram was recorded in the patients, and after being stored for 45-60 minutes, Three-dimensional PET/CT images were taken from the skull to the tip of the foot. A General Electric Discovery PET/CT 600 device was used for imaging. CT imaging, attenuation correction, and anatomical correlation were performed with a spiral 16-slice scanner at 120 kV and 172 mAs. During imaging, images were taken for approximately 2-3 min in each bed position. Axial, coronal, and sagittal fusion images were created using the Iterative reconstruction method. SUV_{max} were calculated from PET images. In the PET images, the region of interest (ROI) was placed within the primary tumor, avoiding the peripheral area. The following formula was used to calculate the SUV_{max}: [Activity in ROI (mCi/mL)×Body Weight (grams)]÷Injected Dose (mCi)

Statistical Analysis

The data obtained from our study were evaluated using SPSS 23.0 software. The normality of the data was analyzed using the Kolmogorov-Smirnov test. Because the parametric conditions of the data were not met, the Mann-Whitney U test was used for two independent groups and the Kruskal-Wallis test for more than two independent groups. When analysis of variance was used for comparisons with more than two groups, Tukey's T2 test was used to determine which group was different from the others when the homogeneity assumption was met, and Tamhane's T2 test was used when the homogeneity assumption was not met. The chi-square test was used to evaluate the data obtained by counting. The p-values ≤0.05 were accepted statistically significant.

Results

The mean bone marrow SUV_{max} was 2.3 (range: 1-7.6). Forty-one (58%) patients had bone marrow enhancement visualized on PET/CT, whereas 30 (42%) did not. The correlation between the rates of plasma cell infiltration and the rates of visualized bone marrow enhancement was statistically significant (p=0.037). There was no significant correlation between bone marrow plasma cell infiltration rate and bone marrow SUV_{max} value (p=0.072) (Table 1). There was no significant correlation between plasma cell infiltration rates and the presence of lytic lesions with increased ^{18}F-FDG uptake >5 mm on PET/CT (p=0.05). In addition, no significant correlation was found between plasma cell infiltration rate and SUV_{max} of the lytic lesion (p=0.07).

No significant correlation was found between plasma cell infiltration rate and SII (p=0.187). No significant correlation was found between bone marrow SUV_{max} and SII (p=0.446) (Table 1). There was a significant correlation between bone lytic lesion SUV_{max} and SII (p=0.025, r=0.330). There was a significant correlation between bone marrow SUV_{max} and creatinine elevation (p=0.032) (Table 1). There was also a significant correlation between the presence of lytic lesions in bone and creatinine elevation (p=0.026). However, there was no significant correlation between the SUV_{max} of lytic lesions in bone and creatinine elevation (p=0.156). However, no significant correlation was found between bone marrow SUV_{max} and parameters such as platelet, hemoglobin, calcium, beta- 2 microglobulin, and albumin (p=0.977, p=0.806, p=0.505, p=0.216, p=0.423, respectively) (Table 1).

Discussion

No significant correlation was found between plasma cell infiltration rate. The presence of bone marrow involvement and the extent of extramedullary tissue involvement are important factors affecting the prognosis and clinical management of patients with multiple myeloma.

In their study, Sager et al. (9) found a significant correlation between bone marrow biopsy cellularity, plasma cell ratio, and bone marrow SUV_{max}. In conclusion, the correlation between bone marrow SUV_{max} and plasma cell ratio suggested that PET/CT could prevent repeated bone marrow biopsies during follow-up.

Ak and Gulbas (10) showed that increased ^{18}F-FDG uptake in the bone marrow of patients with multiple myeloma was associated with the percentage of plasma cell infiltration in the bone marrow. Therefore, the authors stated that the ^{18}F-FDG-PET/CT study may be a valuable tool for estimating the levels of myeloma cells in bone marrow, and it is an imaging method that can be used in response to treatment and follow-up of patients.

However, our study found that plasma cell infiltration rates were also high in patients with visually increased bone marrow. Still, we did not find any significant correlation between bone marrow SUV_{max} and plasma cell infiltration rates. This may be due to the limited number of patients or the individual differences in the fields on which we based the bone marrow SUV_{max} levels.

Cengiz et al. (11) in their study, no correlation was found between the ^{18}F-FDG uptake rate of bone marrow and calcium, albumin, and beta-2 microglobulin levels, which is consistent with our study.

However, a significant correlation was observed between the ^{18}F-FDG uptake rate in bone marrow and creatinine elevation. In addition, the presence or absence of lytic lesions in bone was significantly correlated with creatinine elevation. This is related to disease aggressiveness.

Table 1. The relationship between bone marrow SUV_{max} levels and hematological and biochemical parameters

	Plasma cell infiltration rate/ SUV_{max}	SII/SUV_{max}	Platelet/ SUV_{max}	Hemoglobin/ SUV_{max}	beta-2 microglobulin/ SUV_{max}	Calcium/ SUV_{max}	Creatinine/ SUV_{max}	Albumin/ SUV_{max}
r	0.215	0.93	0.04*	-0.03	0.153	0.083	-0.567	0.101
p	0.07	0.446	0.977	0.806	0.216	0.505	0.03*	0.423

SUV_{max}: Maximum standardized uptake value, *= p< 0.05, SII: Systemic inflammatory index

According to Kim et al., (12), regarding hematological parameters, a high neutrophil-to-lymphocyte ratio, low platelet count, and high c-reactive protein were found to be independently negatively associated with overall survival. In a study by Shi et al., (13) high neutrophil-to-lymphocyte ratio and low platelet-to-lymphocyte ratio were compatible with poor prognostic clinical results and suggested their utility as prognostic biomarkers.

Recently, the SII based on peripheral platelet, neutrophil, and lymphocyte counts has been shown to be a promising prognostic indicator in various diseases.

In our study, there was a significant correlation between SII and the SUV_{max} value of the lytic lesion in the bone (p=0.025, r=0.330). Many studies have reported that high tumor lesion SUV_{max} and SII values increase tumor aggressiveness and poor prognosis (14,15,16). For this reason, we believe that we found a correlation between bone lesion SUV_{max} and SII values in our study. We believe that patients with a high lesion SUV_{max} value will also have a high SII and a worse prognosis. Therefore, it should be kept in mind that anti-inflammatory therapies may be added to such patients during follow-up. The most important limitation of our study is that we could not reach the targeted number of patients and could not evaluate the prognosis of the patients.

Conclusion

No significant correlation was observed between bone and bone marrow uptake and bone marrow plasma cell infiltration rate on ^{18}F-FDG PET/CT. However, our study found that patients with visually increased bone marrow uptake also had high plasma cell infiltration rates. In conclusion, we believe that ^{18}F-FDG PET/CT may be an advantage of bone marrow biopsy in the diagnosis and evaluation of the recurrence of multiple myeloma and may prevent repeated bone marrow biopsies.

In addition, our study showed a significant correlation between the SUV_{max} of lytic lesions in bone and SII (p=0.025, r=0.330). Therefore, we believe that the prognosis will worsen as the SUV_{max} of lytic lesion increases.

In addition, increased serum creatinine levels were associated with bone marrow SUV_{max}. We believe this is also related to the aggressiveness of the disease and poor prognosis.

We found 4 studies investigating the relationship between ^{18}F-FDG-PET/CT parameters and bone marrow plasma cell infiltration rate in multiple myeloma. Although the number of patients included in these studies was insufficient, we believe that further studies would be useful to provide an advantage to bone marrow biopsy, an invasive method for the diagnosis and follow-up of multiple myeloma. In this regard, we believe that our study results are valuable.

Ethics

Ethics Committee Approval: Approval for this study was obtained from the Sivas Cumhuriyet University Non-Invasive Clinical Research Ethics Committee (decision no: 2022-01/21, date: 13.01.2022)..

Informed Consent: Our study was retrospective, and informed consent was obtained from the patients.

Footnote

Authorship Contributions

Surgical and Medical Practices: H.T., Concept: Z.H., Design: Z.H., Data Collection or Processing: Z.H., Analysis or Interpretation: Z.H., Ö.U.B., H.T., Literature Search: Ö.U.B., Writing: Ö.U.B.

Conflict of Interest: No conflict of interest was declared by the authors.

Financial Disclosure: The authors declared that this study has received no financial support.

References

1. Raab MS, Cavo M, Delforge M, Driessen C, Fink L, Flinois A, Gonzalez-McQuire S, Safaei R, Karlin L, Mateos MV, Schoen P, Yong K. Multiple myeloma: practice patterns across Europe. Br J Haematol. 2016;175:66-76.
2. Kazandjian D. Multiple myeloma epidemiology and survival: a unique malignancy. Semin Oncol. 2016;43:676-681.
3. Cowan AJ, Allen C, Barac A, Basaleem H, Bensenor I, Curado MP, Foreman K, Gupta R, Harvey J, Hosgood HD, Jakovljevic M, Khader Y, Linn S, Lad D, Mantovani L, Nong VM, Mokdad A, Naghavi M, Postma M, Roshandel G, Shackelford K, Sisay M, Nguyen CT, Tran TT, Xuan BT, Ukwaja KN, Vollset SE, Weiderpass E, Libby EN, Fitzmaurice C. Global burden of multiple myeloma: a systematic analysis for the global burden of disease study 2016. JAMA Oncol. 2018;4:1221-1227.
4. Medical Masterclass contributors; Firth J. Haematology: multiple myeloma. Clin Med (Lond). 2019;19:58-60.
5. Callander NS, Baljevic M, Adekola K, Anderson LD, Campagnaro E, Castillo JJ, Costello C, Devarakonda S, Elsedawy N, Faiman M, Garfall A, Godby K, Hillengass J, Holmberg L, Htut M, Huff CA, Hultcrantz M, Kang Y, Larson S, Liedtke M, Martin T, Omel J, Sborov D, Shain K, Stockerl-Goldstein K, Weber D, Berardi RA, Kumar R, Kumar SK. NCCN Guidelines® Insights: Multiple Myeloma, Version 3.2022. J Natl Compr Canc Netw. 2022;20:8-19.
6. Nanni C, Zamagni E. Therapy assessment in multiple myeloma with PET. Eur J Nucl Med Mol Imaging. 2017;44(Suppl 1):111-117.
7. Beyer T, Townsend DW, Blodgett TM. Dual-modality PET/CT tomography for clinical oncology. Q J Nucl Med. 2022;46:24-34.
8. Dammacco F, Rubini G, Ferrari C, Vacca A, Racanelli V. ^{18}F-FDG PET/CT: a review of diagnostic and prognostic features in multiple myeloma and related disorders. Clin Exp Med. 2015;15:1-18.
9. Sager S, Ergül N, Ciftci H, Cetin G, Güner SI, Cermik TF. The value of FDG PET/CT in the initial staging and bone marrow involvement of patients with multiple myeloma. Skeletal Radiol. 2011;40:843-847.
10. Ak I, Gulbas Z. F-18 FDG uptake of bone marrow on PET/CT scan: it's correlation with CD38/CD138 expressing myeloma cells in bone marrow of patients with multiple myeloma. Ann Hematol. 2011;90:81-87.

11. Cengiz A, Arda HÜ, Döğer F, Yavaşoğlu İ, Yürekli Y, Bolaman AZ. Correlation between baseline 18F-FDG PET/CT findings and CD38- and CD138-expressing myeloma cells in bone marrow and clinical parameters in patients with multiple myeloma. Turk J Haematol. 2018;35:175-180.
12. Kim DS, Yu ES, Kang KW, Lee SR, Park Y, Sung HJ, Choi CW, Kim BS. Myeloma prognostic index at diagnosis might be a prognostic marker in patients newly diagnosed with multiple myeloma. Korean J Intern Med. 2017;32:711-721.
13. Shi L, Qin X, Wang H, Xia Y, Li Y, Chen X, Shang L, Tai YT, Feng X, Acharya P, Acharya C, Xu Y, Deng S, Hao M, Zou D, Zhao Y, Ru K, Qiu L, An G. Elevated neutrophil-to-lymphocyte ratio and monocyte-to-lymphocyte ratio and decreased platelet-to-lymphocyte ratio are associated with poor prognosis in multiple myeloma. Oncotarget. 2017;8: 18792-18801.
14. Dong X, Wang R, Ying X, Xu J, Yan J, Xu P, Peng Y, Chen B. Construction and validation of an ^{18}F-FDG-PET/CT-based prognostic model to predict progression-free survival in newly diagnosed multiple myeloma patients. Hematology. 2024;29:2329029.
15. Liu S, Shi J, Guo H, Xu F, Wei M, Sun K, Chen Y. Prognostic significance of the inflammatory index-based scoring system in patients preliminarily diagnosed with multiple myeloma in the bortezomib-based chemotherapy era. Cancer Manag Res. 2019;11:9409-9420.
16. Zhang L, Chen S, Wang W, Wang Y, Liang Y. Inflammatory and Nutritional Scoring System for Predicting Prognosis in Patients with Newly Diagnosed Multiple Myeloma. J Inflamm Res. 2023;16:7-17.

Original Article

Mol Imaging Radionucl Ther 2025;34:31-37 *DOI:10.4274/mirt.galenos.2024.50470*

Impact of ^{68}Ga-FAPi PET/CT on Staging or Restaging Digestive System Tumors in Patients with Negative or Equivocal ^{18}F-FDG PET/CT Findings

Negatif veya Şüpheli ^{18}F-FDG PET/BT Bulguları olan Digestif Sistem Tümörlü Olguların Evrelenmesi ve Yeniden Evrelenmesinde ^{68}Ga-FAPi PET/BT'nin rolü

Nalan Alan Selçuk[1], Gamze Beydağı[1], Kaan Akçay[1], Emre Demirci[2], Ayşegül Görmez[3], Bala Başak Öven[4], Serkan Çelik[4], Fatma Şen[5], Özge Kapar[6], Levent Kabasakal[7]

[1]*Yeditepe University Faculty of Medicine, Department of Nuclear Medicine, İstanbul, Türkiye*
[2]*University of Missouri Faculty of Medicine, Department of Radiology, Missouri, USA*
[3]*Yeditepe University Faculty of Medicine, Department of Radiology İstanbul, Türkiye*
[4]*Yeditepe University Faculty of Medicine, Department of Medical Oncology, İstanbul, Türkiye*
[5]*Avrasya Hospital, Clinic of Medical Oncology, İstanbul, Türkiye*
[6]*Göztepe Prof. Dr. Süleyman Yalçın City Hospital, Clinic of Pathology, İstanbul, Türkiye*
[7]*İstanbul University-Cerrahpasa, Department of Nuclear Medicine, İstanbul, Türkiye*

Abstract

Objectives: This study aimed to evaluate the potential efficacy of ^{68}Ga-fibroblast activation protein inhibitor (FAPi) positron emission tomography/computed tomography (PET/CT) for detecting, staging, and restaging digestive system malignancies that are ^{18}F-fluorodeoxyglucose (^{18}F-FDG) negative or show equivocal ^{18}F-FDG uptake.

Methods: We conducted a prospective analysis of 30 patients with pathologically confirmed primary tumors or metastases of the digestive system. Participants underwent ^{68}Ga-FAPi PET/CT and ^{18}F-FDG PET/CT imaging for staging or restaging purposes within the same week. The efficacy of ^{68}Ga-FAPi PET/CT was assessed by comparing its ability to detect lesions and influence disease staging with that of ^{18}F-FDG PET/CT.

Results: ^{68}Ga-FAPi PET/CT imaging was performed in 30 patients with ^{18}F-FDG-negative or indeterminate lesions. Of the 30 patients, 23 had gastric cancer and 7 had colorectal cancer. Among all patients, histopathological diagnosis of signet ring cell carcinoma was present in 15 (50%) patients. Primary tumor or local recurrence was detected in 19 (63%) patients, lymph node metastasis in 8 (27%) patients, visceral metastasis in 4 (13%) patients, peritoneal metastasis in 14 (47%) patients, and bone metastasis in 3 (10%) patients on ^{68}Ga-FAPi PET/CT images. All patients underwent histopathological confirmation on ^{68}Ga-FAPi PET/CT images. The disease stage was upgraded in 20 patients (67%) after ^{68}Ga-FAPi PET/CT imaging. Of the 20 patients, 12 had no evidence of recurrence or metastasis on ^{18}F-FDG PET/CT.

Conclusion: Based on our study, ^{68}Ga-FAPi PET/CT alters the disease stage in the majority of gastrointestinal malignancies with negative or equivocal ^{18}F-FDG PET/CT findings. ^{68}Ga-FAPi PET/CT appears to be effective in both staging and restaging of gastrointestinal malignancies, such as signet-ring cell carcinomas of the stomach that frequently show low ^{18}F-FDG -avidity.

Keywords: ^{68}Ga-FAPi PET/CT imaging, tumor microenvironment, gastrointestinal malignancies

Address for Correspondence: Nalan Alan Selçuk, Yeditepe University Faculty of Medicine, Department of Nuclear Medicine, İstanbul, Türkiye
E-mail: nalanselcuk@yahoo.com **ORCID ID:** orcid.org/0000-0002-9216-658X
Received: 02.10.2024 **Accepted:** 23.12.2024 **Publication Date:** 07.02.2025

Cite this article as: Selçuk NA, Beydağı G, Akçay K, Demirci E, Görmez A, Öven BB, Çelik S, Şen F, Kapar Ö, Kabasakal L. Impact of 68Ga-FAPi PET/CT on staging or restaging digestive system tumors in patients with negative or equivocal 18F-FDG PET/CT findings. Mol Imaging Radionucl Ther. 2025;34:31-37.

Öz

Amaç: Bu çalışmanın amacı, ^{18}F-florodeoksiglukoz (^{18}F-FDG) negatif veya şüpheli ^{18}F-FDG tutulumu gösteren digestif sistem malignitelerinin evrelenmesi ve yeniden evrelenmesi için ^{68}Ga-Fibroblast Aktivasyon Proteini İnhibitörü (FAPi) pozitron emisyon tomografisi/bilgisayarlı tomografinin (PET/BT) potansiyel etkinliğini değerlendirmektir.

Yöntem: Çalışma, patolojik olarak doğrulanmış primer tümörleri veya sindirim sistemi metastazları olan 30 hastada prospektif olarak gerçekleştirildi. Hastalara aynı hafta içerisinde evreleme veya yeniden evreleme amacıyla ^{68}Ga-FAPi PET/BT ve ^{18}F-FDG PET/BT görüntülemesi gerçekleştirildi. ^{68}Ga-FAPi PET/BT'nin etkinliği, lezyonları tespit etme yeteneği ve hastalığın evresini değiştirme potansiyeli açısından ^{18}F-FDG PET/BT ile karşılaştırılarak değerlendirildi.

Bulgular: ^{18}F-FDG-negatif veya şüpheli lezyonlara sahip 30 hastada ^{68}Ga-FAPi PET/BT görüntülemesi gerçekleştirildi. Hastaların 23'ü mide, 7'si kolorektal kanser tanısı almıştı. Tüm hastalar arasında, 15 hastada (%50) patolojik tanı olarak taşlı yüzük hücreli karsinom vardı. ^{68}Ga-FAPi PET/BT görüntülerinde, 19 hastada (%63) primer tümör veya lokal nüks, 8 hastada (%27) lenf nodu metastazı, 4 hastada (%13) visseral metastaz, 14 hastada (%47) peritoneal metastaz ve 3 hastada (%10) kemik metastazı tespit edildi. Tüm hastalarda ^{68}Ga-FAPi PET/BT görüntülemesinin ardından en az bir lezyondan histopatolojik doğrulama yapıldı. ^{68}Ga-FAPi PET/BT görüntülemesinden sonra 20 hastanın (%67) hastalık evresi yükseldi. Bu 20 hastanın 12'sinde ^{18}F-FDG PET/BT'de nüks veya metastaz tespit edilmedi ve ^{18}F-FDG PET/BT tamamen negatifti.

Sonuç: Çalışmamıza göre, ^{68}Ga-FAPi PET/BT, negatif veya şüpheli ^{18}F-FDG PET/BT bulguları olan digestif sistem malignitelerde hastalığın evresini önemli oranda değiştirmektedir. ^{68}Ga-FAPi PET/BT, özellikle mide taşlı yüzük hücreli karsinomları gibi düşük ^{18}F-FDG-afinitesi gösteren digestif sistem malignitelerin evreleme ve yeniden evrelemesinde etkili görünmektedir.

Anahtar kelimeler: ^{68}Ga-FAPi PET/BT görüntüleme, tumor mikroçevre, gastrointestinal malignancies, digestif sistem tümörleri

Introduction

The World Health Organization (WHO) reclassified digestive system tumors in 2020 and emphasized the importance of molecular pathology in clinical practice (1). According to the WHO, approximately 5 million new cases and 3.6 million deaths from digestive system cancers will occur worldwide in 2020, and the incidence of various types of digestive system cancers is gradually increasing (2,3). Most cancers of the digestive tract have a poor prognosis and differ in clinical presentation because of the involvement of multiple organs (4,5). Therefore, early diagnosis and accurate evaluation are of great clinical importance in the treatment of these tumors.

Malignancies in the digestive system are investigated using standard imaging techniques, such as biomarkers, ultrasound, and endoscopic procedures (6,7). However, these techniques have numerous drawbacks, including the inability to accurately determine the stage and metastasis of cancers of the digestive system. ^{18}F-FDG positron emission tomography/computed tomography (PET/CT) is currently used as a standard imaging method in the clinical applications of oncology, for preoperative systemic evaluation, and for determining tumor stage. However, it may be inadequate for imaging certain types of cancer, such as signet-ring cell cancers, mucinous-serous adenocarcinomas, and peritoneal tumors, which have low glucose metabolism (8,9,10). Another important factor affecting the sensitivity to ^{18}F-FDG PET/CT is the size of the tumor (11). In addition, the physiological uptake of ^{18}F-FDG through the gastrointestinal tract may lead to false-positive results, limiting the use of ^{18}F-FDG-PET/CT (12). Therefore, the search for new tumor diagnostic methods has always been an important issue.

PET/CT imaging methods based on fibroblast activation protein (FAP) expressed by cancer-associated fibroblasts (CAFs) in cancer tissues have recently been developed. FAP was first demonstrated in malignant sarcoma cells in 1988 (13). FAP is a type 2 transmembrane serine protease consisting of 760 amino acids with endopeptidase and dipeptidyl peptidase activities (14). It is expressed on the surface of CAFs, which are also found in many tumor tissues. The current FAP inhibitors (FAPi) are peptidomimetic quinoline derivatives that bind to FAP with high affinity and can be used for PET imaging by binding to the ^{68}Ga (15).

CAFs differ from other fibroblasts in that they express higher levels of FAP in the tumor microenvironment. Therefore, FAP is expressed at a very low level in healthy tissues, which allows ^{68}Ga-FAPi PET/CT to provide low background uptake. The low background uptake of ^{68}Ga-FAPi PET/CT provides technical advantages, such as higher tumor detection sensitivity. The requirement for supportive stroma in tumor tissue larger than 1-2 mm in size and the fact that the stromal volume is higher than the cancer cell volume provide an advantage for ^{68}Ga-FAPi PET/CT (16).

Studies comparing ^{18}F-FDG PET/CT with ^{68}Ga-FAPi PET/CT have demonstrated the contribution of ^{68}Ga-FAPi PET/CT in the staging of digestive system tumors (17). However, there is limited information on the success of ^{68}Ga-FAPi PET/CT in ^{18}F-FDG-negative patients. The aim of this study was to detect ^{18}F-FDG-negative or equivocal ^{18}F-F-FDG lesions using ^{68}Ga-FAPi PET/CT and to evaluate the contribution of ^{68}Ga-FAPi PET/CT to the clinical staging or restaging of digestive tumors.

Materials and methods

Patients

This single-center prospective clinical trial was conducted between September 2020 and March 2024, a total of 30 patients with digestive tumors enrolled for ^{18}F-FDG PET/CT with the indication of staging or restaging who met the following inclusion criteria were offered a ^{68}Ga-FAPi PET/CT: (a) low ^{18}F-F-FDG affinity in the metastasis sites of tumor on ^{18}F-FDG PET/CT; (b) an elevation in tumor markers without any focal findings on ^{18}F-FDG PET/CT; (c) presence of an indeterminate finding on ^{18}F-FDG PET/CT; (d) the presence of a lesion in the CT component of ^{18}F-FDG PET/CT that does not exhibit ^{18}F-FDG avidity; (e) patients with stage 1-3 disease diagnosed on ^{18}F-FDG PET/CT. The term indeterminate finding was assigned to areas exhibiting uptake indistinguishable from the background that could not be identified as abnormal.

The exclusion criteria were as follows: (a) aged 18 years; (b) having two or more primary diseases; (c) patients identified as stage 4 on ^{18}F-FDG -PET/CT; (d) pregnant or suspected of being pregnant; (e) inability to remain still during the scan (20-30 minutes).

Informed consent was obtained from all patients. This prospective study was approved by the Yeditepe University Clinical Research Ethics Committee (decision no: 1576, date: 02.03.2022).

Preparation and Quality Control of ^{68}Ga-FAPi

^{68}Ga-DOTA-FAPi-04 was prepared using a modular-based fully automated synthesizer (GRP V4, Scintomics GmbH, Germany). Briefly, the ^{68}Ga obtained from the ^{68}Ge/^{68}Ga generator (iThemba LABS) was sent to the reaction vial containing DOTA-FAPi-04. After completion of the labeling process, the reaction solution was purified with an extraction cartridge and subjected to sterile filtration to prepare the final patient dose. The total synthesis time was 20-25 minutes. The radiochemical purity and radiolabeling efficiency ^{68}Ga-FAPi were determined by combining a radioactive detector with reversed-phase high-pressure liquid chromatography (retinitis pigmentosa-high-performance liquid chromatography). ^{68}Ga-FAPi with a radiochemical purity of ≥ 95% was administered to patients.

^{68}Ga-FAPi and ^{18}F-FDG PET/CT Imaging

Whole-body imaging of ^{68}Ga-FAPi and ^{18}F-FDG PET/CT was performed using a PET scanner (Discovery PET/CT 710, General Electric Medical Systems, Milwaukee, WI, USA) with integrated 64-slice CT, high resolution, time-of-flight function, and LYSO crystal. After intravenous injection of radiopharmaceuticals with an average activity of 240±60 MBq (range: 122-312 MBq), patients were fixed supine on the bed of the PET scanner 60 minutes after injection. CT and PET images were acquired from the vertex region to mid-thigh. ^{68}Ga-FAPi PET/CT was performed within 7 days after ^{18}F-FDG PET/CT.

Evaluation of ^{68}Ga-FAPİ PET/CT and ^{18}F-FDG PET/CT Images

Activity uptake in the tumor was measured by maximum standard uptake value (SUV_{max}) using circular regions of interest drawn around the lesions with focal uptake in transaxial slices and automatically adapted to a 3D voxel area within the 60% iso-contour. All images were reviewed by three senior nuclear medicine physicians who reached consensus for confirmation.

Statistical Analysis

Statistical analysis were performed using SPSS software (version 25.0; IBM Inc.). Descriptive analyses were conducted to assess the characteristics of the patients and their tumors. The mean and standard deviation were calculated for normally distributed measurements, and the median and range were calculated for non-normal measurements. Diagnostic parameters were calculated using a simple matrix method. Using the sample size, 95% Confidence Intervals were also calculated. Pearson's chi-square test was used to compare ^{68}Ga-FAPi PET/CT and ^{18}F-FDG PET/CT. McNemar's test was used to evaluate the staging accuracy of ^{68}Ga-FAPi PET/CT and ^{18}F-FDG PET/CT. A P-value of less than 0.05 was considered statistically significant.

Results

A total of 30 patients were included in the study. Of all patient group for 14 (47%) patients, ^{68}Ga-FAPi PET/CT was performed for restaging because of suspected progressive disease, whereas the 16 (53%) patients with new diagnoses underwent PET imaging for primary staging. The mean age of the patients was 52.7±12.0 (range: 35-77 years). Of the 30 patients, 23 had gastric (77%), and 7 had colorectal (23%). Among all patients, histopathological diagnosis of signet ring cell carcinoma was present in 15 (50%) patients. The demographic characteristics of patients are presented in Table 1.

In half of the patients (n=15), ^{18}F-FDG PET/CT findings were completely negative, while others had equivocal findings. ^{68}Ga-FAPi PET/CT was performed in these patients due to suspicion of potential oversight in staging and evaluation, prompted by clinical progression and/or elevated tumor markers, such as CA 19-9 and CEA. Primary tumor or local

Table 1. Patient characteristics (n=30)	
Characteristic	**Value**
Age, mean ± SD	52.7±12.0
Gender, % (n)	
Female	57% (17)
Male	43% (13)
Primary tumor sites, % (n)	
Gastric	77% (23)
Signet-ring cell	47% (14)
Colorectal	23% (7)
Signet-ring cell	3% (1)
Metastasis sites on ^{68}Ga-FAPi PET/CT, % (n)	
Primary location/local recurrence	63% (19)
Lymph node	27% (8)
Visceral metastasis	13% (4)
Peritoneal metastasis	47% (14)
Bone	10% (3)
Metastasis sites on ^{18}F-FDG PET/CT, % (n)	
Primary location/local recurrence	43% (13)
Lymph node	10% (3)
Visceral metastasis	-
Peritoneal metastasis	-
Bone	-
Indication for imaging, % (n)	
Staging	53% (16)
Restaging	47% (14)

SD: Standard deviation, PET/CT: Positron emission tomography/computed tomography

recurrence was detected in 19 (63%) patients, lymph node metastasis in 8 (27%) patients, visceral metastasis in 4 (13%) patients, peritoneal metastasis in 14 (47%) patients, and bone metastasis in 3 (10%) patients on ^{68}Ga-FAPi PET/CT images. For ^{18}F-FDG PET/CT, primary tumor or local recurrence was detected in 13 (43%) patients and lymph node metastasis in 3 (10%) patients. Otherwise, visceral, peritoneal, and bone metastases could not be detected on ^{18}F-FDG PET/CT (Table 1). ^{68}Ga-FAPi PET/CT demonstrated a higher detection rate for primary lesions at 96%, compared to 71% with ^{18}F-FDG PET/CT.

At least one lesion in all patients was confirmed histopathologically after ^{68}Ga-FAPi PET/CT imaging. In one patient, although peritoneal fluid sampling was negative, ^{68}Ga-FAPi PET/CT revealed signs consistent with peritoneal carcinomatosis. Since the findings of peritoneal carcinomatosis were confirmed radiologically in the patient's subsequent follow-up visits, clinical follow-up confirmed that the cytology result was false negative. In one patient, despite the presence of a primary tumor on CT and/or magnetic resonance imaging (MRI), both ^{68}Ga-FAPi and ^{18}F-FDG PET/CT findings were negative.

Although no findings were detected in 15 patients on ^{18}F-FDG PET/CT, ^{68}Ga-FAPi PET/CT identified 2 patients (7%) as stage 2, 1 patient (3%) as stage 3, and 9 patients (30%) as stage 4 (Table 2). While there was clinical suspicion in 2 patients, no evidence of recurrence or metastasis was found in ^{18}F-FDG and ^{68}Ga-FAPi PET/CT as well as CT and/or MRI. A patient diagnosed with signet ring cell carcinoma of the stomach who presented for staging showed false-negative results on both ^{18}F-FDG and ^{68}Ga-FAPi PET/CT. We found that 12 of 15 patients with negative ^{18}F-FDG PET/CT

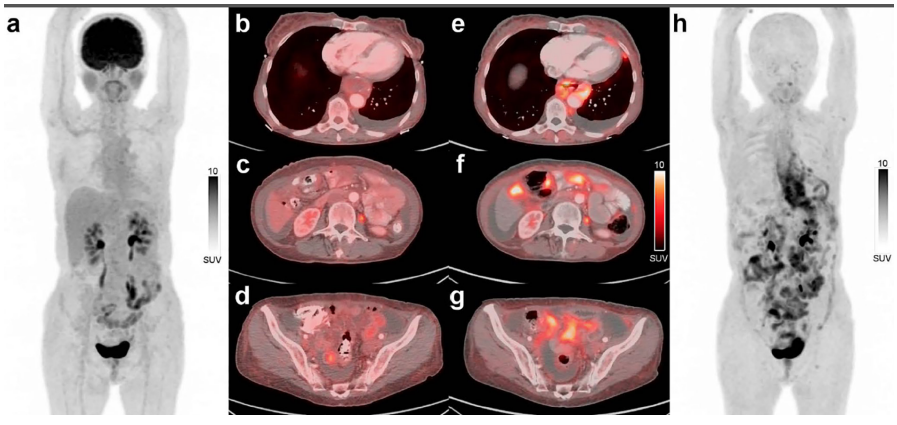

Figure 1. A 63-year-old female patient was diagnosed with gastric adenocarcinoma. Subsequent abdominal magnetic resonance imaging revealed an increase in peritoneal effusion. ^{18}F-FDG-PET/CT did not reveal any malignant lesions that would explain the effusion (a-d). In contrast, the ^{68}Ga-FAPi PET/CT scan revealed widespread peritoneal metastases. These findings observed on the ^{68}Ga -FAPi PET/CT scan (e-h) were later confirmed by histopathologic examination.

PET/CT: Positron emission tomography/computed tomography, SUV: Standard uptake value, FAPİ: Fibroblast activation protein inhibitor

results (80%) experienced an increase in disease stage after undergoing ^{68}Ga-FAPi PET/CT. Additionally, 8 of 15 patients with initially staged 1-3 on ^{18}F-FDG PET/CT (53%) showed an elevation in their primary disease stage when assessed with ^{68}GaFAPi PET/CT. Notably, a discrepancy in staging between ^{68}Ga-FAPi and ^{18}F-FDG PET/CT was observed in 67% of patients, leading to significant alterations in their oncologic treatment plans (Table 2). Our findings indicate that staging with ^{68}Ga-FAPi PET/CT is statistically more effective than ^{18}F-FDG PET/CT (Pearson chi-square value of 27.18; p=0.007).

The mean SUV_{max} values of the primary tumors in gastric and colorectal cancer were 14.8±5.8 (range: 5.5-21.8) and 9.5±4.2 (range: 5.3-13.6), respectively. Notably, all peritoneal metastases were negative on ^{18}F-FDG PET/CT, whereas they exhibited significant uptake on ^{68}Ga-FAPi PET/CT, with a mean SUV_{max} value of 10.5±4.9 (range: 3.6-21.8) (Figure 2).

A histopathological diagnosis of signet ring cell cancer was made in 15 patients (50%). Among these, 14 patients (47%) had gastric signet ring cell cancer, and 1 patient (3%) had colonic signet ring cell malignancy (Table 1). In patients with signet ring cell cancer, 45% of primary lesions (5/11) and 80% of lymph node metastases (4/5) were negative on ^{18}F-FDG PET/CT, whereas all these lesions demonstrated increased uptake on ^{68}Ga-FAPi PET/CT. Additionally, peritoneal metastases were identified in 4 patients using ^{68}Ga-FAPi PET/CT, whereas these lesions were negative on ^{18}F-FDG PET/CT. The mean SUV_{max} for primary lesions was 13.4±5.2 (range: 5.5-17.0) on ^{68}Ga-FAPi PET/CT and 6.8±2.1 (range: 3.8-10.1) on ^{18}F-FDG PET/CT. For peritoneal metastases, the mean SUV_{max} on ^{68}Ga-FAPi PET/CT was 10.6±3.6 (range: 5.9-14.5) (Figure 2).

Discussion

In this study, ^{18}F-FDG-positive cases were excluded because they were already well documented. Our study highlights the diagnostic superiority of ^{68}Ga-FAPi PET/CT over ^{18}F-FDG PET/CT in staging digestive system malignancies, particularly when ^{18}F-FDG PET/CT results are equivocal or negative. The pivotal role of ^{68}Ga-FAPi PET/CT is attributed to its targeted imaging of CAFs, which are prominently expressed in the stromal components of gastrointestinal tumors. This expression pattern significantly enhances tumor detection sensitivity, highlighting the critical role of stromal involvement in gastrointestinal cancer pathology.

^{18}F-FDG PET/CT and CT demonstrate suboptimal lesion detectability, primarily due to the mucinous types of gastric cancer and signet ring cell carcinoma, which constitute the majority of cases in this study and typically manifest as small, diffusely growing patterns characterized by a scarcity of tumor cells (12). Some lesions exhibit low expression of tumor glucose transporters but high levels of dephosphorylation, resulting in lessened accumulation of ^{18}F-FDG PET/CT (18,19). Furthermore, in contrast to the relatively high physiological uptake of ^{18}F-FDG PET/CT in the gastrointestinal tract, the low background uptake of ^{68}Ga-FAPi PET/CT in the abdominopelvic cavity contributes to the superior performance of ^{68}Ga-FAPi PET/CT (20,21).

As with the clinical presentation of gastrointestinal cancers, imaging characteristics and workflows can exhibit substantial variability, resulting in unequal diagnostic efficacy among different imaging modalities (22). The findings of this study indicate that ^{68}Ga-FAPi PET/CT holds considerable promise for detecting disease extent in gastrointestinal cancer, a conclusion that is consistent with other published reports (23,24,25). Many other studies have shown that ^{68}Ga-FAPi PET/CT is superior to other modalities, such as MRI, CT, and ^{18}F-FDG PET/CT, in digestive tract malignancies. However, very few studies have investigated the effect of ^{68}Ga-FAPi PET/CT. The current study is one of the few studies that emphasizes stage changes after ^{68}Ga-FAPi PET/CT performed for staging or restaging of gastrointestinal tumors correlated with biopsy. The results demonstrated that ^{68}Ga-FAPi PET/CT changed disease staging in approximately 67% of cases with ^{18}F-FDG-negative or equivocal lesions. This is a significant finding for accurate staging and the application of correct treatment algorithms.

In our study, all patients had histopathological confirmation after ^{68}Ga-FAPi PET/CT images. ^{68}Ga-FAPi PET/CT findings of one patient were compatible with peritoneal carcinomatosis, although the peritoneal fluid sample was negative. However, on clinical radiological follow-up, these

Table 2. Stage changes according to both ^{18}F-FDG PET/CT and ^{68}Ga-FAPi PET/CT

Staging/re-staging (n=30)	Negative	Stage 1	Stage 2	Stage 3	Stage 4	Equal	Upstage
Staging with ^{18}F-FDG-PET/CT	15 (50%)	5 (17%)	7 (23%)	3 (10%)	-	10 (33%)	-
Staging with ^{68}Ga-FAPi PET/CT	3 (10%)*	3 (10%)	4 (13%)	5 (17%)	15 (50%)	10 (33%)	20 (67%)

*A patient diagnosed with signet ring cell carcinoma of the stomach who presented for staging showed false-negative results on both [^{18}F]FDG PET/CT and ^{68}Ga-FAPi PET/CT. In the other two patients who had negative ^{68}Ga-FAPi PET/CT results, no lesions consistent with malignancy were detected by other radiological methods or during follow-up, indicating true negative resultsPET/CT: Positron emission tomography/computed tomography, FAPi: Fibroblast activation protein inhibitor

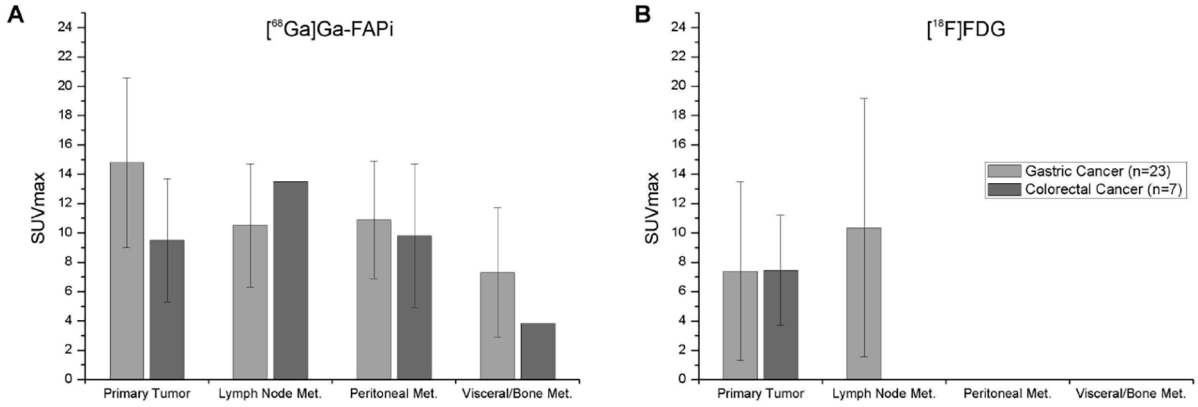

Figure 2. SUV_{max} values from ^{68}Ga-FAPi PET/CT and ^{18}F-FDG PET/CT, categorized by primary malignancy diagnosis and metastasis location, are presented
SUV_{max}: Maximum standard uptake value, PET/CT: Positron emission tomography/computed tomography

findings confirmed that the pathology result was false negative. In another patient, despite the presence of a tumor, the ^{68}Ga-FAPi and ^{18}F-FDG PET/CT findings were negative.

^{68}Ga-FAPi PET/CT showed more peritoneal implants and lymph node metastases than ^{18}F-FDG PET/CT, which led to upstaging based on the tumor-node-metastasis system. In addition, ^{68}Ga-FAPi PET/CT detected more primary lesions than ^{18}F-FDG PET/CT in individuals diagnosed with digestive system malignancy, with detection rates of 96% and 71%, respectively. These results are consistent with literature (17,21). Recent research has also highlighted the promising potential of ^{68}Ga-FAPi PET/CT in guiding the clinical management of pancreatic and gastric cancer (26,27). Koerber et al. (25) have shown that ^{68}Ga-FAPi PET/CT resulted in changes in treatment classified as high, intermediate, and low in 19%, 33%, and 29% of patients, respectively. In our study, we observed that 80% (12/15) of patients with no detectable uptake in the primary tumor and/or metastasis sites on ^{18}F-FDG PET/CT showed increased uptake on ^{68}Ga-FAPi PET/CT. In addition, we demonstrated that of the patients identified by ^{18}F-FDG PET/CT at any stage (stage 1, 2, 3), 53% showed an increase in the primary disease stage when examined by ^{68}Ga-FAPi PET/CT. In summary, 67% of patients showed a difference in staging between ^{68}Ga-FAPi PET/CT and ^{18}F-FDG PET/CT, leading to significant changes in their oncologic treatment strategies.

In agreement with the literature, we found a higher SUV_{max} on ^{68}Ga-FAPi PET/CT than on ^{18}F-FDG PET/CT in primary tumors (17). However, it is worth noting that we did not include patients with high ^{18}F-FDG uptake in our study. The lesions of the patients in our study had either no ^{18}F-FDG uptake or very low uptake outside the primary lesion, which could not be distinguished from the background. Therefore, our patients were expected to have a higher SUV_{max} on ^{68}Ga-FAPi PET/CT. In our study, higher uptake was observed in primary lesions of gastric cancer (SUV_{max}: 14.8) than in colorectal cancer (SUV_{max}: 9.5) on ^{68}Ga-FAPi PET/CT.

The role of ^{18}F-FDG-PET/CT in signet ring cell carcinoma is of limited diagnostic value in terms of both primary lesions and metastases. Peritoneal metastases are often overlooked in ^{18}F-FDG PET/CT. This is because these tumors are mucin-rich, do not consume glucose, and express low levels of glucose transporters (28,29). In addition, the peritoneal implants are usually small and can be missed even with diagnostic tools such as CT and/or MRI. In this context, previous studies have shown that ^{68}Ga-FAPi PET/CT is extremely sensitive in signet ring cell carcinomas (30,31). In our study, 45% of primary lesions (5/11) and 80% of lymph node metastases (4/5) of patients with signet ring cell carcinoma were negative on ^{18}F-FDG PET/CT. Of these patients, 4 had peritoneal metastasis, which could not be detected by ^{18}F-FDG PET/CT. The average SUV_{max} was 13.4 for the primary tumor and 10.6 for the peritoneal metastasis.

Conclusion

In conclusion, ^{68}Ga-FAPi PET/CT is superior for staging and restaging indications in digestive system tumors, especially in patients with ^{18}F-FDG-negative or equivocal lesions, such as signet ring cell carcinoma. The strength of our study lies in its ability to stage cases in which ^{18}F-FDG PET/CT fails to resolve using ^{68}Ga-FAPi PET/CT and in corroborating these findings with biopsy results in all patients. The ^{68}Ga-FAPi

PET/CT modality is a promising imaging modality for the diagnosis and management of FDG-negative GI tumors. The use of this method has the potential to introduce new applications for tumor staging or restaging. Future studies should explore the longitudinal impact of ^{68}Ga-FAPi PET/CT-guided treatment decisions on patient outcomes, potentially establishing this modality as a standard component of gastrointestinal cancer management protocols.

Ethics

Ethics Committee Approval: This prospective study was approved by the Yeditepe University Clinical Research Ethics Committee (decision no: 1576, date: 02.03.2022).

Informed Consent: Informed consent was obtained from all patients.

Footnotes

Authorship Contributions

Surgical and Medical Practices: A.G., S.Ç., F.Ş., Ö.K., Concept: N.A.S., L.K., Design: N.A.S., E.D., L.K., Data Collection or Processing: N.A.S., G.B., Analysis or Interpretation: N.A.S., G.B., K.A., Literature Search: N.A.S., Writing: N.A.S., G.B., K.A., E.D., L.K.

Conflict of Interest: No conflict of interest was declared by the authors.

Financial Disclosure: The authors declared that this study has received no financial support.

References

1. Nagtegaal ID, Odze RD, Klimstra D, et al. The 2019 WHO classification of tumours of the digestive system. Histopathology. 2020;76:182-8.
2. Sung H, Ferlay J, Siegel RL, et al. Global cancer statistics 2020: GLOBOCAN estimates of incidence and mortality worldwide for 36 cancers in 185 countries. CA Cancer J Clin. 2021;71:209-249.
3. Bray F, Ferlay J, Soerjomataram I, et al. Global cancer statistics 2018: GLOBOCAN estimates of incidence and mortality worldwide for 36 cancers in 185 countries. CA Cancer J Clin. 2018;68:394-424.
4. Arjmand MH, Moradi A, Rahimi HR, et al. Prognostic value of HIF-1α in digestive system malignancies: evidence from a systematic review and meta-analysis. Gastroenterol Hepatol Bed Bench. 2022;15:108-19.
5. Peng D, He J, Liu H, et al. FAPI PET/CT research progress in digestive system tumours. Dig Liver Dis. 2022;54:164-9.
6. Bergholt MS, Zheng W, Lin K, et al. In vivo diagnosis of gastric cancer using Raman endoscopy and ant colony optimization techniques. Int J Cancer. 2011;128:2673-80.
7. Xue H, Ge HY, Miao LY, et al. Differential diagnosis of gastric cancer and gastritis: the role of contrast-enhanced ultrasound (CEUS). Abdom Radiol (NY). 2017;42:802-9.
8. Berger KL, Nicholson SA, Dehdashti F, et al. FDG PET evaluation of mucinous neoplasms: correlation of FDG uptake with histopathologic features. AJR Am J Roentgenol. 2000;174:1005-8.
9. Jayaprakasam VS, Paroder V, Schöder H. Variants and pitfalls in PET/CT imaging of gastrointestinal cancers. Semin Nucl Med. 2021;51:485-501.
10. Chandekar KR, Prashanth A, Vinjamuri S, et al. FAPI PET/CT imaging-an updated review. Diagnostics (Basel). 2023;13:2018.
11. Mukai K, Ishida Y, Okajima K, et al. Usefulness of preoperative FDG-PET for detection of gastric cancer. Gastric Cancer. 2006;9:192-6.
12. Yun M. Imaging of gastric cancer metabolism using 18 F-FDG PET/CT. J Gastric Cancer. 2014;14:1-6.
13. Rettig WJ, Garin-Chesa P, Beresford HR, et al. Cell-surface glycoproteins of human sarcomas: differential expression in normal and malignant tissues and cultured cells. Proc Natl Acad Sci U S A. 1988;85:3110-4.
14. Scanlan MJ, Raj BK, Calvo B, et al. Molecular cloning of fibroblast activation protein alpha, a member of the serine protease family selectively expressed in stromal fibroblasts of epithelial cancers. Proc Natl Acad Sci U S A. 1994 ;91:5657-61.
15. Calais J, Mona CE. Will FAPI PET/CT replace FDG PET/CT in the next decade? point-an important diagnostic, phenotypic, and biomarker role. AJR Am J Roentgenol. 2021;216:305-6.
16. Guo W, Pang Y, Yao L, et al. Imaging fibroblast activation protein in liver cancer: a single-center post hoc retrospective analysis to compare [68Ga]Ga-FAPI-04 PET/CT versus MRI and [18F]-FDG PET/CT. Eur J Nucl Med Mol Imaging. 2021;48:1604-17.
17. Liu X, Liu H, Gao C, et al. Comparison of 68Ga-FAPI and 18F-FDG PET/CT for the diagnosis of primary and metastatic lesions in abdominal and pelvic malignancies: a systematic review and meta-analysis. Front Oncol. 2023;13:1093861.
18. Hofman MS, Hicks RJ. How we read oncologic FDG PET/CT. Cancer Imaging. 2016;16:35.
19. Flavell RR, Naeger DM, Aparici CM, et al. Malignancies with low fluorodeoxyglucose uptake at pet/ct: pitfalls and prognostic importance: resident and fellow education feature. Radiographics. 2016;36:293-4.
20. Blake MA, Singh A, Setty BN, et al. Pearls and pitfalls in interpretation of abdominal and pelvic PET-CT. Radiographics. 2006;26:1335-53.
21. Chen H, Pang Y, Wu J, et al. Comparison of [68Ga]Ga-DOTA-FAPI-04 and [18F] FDG PET/CT for the diagnosis of primary and metastatic lesions in patients with various types of cancer. Eur J Nucl Med Mol Imaging. 2020;47:1820-32.
22. Bentley-Hibbert S, Schwartz L. Use of imaging for GI cancers. J Clin Oncol. 2015;33:1729-36.
23. Pang Y, Zhao L, Luo Z, et al. Comparison of 68Ga-FAPI and 18F-FDG Uptake in Gastric, Duodenal, and Colorectal Cancers. Radiology. 2021;298:393-402.
24. Guo W, Chen H. 68Ga FAPI PET/CT imaging in peritoneal carcinomatosis. Radiology. 2020;297:521.
25. Koerber SA, Staudinger F, Kratochwil C, et al. The role of 68Ga-FAPI PET/CT for patients with malignancies of the lower gastrointestinal tract: first clinical experience. J Nucl Med. 2020;61:1331-36.
26. Röhrich M, Naumann P, Giesel FL, et al. Impact of 68Ga-FAPI PET/CT imaging on the therapeutic management of primary and recurrent pancreatic ductal adenocarcinomas. J Nucl Med. 2021;62:779-86.
27. Kuten J, Levine C, Shamni O, et al. Head-to-head comparison of [68Ga]Ga-FAPI-04 and [18F]-FDG PET/CT in evaluating the extent of disease in gastric adenocarcinoma. Eur J Nucl Med Mol Imaging. 2022;49:743-50.
28. Mochiki E, Kuwano H, Katoh H, et al. Evaluation of 18F-2-deoxy-2-fluoro-D-glucose positron emission tomography for gastric cancer. World J Surg. 2004;28:247-53.
29. Kawamura T, Kusakabe T, Sugino T, et al. Expression of glucose transporter-1 in human gastric carcinoma: association with tumor aggressiveness, metastasis, and patient survival. Cancer. 2001;92:634-41.
30. Lin R, Lin Z, Chen Z, et al. [68Ga]Ga-DOTA-FAPI-04 PET/CT in the evaluation of gastric cancer: comparison with [18F]FDG PET/CT. Eur J Nucl Med Mol Imaging. 2022;49:2960-71.
31. Alan-Selçuk N, Ergen S, Demirci E, et al. [68Ga]DOTA-FAPI-04 PET/CT imaging in a case of a signet ring cell carcinoma of stomach. Eur J Nucl Med Mol Imaging. 2021;48:4523-4.

Original Article

Mol Imaging Radionucl Ther 2025;34:38-47 *DOI:10.4274/mirt.galenos.2024.21548*

Quality of Life Outcomes Following Radioactive Iodine 131 Therapy in Hyperthyroid Patients: Insights from the Thyroid Patient-Reported Outcome Questionnaire

Hipertiroidi Hastalarında Radyoaktif İyot 131 Tedavisinden Sonra Yaşam Kalitesi Sonuçları: Tiroid Hastası Tarafından Bildirilen Sonuç Anketinden Bakış

Hamdi Afşin, Billur Çalışkan

Bolu Abant Izzet Baysal University Faculty of Medicine, Department of Nuclear Medicine, Bolu, Türkiye

Abstract

Objectives: This study aimed to evaluate the impact of Radioactive iodine 131 (RAI 131) therapy on the quality of life (QoL) of patients with hyperthyroidism using the Thyroid Patient-Reported Outcome (ThyPRO) questionnaire and to quantify the extent of these improvements.

Methods: This two-year, prospective, single-center study was conducted at the University Medical Faculty Hospital. Eighty-four patients (39 males and 45 females) diagnosed with hyperthyroidism due to Graves' disease, toxic multinodular goiter, or toxic adenoma received RAI 131 therapy at doses of 10, 15, 20, or 30 mCi. The ThyPRO questionnaire, consisting of 84 questions across 12 domains, was administered before treatment and six months post-treatment to assess QoL. The primary outcome was the change in ThyPRO scores.

Results: Significant improvements in all post-treatment QoL measures were observed in both males and females ($p<0.001$). The average age of the patients was 58.33±12.45 years. QoL improvements were consistent across all age groups (<50, 50-60, >60 years) and at all levels of hyperthyroidism severity (mild, moderate, and severe). All RAI 131 dose groups (10, 15, 20, and 30mCi) showed significant improvements in QoL, with no significant differences between dose groups. The correlation analysis revealed that age had a weak negative correlation with QoL improvement ($r=-0.20$, $p=0.05$), whereas thyroid hormone levels were significantly correlated with QoL improvement. Multiple regression analysis identified initial ThyPRO score and age as significant predictors of QoL improvement, whereas sex and RAI 131 dose were not significant predictors.

Conclusion: RAI therapy significantly enhanced the QoL of hyperthyroid patients according to demographic and disease severity. These findings support the use of RAI 131 as a primary treatment for hyperthyroidism, highlighting the importance of personalized treatment approaches for optimizing patient outcomes. Future research should focus on long-term QoL outcomes and refine therapeutic strategies.

Keywords: Radioactive iodine 131, hyperthyroidism, quality of life, ThyPRO, thyroid hormone, RAI therapy, QoL improvement, hyperthyroid treatment

Öz

Amaç: Bu çalışmada Tiroid-Hastası-Tarafından-Bildirilen-Sonuç-Anketini (ThyPRO) kullanarak hipertiroidisi olan hastaların yaşam kalitesi üzerine Radyoaktif İyot 131 (RAİ 131) tedavisinin etkisinin değerlendirilmesive bu iyileşmelerin seviyesinin ölçülmesi amaçlanmıştır.

Yöntem: Bu iki yıllık, tek merkezli çalışma tıp fakültesi hastanesinde yapıldı. Toksik adenom, toksik multinodüler guatr ve Graves hastalığı nedeniyle hipertiroridi tanısı alan toplamda 84 hasta (39 erkek ve 45 kadın) 10, 15, 20 ve 30 mCi dozlarında RAİ 131 tedavisi aldı. On iki alanda toplam 84

Address for Correspondence: Hamdi Afşin, Bolu Abant Izzet Baysal University Faculty of Medicine, Department of Nuclear Medicine, Bolu, Türkiye
E-mail: hamdiafsin@hotmail.com **ORCID ID:** orcid.org/0000-0003-1010-3073
Received: 04.07.2024 **Accepted:** 24.11.2024 **Publication Date:** 07.02.2025

Cite this article as: Afşin H, Çalışkan B. Quality of life outcomes following radioactive iodine 131 therapy in hyperthyroid patients: insights from the thyroid patient-reported outcome questionnaire. Mol Imaging Radionucl Ther. 2025;34:38-47.

sorudan oluşan ThyPRO anketi yaşam kalitesini değerlendirmek için tedaviden önce ve tedaviden altı ay sonra uygulandı. Başlıca sonuçlar ThyPRO puanlarındaki değişiklikti.

Bulgular: Hem erkeklerde hem de kadınlarda tüm tedavi sonrası QoL ölçümlerinde anlamlı iyileşmeler gözlendi (p<0,001). Hastaların ortalama yaşı 58,33±12,45 idi. QoL iyileşmeleri tüm yaş gruplarında (<50, 50-60, >60 yaş) ve hipertiroidinin tüm şiddet düzeylerinde (hafif, orta, şiddetli) uyumluydu. Doz grupları arasında anlamlı farklılık olmasada, tüm RAİ 131 doz grupları (10, 15, 20 ve 30 mCi) QoL'de anlamlı iyileşme gösterdi. Korelasyon analizinde yaş QoL iyileşmesi ile zayıf negative korelasyon saptanmışken (r=-0,20, p=0,05) tiroid hormon düzeyleri anlamlı korelasyon saptandı. Multiple regresyon analizi başlangıç ThyPRO puanları ve yaş QoL iyileşmesinin önemli prediktörleri iken cinsiyet ve RAİ 131 dozları önemli prediktör değildi.

Sonuç: RAİ 131 tedavisi çeşitli demografik gruplarda, hastalık şiddetinde ve iyot doz düzeylerinde hipertiroidili hastaların yaşam kalitesini anlamlı olarak artırdı. Bu bulgular en optimum hasta sonuçları için kişiselleştirilmiş tedavinin önemini ışık tutan hipertiroidinin primer tedavisi olarak RAİ 131'in kullanımını destekler. Gelecek araştırmalar uzun dönem yaşam kalitesine ve tedavi stratejilerinin inceliklerine odaklanmalıdır.

Anahtar kelimeler: Radyoaktif iyot 131, hipertiroidizm, yaşam kalitesi, ThyPRO, tiroid hormonu, RAİ tedavisi, yaşam kalitesi iyileşmesi, hipertiroidi tedavisi

Introduction

Hyperthyroidism is characterized by excessive synthesis and secretion of thyroid hormones. Approximately 1% of the population is estimated to be affected by this condition. Graves' disease, toxic multinodular goiter (MNG), and toxic adenoma are common causes of hyperthyroidism. Uncontrolled hyperthyroidism can lead to accelerated tissue metabolism, which can affect various organs, such as the cardiovascular, neurological, gastrointestinal, neuropsychological, and ocular systems, thereby deteriorating quality of life (QoL) (1). Hyperthyroidism can also lead to anxiety and depression, resulting in the loss of productivity. Radioactive iodine 131 (RAI 131) is widely used to reduce thyroid function and excessive thyroid hormone production. It is considered safe and effective for patients with Graves' disease, toxic MNG, or toxic adenoma. Measuring improvements in QoL after treatment is important because hyperthyroidism can have a significant impact on multiple organ systems (2,3).

In the last century, medicine has focused primarily on understanding the causes of various diseases. However, in recent decades, interest in patients' physical and mental well-being. The concept of "QoL" was introduced by Elkinton in 1966 in his editorial "Medicine and the QoL," building on Francis Bacon's idea of harmony in the human body, which was the domain of medicine. Medical care has begun to consider patient perspectives (4,5). Health-related QoL involves assessing the impact of disease and treatment on various aspects of functioning and well-being, including physical, psychological, social, and somatic aspects. Patients with chronic diseases experience not only physical suffering but also emotional distress and decreased QoL. Therefore, therapeutic interventions for chronic diseases should aim to keep patients symptom-free for as long as possible and restore their QoL. The concept of QoL is crucial in various health conditions because it evaluates the effects of diseases and treatments on physical, psychological, social, and functional well-being. The disability paradox, in which individuals report good QoL despite serious and persistent disability, highlights the importance of balancing body, mind, and spirit. Moreover, QoL has significant implications for health economics. The primary objective of treatment is not only to cure the disease but also to assess, maintain, improve, and restore QoL. Two main types of questionnaires are used to evaluate QoL: General measures related to the overall population and disease-specific measures tailored to specific organs affected by the disease. Disease-specific questionnaires are more sensitive to minor changes in QoL than general measures. The Thyroid Patient-Reported Outcome (ThyPRO) is a validated and standardized thyroid-specific questionnaire developed to measure QoL in patients with benign thyroid pathologies (5,6).

The aim of this study was to determine whether there were improvements in the QoL of patients treated with RAI 131 for hyperthyroidism and to quantify the extent of these improvements using the ThyPRO questionnaire.

Material and Methods

Study Design

This prospective, single center study was conducted in Bolu Abant İzzet Baysal University Clinical Research Ethics Committee (decision no:2022/239, date: 25.10.2022)

Patients

The study included 84 patients diagnosed with hyperthyroidism due to Grave' disease, toxic MNG and toxic adenoma who received RAI 131 therapy at doses of 10, 15, 20, or 30 mCi. The cohort comprised 39 males and 45 females, with 7 receiving 10 mCi, 26 receiving 15 mCi, 48 receiving 20 mCi, and 3 receiving 30 mCi doses of RAI 131 (Table 1). The exclusion criteria were age under

Table 1. Comparison of ThyPRO scores according to gender				
Quality of life	**Pre-treatment (mean ± SD)**	**Post-treatment (mean ± SD)**	**Mean change**	***p-value**
Males (n=39)				
Disease symptoms	12.90±1.85	12.60±6.20	-0.30	<0.001
Fatigue	32.80±22.10	5.00±14.50	-27.80	<0.001
Vitality	22.80±18.00	3.40±10.00	-19.40	<0.001
Memory and concentration	20.50±22.00	3.20±10.40	-17.30	<0.001
Nervousness and mental fatigue	28.20±25.00	6.70±19.00	-21.50	<0.001
Psychological well-being	24.60±16.60	5.90±15.50	-18.70	<0.001
Mood	19.90±16.60	3.60±10.10	-16.30	<0.001
Relationships with others	3.00±9.60	0.00	-3.00	<0.001
Daily activities	21.00±23.70	3.40±11.00	-17.60	<0.001
Sexual life	5.50±12.40	2.30±8.90	-3.20	<0.001
Appearance	15.40±22.60	4.00±12.50	-11.40	<0.001
General condition	36.50±28.50	3.80±13.00	-32.70	<0.001
Females (n=45)				
Disease symptoms	13.00±1.90	12.80±6.40	-0.20	<0.001
Fatigue	33.00±22.80	5.20±15.10	-27.80	<0.001
Vitality	23.00±18.40	3.50±10.30	-19.50	<0.001
Memory and concentration	20.70±22.10	3.40±10.50	-17.30	<0.001
Nervousness and mental fatigue	28.40±25.20	6.80±19.40	-21.60	<0.001
Psychological well-being	24.80±16.80	5.90±15.70	-18.90	<0.001
Mood	20.00±16.80	3.70±10.20	-16.30	<0.001
Relationships with others	3.10±9.80	0.00	-3.10	<0.001
Daily activities	21.10±23.90	3.50±11.10	-17.60	<0.001
Sexual life	5.60±12.60	2.40±9.10	-3.20	<0.001
Appearance	15.50±22.80	4.10±12.60	-11.40	<0.001
General condition	36.60±28.60	3.90±13.10	-32.70	<0.001
*Paired t-test, SD: Standard deviation, ThyPRO: Thyroid Patient-Reported Outcome				

18 years and over 90 years, known cancer, and psychiatric disorders.

Data Collection

Hyperthyroidism was defined as a thyroid stimulating hormone (TSH) level of <0.01 mIU/L with elevated free T4 and/or T3 levels. The etiology of hyperthyroidism was evaluated according to clinical presentation, laboratory results, thyroid scintigraphy, uptake studies, and sonographic findings. The appropriate RAI 131 treatment dose was determined. Patients received the optimal dose of RAI 131 therapy and were followed up clinically and with laboratory tests between 1.5 and 6 months after treatment. The final treatment outcomes were assessed at 6 months. Cure was defined as the achievement of euthyroidism or hypothyroidism without antithyroid medication after 131 therapies. Persistent hyperthyroidism indicated treatment failure, and repeat RAI 131 therapy was considered under appropriate conditions.

Questionary Assessment

The QoL of all patients was assessed using the ThyPRO questionnaire before treatment and 6 months after treatment. Patients were administered the ThyPRO questionnaire either in person or via telephone to collect QoL data. The ThyPRO questionnaire consists of 84 short questions categorized into 12 domains: Disease symptoms, fatigue, vitality, memory, and concentration, nervousness and mental fatigue, psychological well-being, mood, relationship with others, daily activities, sexual life, appearance, and general conditions related to thyroid disease. Patients selected one of the five response options

for each question (0= never, 1= very little, 2= somewhat, 3= quite a bit, 4= very much). Each response was scored from 0 to 100, with higher scores indicating worse QoL. The average score for each domain was calculated separately. The survey duration ranged from 15 to 30 min, depending on the researcher and patient conditions. The change in scores before and after RAI 131 therapy was defined as improvement, with positive change scores indicating an improvement in QoL.

Ethical Considerations

Ethical approval was obtained from the Bolu Abant Izzet Baysal University Clinical Research Ethics Committee in October 2022 (decision no: 2022/239, date: 25.10.2022), and the study complied with the Declaration of Helsinki. The patients provided written informed consent to publication of this report.

Statistical Analysis

Continuous variables are expressed as mean ± standard deviation, while categorical variables are presented as frequencies and percentages. The chi-square test was used to compare categorical variables. Paired sample t-tests were performed to determine differences between pre- and posttreatment parameters. Analysis of Variance was employed to compare changes in ThyPRO scores among the different RAI 131 dose groups. Multiple regression analysis was conducted to identify predictors of posttreatment QoL improvement. Statistical analysis were conducted using SPSS version 25.0. Statistical significance was set at $p<0.05$.

Results

Demographic and Treatment Data

The ThyPRO questionnaire was administered to 84 patients, including 39 males (47%) and 45 females (53%). The average age of the patients was 58.33±12.45 years. The distribution of RAI 131 doses administered to the patients was as follows: Seven patients (8%) received a dose of 10 mCi, 26 patients (31%) received a dose of 15 mCi, 48 patients (57%) received a dose of 20 mCi, and 3 patients (4%) received a dose of 30 mCi. These demographic and treatment data provide the context for subsequent analysis of QoL improvement following RAI 131 therapy.

Comparison of ThyPRO Scores According to Gender

In both sex groups, significant improvements in all post-treatment QoL measures were observed. For males, the mean change in scores indicated improvements in disease symptoms, fatigue, vitality, memory and concentration, nervousness and mental fatigue, psychological well-being, mood, relationships with others, daily activities, sexual life, appearance, and general condition ($p<0.001$ for all). Similarly, females showed significant improvements in the QoL measures ($p<0.001$ for all). Table 1 presents the comparison of ThyPRO scores before and after RAI 131 treatment among male and female patients.

Comparison of ThyPRO Scores Among Age Groups

Significant improvements in QoL were observed across all post-treatment measures in all age groups. For patients aged below 50 years, the mean change in scores indicated improvements in disease symptoms, fatigue, vitality, memory and concentration, nervousness and mental fatigue, psychological well-being, mood, relationship with others, daily activities, sexual life, appearance, and general condition (all $p< 0.001$). Similarly, patients aged 50-60 years and over 60 years showed significant improvements in the same QoL measures ($p<0.001$ for all). Table 2 presents the comparison of ThyPRO scores before and after treatment with RAI 131 among the different age groups.

Comparison of ThyPRO Scores According to Hyperthyroidism Severity

Significant improvements in QoL were observed across all post-treatment measures in patients with mild, moderate, or severe hyperthyroidism. For patients with mild hyperthyroidism, the mean change in scores indicated improvements in disease symptoms, fatigue, vitality, memory and concentration, nervousness and mental fatigue, psychological well-being, mood, relationship with others, daily activities, sexual life, appearance, and general condition ($p<0.001$ for all) (Table 3). Similarly, patients with moderate and severe hyperthyroidism showed significant improvements in QoL measures (all $p<0.001$).

Comparison of ThyPRO Scores among RAI 131 Dose Groups

Significant improvements were observed in all QoL measures post-treatment across the different RAI 131 dose groups. Patients receiving 10 mCi, 15 mCi, 20 mCi, and 30 mCi doses all showed significant improvements in disease symptoms, fatigue, vitality, memory and concentration, nervousness and mental fatigue, psychological well-being, mood, relationship with others, daily activities, sexual life, appearance, and general condition ($p<0.001$ for all). Table 4 presents the comparison of ThyPRO scores before and after treatment with RAI 131 among the different dose groups.

Correlation Between Demographic Factors, Thyroid Hormone Normalization, and QoL Improvement

Correlation analysis revealed significant relationships between certain demographic factors, thyroid hormone

Table 2. Comparison of ThyPRO scores among age groups				
Quality of life	**Pre-treatment (mean ± SD)**	**Post-treatment (mean ± SD)**	**Mean change**	***p-value**
<50 Years (n=20)				
Disease symptoms	13.00±2.00	12.70±6.30	-0.30	<0.001
Fatigue	33.00±23.00	5.20±15.00	-27.80	<0.001
Vitality	23.00±18.50	3.50±10.20	-19.50	<0.001
Memory and concentration	20.70±22.20	3.40±10.60	-17.30	<0.001
Nervousness and mental fatigue	28.40±25.30	6.80±19.50	-21.60	<0.001
Psychological well-being	24.80±16.90	5.90±15.80	-18.90	<0.001
Mood	20.00±16.90	3.70±10.30	-16.30	<0.001
Relationships with others	3.10±9.90	0.00	-3.10	<0.001
Daily activities	21.10±23.90	3.50±11.20	-17.60	<0.001
Sexual life	5.60±12.70	2.40±9.20	-3.20	<0.001
Appearance	15.50±22.90	4.10±12.70	-11.40	<0.001
General condition	36.60±28.70	3.90±13.20	-32.70	<0.001
50-60 Years (n=34)				
Disease symptoms	13.10±1.80	12.80±6.50	-0.30	<0.001
Fatigue	33.20±22.60	5.30±15.20	-27.90	<0.001
Vitality	23.10±18.60	3.60±10.40	-19.50	<0.001
Memory and concentration	20.90±22.30	3.50±10.70	-17.40	<0.001
Nervousness and mental fatigue	28.60±25.40	6.90±19.60	-21.70	<0.001
Psychological well-being	25.00±17.00	6.00±16.00	-19.00	<0.001
Mood	20.10±17.00	3.80±10.40	-16.30	<0.001
Relationships with others	3.20±10.00	0.00	-3.20	<0.001
Daily activities	21.20±24.00	3.60±11.30	-17.60	<0.001
Sexual life	5.70±12.80	2.50±9.30	-3.20	<0.001
Appearance	15.60±23.00	4.20±12.80	-11.40	<0.001
General condition	36.70±28.80	4.00±13.30	-32.70	<0.001
>60 Years (n=30)				
Disease symptoms	13.20±1.70	12.90±6.60	-0.30	<0.001
Fatigue	33.40±22.40	5.40±15.30	-28.00	<0.001
Vitality	23.20±18.70	3.70±10.50	-19.50	<0.001
Memory and concentration	21.10±22.40	3.60±10.80	-17.50	<0.001
Nervousness and mental fatigue	28.80±25.50	7.00±19.70	-21.80	<0.001
Psychological well-being	25.20±17.10	6.10±16.10	-19.10	<0.001
Mood	20.20±17.10	3.90±10.50	-16.30	<0.001
Relationships with others	3.30±10.10	0.00	-3.30	<0.001
Daily activities	21.30±24.10	3.70±11.40	-17.60	<0.001
Sexual life	5.80±12.90	2.60±9.40	-3.20	<0.001
Appearance	15.70±23.10	4.30±12.90	-11.40	<0.001
General condition	36.80±28.90	4.10±13.40	-32.70	<0.001

*Paired t-test, SD: Standard deviation, ThyPRO: Thyroid Patient-Reported Outcome

Table 3. Comparison of ThyPRO scores according to hyperthyroidism severity				
Quality of life	**Pre-treatment (mean ± SD)**	**Post-treatment (mean ± SD)**	**mean Change**	***p-value**
Mild (n=30)				
Disease symptoms	13.10±1.80	12.80±6.50	-0.30	<0.001
Fatigue	33.20±22.60	5.30±15.20	-27.90	<0.001
Vitality	23.10±18.60	3.60±10.40	-19.50	<0.001
Memory and concentration	20.90±22.30	3.50±10.70	-17.40	<0.001
Nervousness and mental fatigue	28.60±25.40	6.90±19.60	-21.70	<0.001
Psychological well-being	25.00±17.00	6.00±16.00	-19.00	<0.001
Mood	20.10±17.00	3.80±10.40	-16.30	<0.001
Relationships with others	3.20±10.00	0.00	-3.20	<0.001
Daily activities	21.20±24.00	3.60±11.30	-17.60	<0.001
Sexual life	5.70±12.80	2.50±9.30	-3.20	<0.001
Appearance	15.60±23.00	4.20±12.80	-11.40	<0.001
General condition	36.70±28.80	4.00±13.30	-32.70	<0.001
Moderate (n=40)				
Disease symptoms	13.20±1.70	12.90±6.60	-0.30	<0.001
Fatigue	33.40±22.40	5.40±15.30	-28.00	<0.001
Vitality	23.20±18.70	3.70±10.50	-19.50	<0.001
Memory and concentration	21.10±22.40	3.60±10.80	-17.50	<0.001
Nervousness and mental fatigue	28.80±25.50	7.00±19.70	-21.80	<0.001
Psychological well-being	25.20±17.10	6.10±16.10	-19.10	<0.001
Mood	20.20±17.10	3.90±10.50	-16.30	<0.001
Relationships with others	3.30±10.10	0.00	-3.30	<0.001
Daily activities	21.30±24.10	3.70±11.40	-17.60	<0.001
Sexual life	5.80±12.90	2.60±9.40	-3.20	<0.001
Appearance	15.70±23.10	4.30±12.90	-11.40	<0.001
General condition	36.80±28.90	4.10±13.40	-32.70	<0.001
Severe (n=14)				
Disease symptoms	13.30±1.60	13.00±6.70	-0.30	<0.001
Fatigue	33.60±22.20	5.50±15.40	-28.10	<0.001
Vitality	23.30±18.80	3.80±10.60	-19.50	<0.001
Memory and concentration	21.30±22.50	3.70±10.90	-17.60	<0.001
Nervousness and mental fatigue	29.00±25.60	7.10±19.80	-21.90	<0.001
Psychological well-being	25.40±17.20	6.20±16.20	-19.20	<0.001
Mood	20.30±17.20	4.00±10.60	-16.30	<0.001
Relationships with others	3.40±10.20	0.00	-3.40	<0.001
Daily activities	21.40±24.20	3.80±11.50	-17.60	<0.001
Sexual life	5.90±13.00	2.70±9.50	-3.20	<0.001
Appearance	15.80±23.20	4.40±13.00	-11.40	<0.001
General condition	36.90±29.00	4.20±13.50	-32.70	<0.001

SD: Standard deviation, ThyPRO: Thyroid Patient-Reported Outcome, *Paired t-test

Table 4. Comparison of ThyPRO Scores among RAI 131 Dose Groups

Quality of life	Ten mCi (n=7) Pre-treatment (mean ± SD)	Ten mCi (n=7) Post-treatment (mean ± SD)	Mean change (10 mCi)	Fifteen mCi (n=26) Pre-treatment (mean ± SD)	Fifteen mci (n=26) post-treatment (mean ± SD)	Mean change (15 mCi)	Twenty mCi (n=48) Pre-treatment (mean ± SD)	Twenty mCi (n=48) post-treatment (mean ± SD)	Mean change (20 mCi)	Thirty mCi (n=3) pre-treatment (mean ± SD)	Thirty mci (n=3) post-treatment (mean ± SD)	Mean change (30 mCi)	*p-value
Disease symptoms	12.9±1.8	12.6±6.2	-0.3	13.0±1.9	12.7±6.3	-0.3	13.1 ± 1.9	12.8 ± 6.5	-0.3	13.2 ± 1.7	12.9 ± 6.6	-0.3	<0.001
Fatigue	32.8±22.1	5.0±14.5	-27.8	33.0±22.8	5.2±15.1	-27.8	33.2 ± 22.6	5.3 ± 15.2	-27.9	33.4 ± 22.4	5.4 ± 15.3	-28.0	<0.001
Vitality	22.8±18.0	3.4±10.0	-19.4	23.0±18.4	3.5±10.3	-19.5	23.2 ± 18.6	3.6 ± 10.4	-19.5	23.4 ± 18.7	3.7 ± 10.5	-19.7	<0.001
Memory and concentration	20.5±22.0	3.2±10.4	-17.3	20.7±22.1	3.4±10.5	-17.3	20.9 ± 22.3	3.5 ± 10.7	-17.4	21.1 ± 22.4	3.6 ± 10.8	-17.5	<0.001
Nervousness and mental fatigue	28.2±25.0	6.7±19.0	-21.5	28.4±25.2	6.8±19.4	-21.6	28.6 ± 25.4	6.9 ± 19.6	-21.7	28.8 ± 25.5	7.0 ± 19.7	-21.8	<0.001
Psychological well-being	24.6±16.6	5.9±15.5	-18.7	24.8±16.8	5.9±15.7	-18.9	25.0 ± 17.0	6.0 ± 16.0	-19.0	25.2 ± 17.1	6.1 ± 16.1	-19.1	<0.001
Mood	19.9±16.6	3.6±10.1	-16.3	20.0±16.8	3.7±10.2	-16.3	20.1 ± 17.0	3.8 ± 10.4	-16.3	20.2 ± 17.1	3.9 ± 10.5	-16.3	<0.001
Relationships with others	3.0±9.6	0.0	-3.0	3.1±9.8	0.0	-3.1	3.2 ± 10.0	0.0	-3.2	3.3 ± 10.1	0.0	-3.3	<0.001
Daily activities	21.0±23.7	3.4±11.0	-17.6	21.1±23.9	3.5±11.1	-17.6	21.2 ± 24.0	3.6 ± 11.2	-17.6	21.3 ± 24.1	3.7 ± 11.3	-17.6	<0.001
Sexual Life	5.5±12.4	2.3±8.9	-3.2	5.6±12.6	2.4±9.1	-3.2	5.7 ± 12.8	2.5 ± 9.3	-3.2	5.8 ± 12.9	2.6 ± 9.4	-3.2	<0.001
Appearance	15.4±22.6	4.0±12.5	-11.4	15.5±22.8	4.1±12.6	-11.4	15.6 ± 23.0	4.2 ± 12.8	-11.4	15.7 ± 23.1	4.3 ± 12.9	-11.4	<0.001
General condition	36.5±28.5	3.8±13.0	-32.7	36.6±28.6	3.9±13.1	-32.7	36.7 ± 28.8	4.0 ± 13.3	-32.7	36.8 ± 28.9	4.1 ± 13.4	-32.7	<0.001

*ANOVA test, SD: Standard deviation, ThyPRO: Thyroid Patient-Reported Outcome, RAI 131: Radioactive iodine

levels, and QoL improvement, as measured by changes in ThyPRO scores. Age had a weak negative correlation with QoL improvement (r=-0.20, p=0.05), indicating that younger patients tended to experience greater improvements in QoL. Sex was not significantly correlated with QoL improvement (r=0.10, p=0.30).

Thyroid hormone levels were significantly correlated with improvements in QoL. T3 levels showed a moderate positive correlation (r=0.45, p=0.001), T4 levels showed a positive correlation (r=0.40, p=0.003), and TSH levels showed a moderate negative correlation (r=-0.35, p=0.007). These correlations suggest that better normalization of thyroid hormone levels is associated with greater improvement in QoL (Table 5).

Multiple Regression Analysis of Predictors of QoL Improvement

Multiple regression analysis was conducted to identify predictors of QoL improvement, as measured by changes in ThyPRO scores. The initial ThyPRO score was found to be a significant predictor of QoL improvement, with a coefficient (B) of -0.50 (p<0.001), indicating that higher initial scores were associated with greater improvements. Age was also a significant predictor (B=0.05, p=0.015), suggesting that older patients experienced slightly greater QoL improvement. Sex did not significantly predict QoL improvement (B=0.10, p= 0.620). The dose of RAI 131 was not a significant predictor across the different dose groups: 10 mCi (reference group), 15 mCi (B=0.15, p=0.550), 20 mCi (B=0.20, p=0.503), and 30 mCi (B=0.25, p=0.480) (Table 6).

Discussion

The present study showed significant improvements in QoL among patients with hyperthyroidism treated with RAI 131, as assessed using the ThyPRO questionnaire. These improvements were consistent across various

Table 5. Correlation between demographic factors, thyroid hormone normalization, and quality of life improvement (change in ThyPRO score)		
Demographic factor	**Pearson's correlation coefficient (r)**	***p-value**
Age	-0.20	0.05
Gender (male= 0, female= 1)	0.10	0.30
Hormone level		
T3	0.45	0.001
T4	0.40	0.003
TSH	-0.35	0.007
*Pearson correlation coefficient, ThyPRO: Thyroid Patient-Reported Outcome, TSH: Thyroid-stimulating hormone		

Table 6. Multiple regression analysis of predictors of quality of life improvement (change in ThyPRO score)					
Predictor Variable	**Coefficient (B)**	**Standard error (SE)**	**Beta (β)**	**t-value**	***p-value**
Initial ThyPRO score	-0.50	0.10	-0.60	-5.00	<0.001
Age	0.05	0.02	0.20	Şub.50	0.015
Gender (male= 0, female= 1)	0.10	0.20	0.05	0.50	0.620
Dose of RAI 131 (10 mCi)					
Dose of RAI 131 (15 mCi)	0.15	0.25	0.10	0.60	0.550
Dose of RAI 131 (20 mCi)	0.20	0.30	0.12	0.67	0.503
Dose of RAI 131 (30 mCi)	0.25	0.35	0.15	0.71	0.480
*Regression analysis, RAI 131: Radioactive iodine, ThyPRO: Thyroid Patient-Reported Outcome					

demographic groups, including sex, age, disease severity, and RAI 131 dose levels. Our findings align with those of previous studies, emphasizing the efficacy and safety of RAI 131 in enhancing QoL in patients with hyperthyroidism.

Significant improvements were observed across all QoL measures for both males and females post-treatment. Both genders showed notable enhancements in disease symptoms, fatigue, vitality, memory, and concentration, nervousness and mental fatigue, psychological well-being, mood, relationships with others, daily activities, sexual life, appearance, and general condition.

These findings align with Kaniuka-Jakubowska et al. (7) study on patients with nontoxic goiter treated with RAI 131, in which significant QoL improvements were reported regardless of thyroid gland size. Our results corroborate their conclusion that RAI 131 effectively enhances QoL across different demographic groups, although our study did not find a significant gender difference in QoL improvement, which is consistent with the existing literature.

Improvements in QoL were significant across all age groups: <50 years, 50-60 years, and >60 years. Younger patients (<50 years) experienced slightly greater improvements in vitality, memory, and concentration than older age groups. The age-related differences in QoL improvement were modest, indicating that RAI 131 was effective across all ages.

Larisch et al. (8) reported similar findings in their study on subclinical hyperthyroidism, where RAI therapy improved QoL and biochemical parameters, emphasizing the importance of pretreatment QoL assessment in therapeutic decision-making. Our results support this finding, showing that age is a factor but not a barrier to significant improvement in QoL after 131 weeks of therapy.

Patients with mild, moderate, and severe hyperthyroidism showed significant improvements in QoL after treatment. Consistent mean changes across different severity levels highlight the efficacy of RAI 131 in improving QoL, regardless of initial disease severity. This finding is consistent with that of Mirallié et al. (9). Who reported QoL improvements in thyroidectomy patients, and Helvacı et al. (10). Who found no significant differences in depression and anxiety scores between RAI-treated and untreated thyroid cancer survivors. Our study extends these findings to patients with hyperthyroidism, confirming that RAI 131 effectively enhances QoL across various severity levels of the disease.

All dose groups (10, 15, 20, and 30 mCi) showed significant improvement in QoL across all measures, with no significant differences between dose groups. This suggests that a low dose of 10 mCi is sufficient to achieve substantial improvement in QoL in patients with

hyperthyroidism. Törring et al. (11) reported negative QoL impacts in patients with Graves' disease treated with RAI, which is in contrast with our findings. However, our study included patients with various hyperthyroid etiologies, which may explain this discrepancy. Our results suggest that RAI 131 dosage can be tailored to patient needs without compromising QoL outcomes, supporting the safety and efficacy of lower doses.

The correlation analysis revealed that age had a weak negative correlation with QoL improvement, indicating that younger patients tend to experience greater QoL improvement. Thyroid hormone levels were significantly correlated with QoL improvement, emphasizing the importance of hormone normalization for improving QoL outcomes. These findings align with those of Wu et al. (12), who found significant improvements in QoL and reductions in depression and anxiety symptoms among patients with thyroid cancer receiving RAI and behavioral support. Our study reinforces the importance of achieving a hormonal balance for optimal QoL improvement in patients with hyperthyroidism.

Multiple regression analysis identified initial ThyPRO score and age as significant predictors of QoL improvement. Higher initial ThyPRO scores were associated with greater QoL improvement, and older patients experienced slightly greater QoL improvement. Sex and RAI 131 dose were not significant predictors. This finding supports the findings of Taïeb et al. (13) Who emphasized the importance of early levothyroxine initiation post-RAI therapy for improving QoL in patients with Graves' disease. Our findings suggest that although demographic factors and initial QoL levels influence outcomes, the dosage of RAI 131 can be flexible without adversely affecting QoL improvement.

Study Limitations

Although our study demonstrated significant results, there are some limitations that should be acknowledged. A sample size of 84 patients is sufficient, limiting the generalizability of the findings. A larger sample size would provide more robust data and increase external validity. The results of this study were conducted at a single center, and they may not be applicable to other settings or populations. The ThyPRO questionnaire, which relies on self-reported data, is susceptible to response bias and inaccuracy. Future studies should incorporate objective measures of health and quality of life. The exclusion of patients with known cancers or psychiatric disorders limits the applicability of the findings. Including a more diverse patient population would provide a more comprehensive understanding of RAI 131 therapy's impact. The absence of a control group receiving alternative treatments or no treatment impedes direct comparisons of the effectiveness of RAI 131 with other interventions.

Conclusion

RAI 131 therapy significantly enhances the QoL of hyperthyroid patients, with improvements observed across various demographic groups, disease severity, and dosage levels. These findings support the continued use of RAI 131 as a primary treatment modality for hyperthyroidism, emphasizing the importance of personalized treatment approaches to optimize patient outcomes. Further research should focus on long-term QoL outcomes and refine therapeutic strategies to maximize patient well-being.

Ethics

Ethics Committee Approval: This prospective, single center study was conducted in Bolu Abant İzzet Baysal University Clinical Research Ethics Committee (decision no:2022/239, date: 25.10.2022)

Informed Consent: The patients provided written informed consent to publication of this report.

Footnotes

Authorship Contributions

Surgical and Medical Practices: H.A., B.Ç., Concept: H.A., Design: H.A., B.Ç., Data Collection or Processing: H.A., Analysis or Interpretation: H.A, B.Ç., Literature Search: H.A., Writing: H.A.

Conflict of Interest: No conflict of interest was declared by the authors.

Financial Disclosure: The authors declared that this study has received no financial support.

References

1. Wiersinga WM, Poppe KG, Effraimidis G. Hyperthyroidism: aetiology, pathogenesis, diagnosis, management, complications, and prognosis. Lancet Diabetes Endocrinol. 2023;11:282-98.
2. Lutterman SL, Zwaveling-Soonawala N, Verberne HJ, et al. The efficacy and short- and long-term side effects of radioactive iodine treatment in pediatric graves' disease: a systematic review. Eur Thyroid J. 2021;10:353-63.
3. Liu X, Wong CKH, Chan WWL, et al. Outcomes of graves' disease patients following antithyroid drugs, radioactive iodine, or thyroidectomy as the first-line treatment. Ann Surg. 2021;273:1197-206.
4. Marquez DX, Aguiñaga S, Vásquez PM, et al. A systematic review of physical activity and quality of life and well-being. Transl Behav Med. 2020;10:1098-109.
5. Vita R, Caputo A, Quattropani MC, Watt T, Feldt-Rasmussen U, Puleio P, et al. Quality of life in patients with hyperthyroidism: where do we stand? Mediterranean Journal of Clinical Psychology. 2020;8.
6. Cramon PK, Bjorner JB, Groenvold M, et al. Implementation of thyroid-related patient-reported outcomes in routine clinical practice. Front Endocrinol (Lausanne). 2022;1000682.
7. Kaniuka-Jakubowska S, Lewczuk A, Majkowicz M, Piskunowicz M, Mizan-Gross K, Zapaśnik A, et al. Nontoxic goiter (NTG) and radioiodine:

what do patients think about it? Quality of life in patients with NTG before and after 131-I therapy. Frontiers in Endocrinology. 2018;9:114.

8. Larisch R, Midgley JEM, Dietrich JW, et al. Effect of radioiodine treatment on quality of life in patients with subclinical hyperthyroidism: a prospective controlled study. Nuklearmedizin. 2024:176-87.
9. Mirallié E, Borel F, Tresallet C, et al. Impact of total thyroidectomy on quality of life at 6 months: the prospective ThyrQoL multicentre trial. Eur J Endocrinol. 2020;182:195-205.
10. Helvacı BC, Yalçın MM, Yalcın ŞNG, et al. Differentiated thyroid cancer: effect on quality of life, depression, and anxiety. Hormones (Athens). 2023;22:367-74.
11. Törring O, Watt T, Sjölin G, et al. Impaired quality of life after radioiodine therapy compared to antithyroid drugs or surgical treatment for graves' hyperthyroidism: a long-term follow-up with the thyroid-related patient-reported outcome questionnaire and 36-item short form health status survey. Thyroid. 2019;29:322-31.
12. Wu HX, Zhong H, Xu YD, et al. Psychological and behavioral intervention improves the quality of life and mental health of patients suffering from differentiated thyroid cancer treated with postoperative radioactive iodine-131. Neuropsychiatr Dis Treat. 2016;12:1055-60.
13. Taïeb D, Bournaud C, Eberle MC, et al. Quality of life, clinical outcomes and safety of early prophylactic levothyroxine administration in patients with Graves' hyperthyroidism undergoing radioiodine therapy: a randomized controlled study. Eur J Endocrinol. 2016;174:491-502.

Original Article

Mol Imaging Radionucl Ther 2025;34:48-54 *DOI:10.4274/mirt.galenos.2024.37431*

Correlation of 3T Diffusion-weighted MRI and ^{18}F-FDG-PET/CT in Liver Metastases: SUV Versus ADC

Karaciğer Metastazlarında 3T Difüzyon Ağırlıklı MRG ve ^{18}F-FDG-PET/BT Korelasyonu: SUV'a Karşı ADC

Ahmet Tanyeri[1], Rıdvan Akbulut[1], Emir Hüseyin Nevai[1], Yakup Yürekli[2]

[1]*Aydın Adnan Menderes University, Faculty of Medicine, Department of Radiology, Aydın, Türkiye*
[2]*Aydın Adnan Menderes University Faculty of Medicine, Department of Nuclear Medicine, Aydın, Türkiye*

Abstract

Objectives: Positron emission tomography/computed tomography (PET/CT) and magnetic resonance imaging (MRI) are widely used in the diagnosis and follow-up of liver metastases. Both modalities provide anatomical and functional information and have advantages and disadvantages. The objective of this study was to investigate the correlation between apparent diffusion coefficient (ADC) and standardized uptake value (SUV) values in metastatic liver lesions.

Methods: Abdominal magnetic resonance (MR) scans performed between April 2021 and 2024 using the 3T MR scanner were retrospectively evaluated. Thirty-three patients with liver metastases, less than one month between magnetic resonance imaging (MRI) and PET/CT, no treatment during this period, and lesions larger than 1 cm were included in the study. In each MRI scan, an index lesion was selected for ADC measurement. The radiologist and nuclear medicine specialist measured the same index lesion without the patient being informed of the results.

Results: The mean age of the 33 patients was 59±12 years, with 17 (51%) men and 16 (49%) women. The mean size of the index lesions was 27±9 mm. In MRI, mean ADC_{min}: (0.54±0.2) $\times10^{-3}mm^2/s$; ADC_{mean}: (1.02±0.2) $\times10^{-3}mm^2/s$; ADC_{max}: (1.48±0.44) $\times10^{-3}mm^2/s$; and region of interest area was calculated as 6±4.6 cm^2. In PET/CT, mean SUV_{mean}: 5.8±3.3; SUV_{peak}: 6.8±4.3; SUV_{max}: 10.7±5.6; and metabolic tumor volume: 12.1 (7.4-20.7) cm^3. No statistically significant correlation was found between ADC and SUV values.

Conclusion: There was no correlation between ADC and SUV values in liver metastases. Prospective studies with a large patient group are needed.

Keywords: Liver neoplasms, diffusion magnetic resonance imaging, positron emission tomography computed tomography, apparent diffusion coefficient, standardized uptake value

Öz

Amaç: Pozitron emisyon tomografisi/bilgisayarlı tomografi (PET/BT) ve manyetik rezonans görüntüleme (MRG) karaciğer metastazlarının tanı ve takibinde yaygın olarak kullanılmaktadır. Anatomik ve fonksiyonel bilgi sağlayan her iki modalitenin de avantaj ve dezavantajları vardır. Bu çalışmanın amacı metastatik karaciğer lezyonlarında görünür difüzyon katsayısı (ADC) değerleri ile standardize uptake değeri (SUV) değerleri arasındaki korelasyonu araştırmaktır.

Yöntem: Nisan 2021 ve 2024 tarihleri arasında 3T MR cihazı kullanılarak gerçekleştirilen abdominal MR taramaları retrospektif olarak değerlendirilmiştir. Çalışmaya, karaciğer metastazı olan ve lezyonları 1 cm'den büyük olan 33 hasta dahil edildi. Bu hastalar, bir aydan kısa süre içinde MRG ve PET/BT taramalarından geçti ve bu süreçte herhangi bir tedavi almadı. Her MRG taramasında, ADC ölçümü için bir indeks lezyon seçildi. Radyolog ve nükleer tıp uzmanı, birbirlerinin sonuçlarından habersiz bir şekilde aynı indeks lezyon üzerinde ölçüm yaptı.

Address for Correspondence: Ahmet Tanyeri, Aydın Adnan Menderes University Faculty of Medicine, Department of Radiology, Aydın, Türkiye
E-mail: dr.a.tanyeri@gmail.com **ORCID ID:** orcid.org/0000-0002-1097-1172
Received: 29.07.2024 **Accepted:** 13.10.2024 **Publication Date:** 07.02.2025

Cite this article as: Tanyeri A, Akbulut R, Nevai EH, Yürekli Y. Correlation of 3T diffusion-weighted MRI and ^{18}F-FDG-PET/CT in liver metastases: SUV versus ADC. Mol Imaging Radionucl Ther. 2025;34:48-54.

Öz

Bulgular: Ortalama yaşı 59±12 olan 33 hastanın 17'si (%51) erkek, 16'sı (%49) kadındı. İndeks lezyonların ortalama boyutu 27±9 mm idi. MRG'de ortalama ADC_{min}: (0,54±0,2) $\times 10^{-3} mm^2/s$; ADC_{ort}: (1,02±0,2) $\times 10^{-3} mm^2/s$; ADC_{maks}: (1,48±0,44) $\times 10^{-3} mm^2/s$; ve ilgi alanı 6±4,6 cm^2 olarak hesaplandı. PET/BT'de ortalama SUVmean: 5,8±3,3; SUV_{pik}: 6,8±4,3; SUV_{maks}: 10,7±5,6; ve metabolik tümör hacmi: 12,1 (7,4-20,7) cm^3. ADC ve SUV değerleri arasında istatistiksel olarak anlamlı bir korelasyon bulunmadı.

Sonuç: Karaciğer metastazlarında ADC ve SUV arasında korelasyon bulunmamıştır. Geniş bir hasta grubuyla yapılacak prospektif çalışmalara ihtiyaç vardır.

Anahtar kelimeler: Karaciğer neoplazmları, difüzyon manyetik rezonans görüntüleme, pozitron emisyon tomografi bilgisayarlı tomografi, görünür difüzyon katsayısı, standardize uptake değeri

Introduction

The liver is the organ most frequently affected organ by metastases in the abdomen. For diagnosing and monitoring these lesions, magnetic resonance imaging (MRI) and ^{18}F-fluorodeoxyglucose (^{18}F-FDG) positron emission tomography/computed tomography (PET/CT) are commonly used imaging techniques. However, PET/CT has several disadvantages, including the exposure of patients to high radiation doses. Additionally, it involves complex preparation procedures for both patients and ^{18}F-FDG and requires long ^{18}F-FDG uptake and scanning times (1). Additionally, PET/CT scan is less sensitive than MRI for detecting liver lesions smaller than 1 cm (2). As a radiation-free alternative, MRI with diffusion-weighted imaging (DWI) sequences has been widely researched for its efficacy in oncological imaging (3), providing anatomical and functional data comparable to PET/CT.

Although apparent diffusion coefficient (ADC) values from DWI provide insights into tissue cellularity and organization, standardized uptake value (SUV) values from PET/CT reflect glucose metabolism (4). Numerous studies have explored the correlation between ADCs and SUVs, hypothesizing a link between the cellular density of malignancies and their glucose metabolism. Despite some variability in the results, most studies have shown a correlation between these two values (3,5,6). Although there has been research on this correlation in various tumor types, such as lung, breast and rectum, we have not found similar studies focusing specifically on liver metastases.

The aim of this study was to investigate the correlation between ADC and SUV values in metastatic liver lesions.

Materials and Methods

This study was approved by the Aydın Adnan Menderes University Rectorate Faculty of Medicine Dean's Office Non-Interventional Clinical Research Ethics Committee (approval no: 20, date: 13.06.2024). Informed consent was not obtained for this retrospective study.

Study Group and Design

All abdominal MRI scans performed between April 2021 and April 2024 using the 3T MRI scanner were evaluated retrospectively. From a total of 2543 examinations, 254 scans with a preliminary diagnosis of liver metastases were selected based on the following inclusion criteria:

Inclusion Criteria

1. The time between MRI and PET/CT should be 1 month.
2. There should be no artifacts in the lesion of interest on the ADC map, and the lesion should not be smaller than 1 cm.
3. There should be no follow-up patients with complete response to treatment.
4. No systemic or local treatment for malignancy should be provided between MRI and PET/CT.
5. Malignancy should be confirmed by histopathological examination.

A total of 33 patients who met the inclusion criteria were included in the study (Figure 1). Each MRI scan revealed one metastasis. In cases of multiple metastases, the most opacified lesion in the contrast-enhanced series, the lesion with the least or no cystic-necrotic component, and the largest lesion were selected as the index lesion. DWI and PET/CT measurements were performed on the same index lesion (Figures 2,3).

Index lesion size on MRI, liver segment, malignancy type, interval between MRI and PET-CT, patient age and sex, and new diagnosis or treatment follow-up were recorded. The correlation between ADC and SUV values was investigated in groups of all metastases, gastrointestinal metastases, and others, and new diagnosis and treatment response follow-up.

DWI and ADC

Images were acquired using a 3T MR scanner (GE Signa Pioneer, GE Healthcare, United States). For abdominal MRI, a body coil with a 30-channel anterior array and a

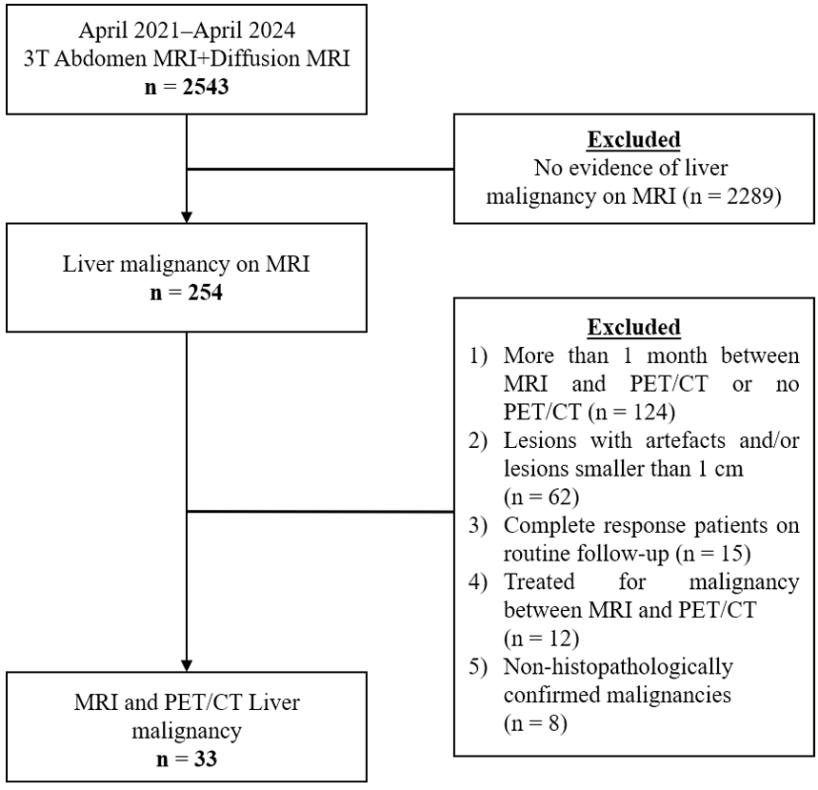

Figure 1. Flowchart showing the selection of the working group

MRI: Magnetic resonance imaging, PET/CT: Positron emission tomography/computed tomography

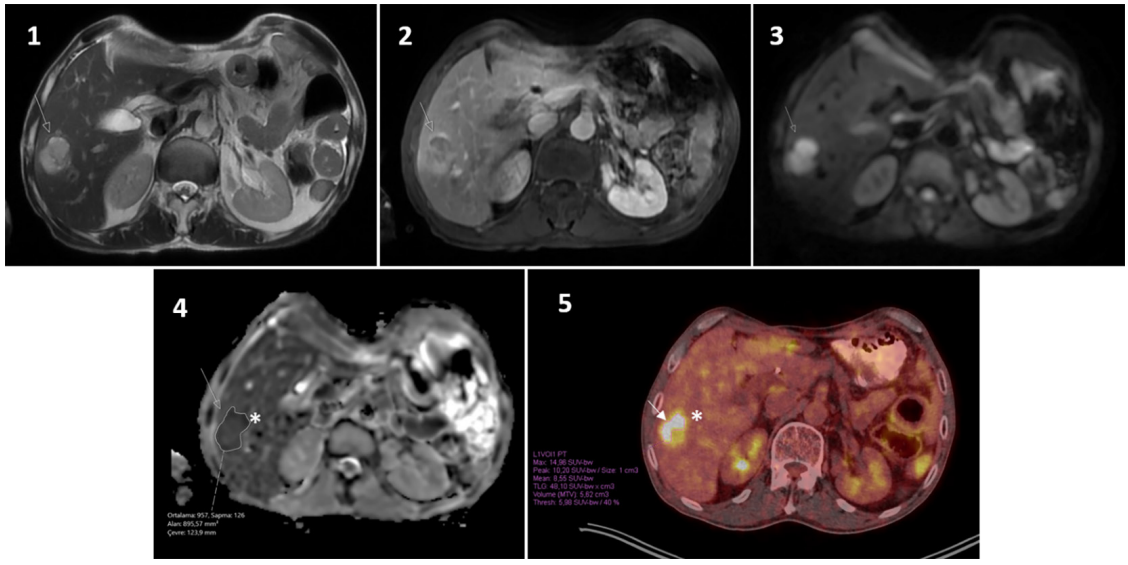

Figure 2. A 58-year-old male patient with metastatic gastric adenocarcinoma/systemic treatment response evaluation (MRI and PET/CT scans) 1–5) Axial T2, contrast-enhanced fat-suppressed T1, DWI, ADC, and PET/CT images from 1–5 show liver metastasis, respectively (white arrow). The 4th figure shows the ROI for the ADC measurement, and the 5th figure shows the VOI (volume of interest) for the SUV measurement (*). ADC_{min}: 0.68×10^{-3} mm^2/s, ADC_{mean}: 0.96×10^{-3} mm^2/s, ADC_{max}: 1.25×10^{-3} mm^2/s, SUV_{mean}: 8.6, SUV_{peak}: 10.2, SUV_{max}: 15 were calculated.

MRI: Magnetic resonance imaging, PET/CT: Positron emission tomography/computed tomography, ADC: Apparent diffusion coefficient, SUV: Standardized uptake value, DWI: Diffusion-weighted imaging, ROI: Region of interest

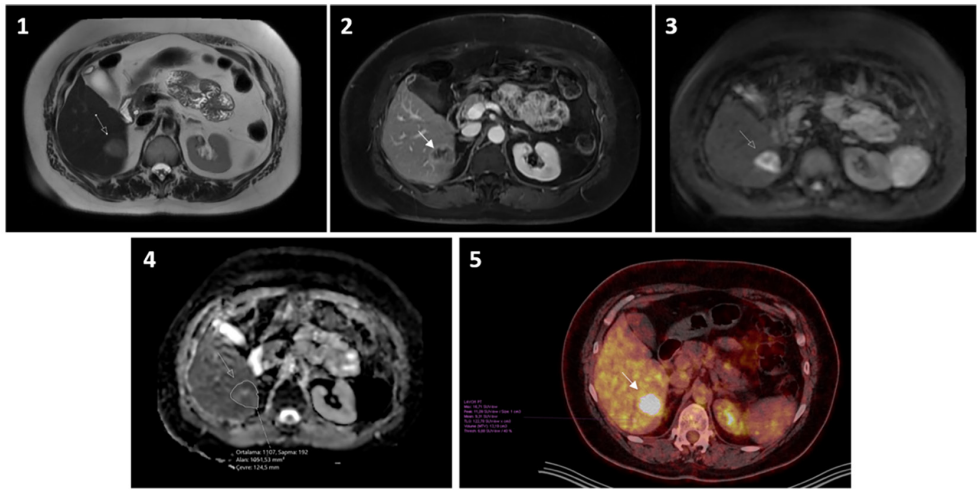

Figure 3. A 46-year-old woman with newly diagnosed metastatic ovarian cancer
(1-5) Axial T2, contrast-enhanced fat-suppressed T1, DWI, ADC, and PET/CT images from 1-5 show liver metastasis, respectively (white arrow). The 4th figure shows the ROI for the ADC measurement, and the 5th figure shows the VOI for the SUV measurement. ADC_{min}: 0.73×10^{-3} mm^2/s, ADC_{mean}: 1.10×10^{-3} mm^2/s, ADCmax: 1.79×10^{-3} mm^2/s, SUV_{mean}: 9.3, SUV_{Mean}: 11.1, SUV_{max}: 16.7 were calculated.

DWI: Diffusion-weighted imaging, ADC: Apparent diffusion coefficient, PET/CT: Positron emission tomography/computed tomography, ROI: Region of interest, SUV: Standardized uptake value

32-channel posterior array configuration was used. DWI was acquired using the echo planar imaging sequence with the following parameters: Echo time of 60-100 ms, repetition time of 4000-8000 ms, field of view of 240-460 mm, matrix size of 128×128, slice thickness of 5 mm with an interslice gap of 1 mm, and b-values of 0, 600, and 1000 s/mm². Before and after 180° pulses, a motion-probing gradient was applied to the DWI images along the x, y, and z axes. The ADC value for each pixel was then reconstructed using b-values of 0 and 1000 s/mm² with the standard software on the console.

Two experienced radiologists blinded to the PET/CT results performed ADC measurements and selected the index lesion to be measured. The region of interest (ROI) in the ADC map was manually drawn in the widest axial plane, avoiding borders at the periphery of the index lesion (7). The minimum, mean, and maximum ADC values of the ROI area were calculated automatically using the image software program (Sectra Workstation v. 24.2, Linköping, Sweden).

PET/CT and SUV

All PET/CT images were acquired using a Siemens scanner (Biograph mCT 20). The scan was performed when blood glucose was below 180 mg/dL after 6-8 hours of fasting. Patients rested in a quiet room after intravenous administration of 270-370 MBq ^{18}F-FDG. After a rest period of 60 min, imaging was performed from the base of the skull to the thigh. The CT transmission scan was acquired at 140 kVp and 110 mA with a slice thickness of 3 mm. The PET scan was acquired for 2-4 minutes per bed position.

An experienced nuclear medicine specialist who was blinded to the MRI findings evaluated the PET/CT scans and measured the SUV of the index lesion. Maximum, peak, and mean SUV and metabolic tumor volume (MTV) were calculated using image processing software (Syngo. via) with semi-automatic ROI drawing in selected index lesions.

Statistical Analysis

Statistical analysis were performed using the Statistical Package for the Social Sciences software (version 26.0, SPSS, Chicago, IL, USA). The Kolmogorov-Smirnov test was used to determine whether the data were suitable for normal distribution. Normally distributed data are expressed as mean ± standard deviation. The correlation between ADCs and SUVs was examined using Pearson's correlation test. A value of $p<0.05$ was considered statistically significant.

Results

The mean age of the 33 patients was 59±12 years; 17 (51%) patients were male and 16 (49%) were female. The mean size of the index lesion was 27±9 mm, and the most common liver sites were segments 6 (27%) and 7 (27%). The most common liver metastases were adenocarcinomas of the gastrointestinal tract (colon: 9, rectum: 5, stomach: 1, esophagus: 1) (49%). The remainder were metastases of the breast (5, 15%), pancreas (3, 9%), ovary (3, 9%),

cervix (2, 6%), bladder (2, 6%), and lung (2, 6%). A total of 30% of the metastases were newly identified, while 70% were followed up for response to treatment. The mean interval between MRI and PET/CT was 14±7 days (Table 1).

In DWI measurements, the mean ADC_{min}: (0.54±0.2) $\times10^{-3}mm^2/s$; ADC_{mean}: (1.02±0.2) $\times10^{-3}mm^2/s$; ADC_{max}: (1.48±0.44) $\times10^{-3}mm^2/s$; and ROI area were calculated as 6±4.6 cm^2. In PET/CT measurements, mean SUV_{mean}: 5.8±3.3; SUV_{peak}: 6.8±4.3; SUV_{max}: 10.7±5.6; and MTV (metabolic tumor volume): 12.1 (7.4-20.7) cm^3 (Table 1). No statistically significant correlation was observed between ADC and SUV measurements (Table 2).

Discussion

This study concluded that there was no significant correlation between ADC and SUV levels in liver metastases. However, in our study, the ADC and SUV values were individually supportive of malignancy (8,9). The ADC has long been used to diagnose and assess treatment response in malignant liver lesions (10,11). With recent advancements in PET/MRI technology, the use of ADC in routine clinical practice has become more widespread, and its correlation with SUV has been explored in several studies. One study involving 68 neoplastic lesions on PET/MRI found a weak correlation between ADC and SUV, suggesting that they may provide complementary information for evaluating treatment response (12). Similarly, another study involving 71 patients with head and neck cancer reported no correlation between ADC and SUV (13). However, in a different study of 56 patients with lymphoma and sarcoma, ADC and SUV were found to be 88% consistent in indicating treatment response (14). Although ADC and SUV are both valuable markers for assessing treatment response, there are inconsistencies in their correlation findings.

Increased glucose uptake with increased cell density requires decreased ADCs and increased SUVs, i.e., an inverse correlation. Previous studies have investigated the presence of this inverse correlation in different tumor types and reported different results. For example, three out of six studies investigating the correlation between SUV and ADC in breast cancer found no correlation between these two variables (15,16,17), whereas three studies found weak to moderate inverse correlations (6,18,19). Furthermore, no correlation was found between SUV max and ADC min in primary cervical cancer (20), whereas a strong inverse correlation was found between SUV max and mean ADC in rectal cancer (21).

There are several reasons for the results of our study. First, in the case of multiple metastases, the ADC and SUV values of the selected index lesion on MRI were assumed to be representative of the other metastases. This assumption can be refuted, but it is currently not possible to measure each metastasis separately. For example, in a hybrid PET/MRI study of liver metastases, the lesion selected for measurement was not clearly defined (22). Second, the cellularity of the tumor and the reflection of glucose metabolism in the complex background of the liver parenchyma may not be the same as in other isolated regions. For example, it has been reported that there is no correlation between ADC and

Table 1. Demographic characteristics of the patients, index lesion, ADC, and SUV

n=33	
Age	59±12
Gender (male/female)	17 (51%)/16 (49%)
Index lesion	
Diameter (mm)	27±9
Liver location	
Segment 6	27%
Segment 7	27%
Segment 8	21%
Segment 4	15%
Segments 2, 3, and 5	10%
Primary tumour	
Gastrointestinal tract	16 (49%)
Breast	5 (15%)
Pancreas	3 (9%)
Over	3 (9%)
Cervix	2 (6%)
Bladder	2 (6%)
Lung	2 (6%)
Newly diagnosed	10 (30%)
Follow-up of treatment response	23 (70%)
Interval between MRI-PET/CT (day)	14±7
Minimum ADC ($\times10^{-3}mm^2/s$)	0.54±0.2
Mean ADC ($\times10^{-3}mm^2/s$)	1.02±0.2
Maximum ADC ($\times10^{-3}mm^2/s$)	1.48±0.44
ADC ROI (cm^2)	6±4.6
SUV_{mean}	5.8±3.3
SUV_{peak}	6.8±4.3
SUV_{max}	10.7±5.6
*MTV (cm^3)	12.1 (7.4-20.7)

*Shown as median (25^{th}-75^{th} percentile)
ADC: Apparent diffusion coefficient, SUV_{mean}: Mean standardized uptake value, SUV_{peak}: Peak standardized uptake value, SUV_{max}: Maximum standardized uptake value, MTV: Metabolic tumor volume

Table 2. Pearson correlation analysis results between ADC and SUV values

		ADC_{min} SUV_{max}	ADC_{min} SUV_{peak}	ADC_{min} SUV_{mean}	ADC_{mean} SUV_{max}	ADC_{mean} SUV_{peak}	ADC_{mean} SUV_{mean}	ADC_{max} SUV_{max}	ADC_{max} SUV_{peak}	ADC_{max} SUV_{mean}
All patients (n=33)	r	-0.130	-0.163	-0.099	0.300	0.276	0.309	0.090	-0.004	0.032
	p	0.470	0.365	0.584	0.399	0.441	0.385	0.805	0.992	0.930
Treatment response follow-up (n=23)	r	-0.330	-0.360	-0.308	0.003	-0.018	0.034	0.210	0.224	0.253
	p	0.124	0.091	0.153	0.990	0.934	0.876	0.337	0.305	0.244
Newly diagnosed (n=10)	r	0.198	0.127	0.188	0.300	0.276	0.309	0.090	-0.004	0.032
	p	0.584	0.726	0.603	0.399	0.441	0.385	0.805	0.992	0.930
Gastrointestinal metastases (n=16)	r	-0.094	-0.145	-0.051	0.308	0.233	0.308	0.160	0.097	0.135
	p	0.729	0.592	0.851	0.245	0.385	0.245	0.553	0.722	0.617
Other metastases (n=17)	r	-0.265	-0.256	-0.230	-0.189	-0.137	-0.109	0.290	0.315	0.332
	p	0.305	0.321	0.375	0.467	0.600	0.678	0.259	0.217	0.193

r: Pearson correlation coefficient, ADC: Apparent diffusion coefficient, SUV: Standardized uptake value

SUV levels in hepatocellular carcinoma (23). In addition, the inclusion of benign lesions (such as hemangiomas and focal nodular hyperplasia) as well as malignant liver lesions in future studies may provide a clearer understanding of how different types of lesions behave within liver tissue. Finally, as suggested in the literature, there is the possibility that cell density and glucose metabolism may not be directly related to each other. Alternatively, this assumption may not be valid for all tumor types.

Study Limitations

The primary limitations of this study were its retrospective nature and limited number of patients. The selected index lesion may be open to question. The criteria and assessment were based on the consensus of two experienced radiologists. The scans were not taken simultaneously; thus, changes in tumor behavior may have occurred during the selected period.

Conclusion

In conclusion, although both MRI and PET/CT are routinely used in the diagnosis and follow-up of liver metastases, their different advantages can confuse the choice of imaging modality. Understanding the strengths and weaknesses of each modality can help healthcare providers make more informed decisions when diagnosing and treating patients. Although ADC is a cheap and rapid tumor biomarker, its standardization and correlation remain under development. Prospective studies with a large patient group are needed.

Ethics

Ethics Committee Approval: This study was approved by the Aydın Adnan Menderes University Rectorate Faculty of Medicine Dean's Office Non-Interventional Clinical Research Ethics Committee (approval no: 20, date: 13.06.2024).

Informed Consent: Informed consent was not obtained for this retrospective study.

Footnotes

Authorship Contributions

Surgical and Medical Practices: A.T., R.A., Y.Y., Concept: A.T., R.A., Y.Y., Design: A.T., Y.Y., Data Collection or Processing: A.T., R.A., E.H.N., Analysis or Interpretation: A.T., E.H.N., Y.Y., Literature Search: A.T., R.A., E.H.N., Y.Y., Writing: A.T., Y.Y.

Conflict of Interest: No conflict of interest was declared by the authors.

Financial Disclosure: The authors declared that this study has received no financial support.

References

1. Wong CS, Gong N, Chu YC, Anthony MP, Chan Q, Lee HF, Chu KM, Khong PL. Correlation of measurements from diffusion weighted MR imaging and FDG PET/CT in GIST patients: ADC versus SUV. Eur J Radiol. 2012;81:2122-2126.
2. Schulz A, Viktil E, Godt JC, Johansen CK, Dormagen JB, Holtedahl JE, Labori KJ, Bach-Gansmo T, Kløw NE. Diagnostic performance of CT, MRI and PET/CT in patients with suspected colorectal liver metastases: the superiority of MRI. Acta Radiol. 2016;57:1040-1048.
3. Gu J, Khong PL, Wang S, Chan Q, Law W, Zhang J. Quantitative assessment of diffusion-weighted MR imaging in patients with primary rectal cancer: correlation with FDG-PET/CT. Mol Imaging Biol. 2011;13:1020-1028.
4. Tyng CJ, Guimarães MD, Bitencourt AGV, Etchebehere ECSC, Souza JA, Costa FP, Bastos CR, Marchiori E, Muglia VF. Correlation of the ADC values assessed by diffusion-weighted MRI and 18F–FDG PET/CT SUV in patients with lung cancer. Appl Cancer Res. 2018;38:9.
5. Usuda K, Funasaki A, Sekimura A, Motono N, Matoba M, Doai M, Yamada S, Ueda Y, Uramoto H. FDG-PET/CT and diffusion-weighted

imaging for resected lung cancer: correlation of maximum standardized uptake value and apparent diffusion coefficient value with prognostic factors. Med Oncol. 2018;35:66.

6. Kitajima K, Yamano T, Fukushima K, Miyoshi Y, Hirota S, Kawanaka Y, Miya M, Doi H, Yamakado K, Hirota S. Correlation of the SUVmax of FDG-PET and ADC values of diffusion-weighted MR imaging with pathologic prognostic factors in breast carcinoma. Eur J Radiol. 2016;85:943-949.
7. Ippolito D, Monguzzi L, Guerra L, Deponti E, Gardani G, Messa C, Sironi S. Response to neoadjuvant therapy in locally advanced rectal cancer: assessment with diffusion-weighted MR imaging and 18FDG PET/CT. Abdom Imaging. 2012;37:1032-1040.
8. Chen X, Cai Q, Xia J, Huang H, Li Z, Song K, Jia N, Liu W. Liver Imaging Reporting and Data System (LI-RADS) v2018: differential diagnostic value of ADC values for benign and malignant nodules with moderate probability (LR-3). Front Oncol. 2023;13:1186290.
9. Watanabe A, Harimoto N, Yokobori T, Araki K, Kubo N, Igarashi T, Tsukagoshi M, Ishii N, Yamanaka T, Handa T, Oyama T, Higuchi T, Shirabe K. FDG-PET reflects tumor viability on SUV in colorectal cancer liver metastasis. Int J Clin Oncol. 2020;25:322-329.
10. Galea N, Cantisani V, Taouli B. Liver lesion detection and characterization: role of diffusion-weighted imaging. J Magn Reson Imaging. 2013;37:1260-1276.
11. Sobeh T, Inbar Y, Apter S, Soffer S, Anteby R, Kraus M, Konen E, Klang E. Diffusion-weighted MRI for predicting and assessing treatment response of liver metastases from CRC- A systematic review and meta-analysis. Eur J Radiol. 2023;163:110810.
12. Rakheja R, Chandarana H, DeMello L, Jackson K, Geppert C, Faul D, Glielmi C, Friedman KP. Correlation between standardized uptake value and apparent diffusion coefficient of neoplastic lesions evaluated with whole-body simultaneous hybrid PET/MRI. AJR Am J Roentgenol. 2013;201:1115-1119.
13. Freihat O, Zoltán T, Pinter T, Kedves A, Sipos D, Repa I, Kovács Á, Zsolt C. Correlation between tissue cellularity and metabolism represented by diffusion-weighted imaging (DWI) and 18F-FDG PET/MRI in head and neck cancer (HNC). Cancers (Basel). 2022;14:847.
14. Theruvath AJ, Siedek F, Muehe AM, Garcia-Diaz J, Kirchner J, Martin O, Link MP, Spunt S, Pribnow A, Rosenberg J, Herrmann K, Gatidis S, Schäfer JF, Moseley M, Umutlu L, Daldrup-Link HE. Therapy response assessment of pediatric tumors with whole-body diffusion-weighted MRI and FDG PET/MRI. Radiology. 2020;296:143-151.
15. Choi BB, Kim SH, Kang BJ, Lee JH, Song BJ, Jeong SH, Yim HW. Diffusion-weighted imaging and FDG PET/CT: predicting the prognoses with apparent diffusion coefficient values and maximum standardized uptake values in patients with invasive ductal carcinoma. World J Surg Oncol. 2012;10:126.
16. Miyake KK, Nakamoto Y, Kanao S, Tanaka S, Sugie T, Mikami Y, Toi M, Togashi K. Journal Club: Diagnostic value of (18)F-FDG PET/CT and MRI in predicting the clinicopathologic subtypes of invasive breast cancer. AJR Am J Roentgenol. 2014;203:272-279.
17. Baba S, Isoda T, Maruoka Y, Kitamura Y, Sasaki M, Yoshida T, Honda H. Diagnostic and prognostic value of pretreatment SUV in 18F-FDG/PET in breast cancer: comparison with apparent diffusion coefficient from diffusion-weighted MR imaging. J Nucl Med. 2014;55:736-742.
18. Nakajo M, Kajiya Y, Kaneko T, Kaneko Y, Takasaki T, Tani A, Ueno M, Koriyama C, Nakajo M. FDG PET/CT and diffusion-weighted imaging for breast cancer: prognostic value of maximum standardized uptake values and apparent diffusion coefficient values of the primary lesion. Eur J Nucl Med Mol Imaging. 2010;37:2011-2020.
19. Byun BH, Noh WC, Lim I, Lee SS, Cho AR, Park JA, Kim KM, Kim HA, Kim EK, Kim BI, Choi CW, Lim SM. A new method for apparent diffusion coefficient measurement using sequential (18)F-FDG PET and MRI: correlation with histological grade of invasive ductal carcinoma of the breast. Ann Nucl Med. 2013;27:720-728.
20. Ho KC, Lin G, Wang JJ, Lai CH, Chang CJ, Yen TC. Correlation of apparent diffusion coefficients measured by 3T diffusion-weighted MRI and SUV from FDG PET/CT in primary cervical cancer. Eur J Nucl Med Mol Imaging. 2009;36:200-208.
21. Jeong JH, Cho IH, Chun KA, Kong EJ, Kwon SD, Kim JH. Correlation between apparent diffusion coefficients and standardized uptake values in hybrid (18)F-FDG PET/MR: Preliminary results in rectal cancer. Nucl Med Mol Imaging. 2016;50:150-156.
22. Stein D, Goldberg N, Domachevsky L, Bernstine H, Nidam M, Abadi-Korek I, Guindy M, Sosna J, Groshar D. Quantitative biomarkers for liver metastases: comparison of MRI diffusion-weighted imaging heterogeneity index and fluorine-18-fluoro-deoxyglucose standardised uptake value in hybrid PET/MR. Clin Radiol. 2018;73:832.
23. Boussouar S, Itti E, Lin SJ, Decaens T, Evangelista E, Chiaradia M, Chalaye J, Baranes L, Calderaro J, Laurent A, Pigneur F, Duvoux C, Azoulay D, Costentin C, Rahmouni A, Luciani A. Functional imaging of hepatocellular carcinoma using diffusion-weighted MRI and (18) F-FDG PET/CT in patients on waiting-list for liver transplantation. Cancer Imaging. 2016;16:4.

Interesting Image

Mol Imaging Radionucl Ther 2025;34:55-57 *DOI:10.4274/mirt.galenos.2024.61214*

A Rare Case of Triple Primary Malignant Neoplasms (RCC and Colon Cancer) Detected by ^{18}F-FDG PET/CT

^{18}F-FDG PET/BT ile Tespit Edilen Nadir Bir Üçlü Primer Malign Neoplazm (RCC ve Kolon Kanseri) Olgusu

Petya Nikolova, Valeria Hadzhiyska, Yavor Gramatikov, Stefani Veneva, Georgi Gaydarov, Elena Raycheva, Mihaela Ilcheva

Alexandrovska University Hospital, Department of Nuclear Medicine, Sofia, Bulgaria

Abstract

Multiple primary malignancies are not uncommon in daily oncology practice, even though their frequency in the same or different organ systems varies. Regardless, early detection and proper planning of therapeutic approaches are essential for successful management. Here, we present a 73-years-old male with adenocarcinoma of the sigmoid who was referred for initial staging with ^{18}F-fluorodeoxyglucose (^{18}F-FDG) positron emission tomography/computed tomography (PET/CT). ^{18}F-FDG PET/CT revealed two metabolically active formations in the sigmoid and ascending colon and a large, heterogeneous tumor lesion in the middle and lower third of the left kidney, with increased ^{18}F-FDG uptake in soft tissue components, suggesting the presence of synchronous neoplasms. The scan also showed ^{18}F-FDG-positive multiple metabolically active lytic bone lesions with soft tissue components, small pulmonary nodules, and mediastinal/hilar lymph nodes with mildly elevated metabolic activity, suggesting secondary foci. Considering these findings, the patient was referred for histological evaluation.

Keywords: ^{18}F-FDG PET/CT, synchronous tumors, colon cancer, renal cell carcinoma

Öz

Çoklu primer maligniteler, aynı veya farklı organ sistemlerinde görülme sıklıkları farklılık gösterse de, günlük onkoloji pratiğinde nadir görülen bir durum değildir. Ne olursa olsun, başarılı bir yönetim için erken teşhis ve terapötik yaklaşımların uygun şekilde planlanması önemlidir. Burada, ^{18}F-florodeoksiglukoz (^{18}F-FDG) pozitron emisyon tomografisi/bilgisayarlı tomografi (PET/BT) ile ilk evreleme için yönlendirilen, sigmoid adenokarsinomlu 73 yaşında bir erkek hastayı sunuyoruz. ^{18}F-FDG PET/BT, yumuşak doku bileşenlerinde artan ^{18}F-FDG alımı ile senkronize neoplazmların varlığını düşündüren, sigmoid ve çıkan kolonlarda metabolik olarak aktif iki oluşumu ve sol böbreğin orta ve alt üçte birlik kısmında büyük, heterojen bir tümöral lezyonu ortaya çıkardı. Taramada ayrıca ikincil odakları düşündüren, yumuşak doku bileşenleri içeren ^{18}F-FDG-pozitif çoklu metabolik olarak aktif litik kemik lezyonları, küçük pulmoner nodüller ve hafif derecede yüksek metabolik aktiviteye sahip mediastinal/hiler lenf düğümleri görüldü. Bu bulgular dikkate alınarak hasta histolojik değerlendirmeye yönlendirildi.

Anahtar kelimeler: ^{18}F-FDG PET/BT, senkron tümörler, kolon kanseri, renal hücreli karsinom

Address for Correspondence: Petya Nikolova MD, Alexandrovska University Hospital, Department of Nuclear Medicine, Sofia, Bulgaria
E-mail: petia.nn@abv.bg **ORCID ID:** orcid.org/0000-0001-9200-3708
Received: 13.02.2024 **Accepted:** 14.05.2024 **Publication Date:** 07.02.2025

Cite this article as: Nikolova P, Hadzhiyska V, Gramatikov Y, Veneva S, Gaydarov G, Raycheva G, Ilcheva M. A rare case of triple primary malignant neoplasms (RCC and colon cancer) detected by ^{18}F-FDG PET/CT. Mol Imaging Radionucl Ther. 2025;34:55-57.

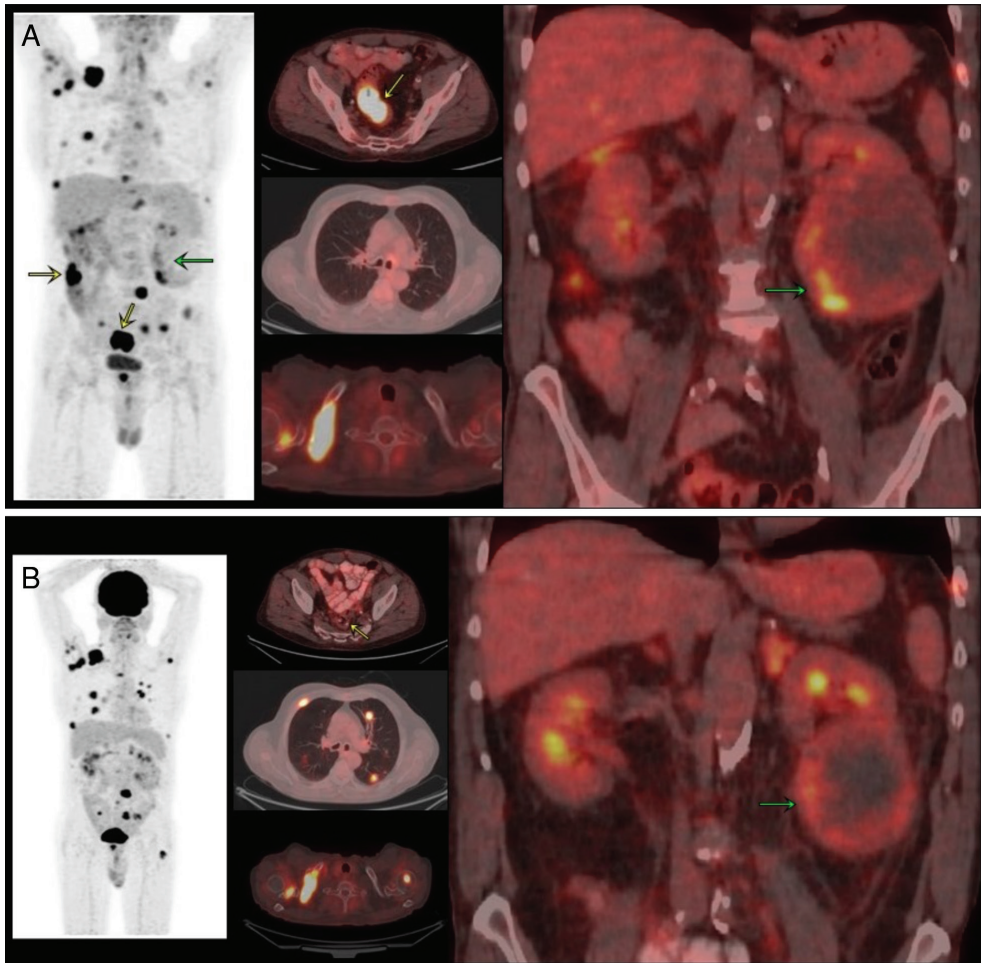

Figure 1. A) A 73-year-old man was referred for staging with ^{18}F-fluorodeoxyglucose (^{18}F-FDG) positron emission tomography/computed tomography (PET/CT) due to adenocarcinoma of the sigmoid colon. MIP and fusion images show two ^{18}F-FDG-avid soft-tissue formations in the sigmoid and ascending colon [maximum standardized uptake value (SUV_{max}): 47.9]-yellow arrows. Also, a large and heterogeneous formation in the middle and lower third of the left kidney (87x95 mm), with increased ^{18}F-FDG uptake in the soft tissue components of the lesion (SUV_{max}: 8.6) - green arrow. The scan showed multiple metabolically active lytic bone lesions with soft tissue components - e.g., in the right clavicle, SUV_{max}: 15.8. ^{18}F-FDG-negative small pulmonary nodules and mediastinal/hilar lymph nodes with mildly elevated metabolic activity were suspected as secondary foci. Considering these findings, the patient was referred for histological evaluation. The patient underwent surgery for the primary colonic lesions and partial resection of the tumor formation in the kidney. Given the low incidence of bone metastasis from colon carcinoma, even in the setting of a high initial T stage, as well as the macromorphological appearance of bone lesions, the latter was assumed to be associated with renal carcinoma. The registered lung nodules were left for observation due to their small size and lack of increased glucose metabolism on staging PET/CT. Multiple primary malignancies are increasingly seen in daily oncology practice, even though their frequency in the same or different organ systems is variable, ranging from 2% to 17% (1). Given the relatively low incidence of renal cell and colon carcinoma, reported at approximately 3.8% and 8.2% of total cancer cases diagnosed each year (2), the clinical scenario of co-occurring cancer is quite rare. According to the literature, in most cases, renal cell carcinoma (RCC) is associated with other primary malignancies, including prostate, bladder, and rectal cancers, as well as non-Hodgkin's lymphoma (3). Regardless of the overall incidence of synchronous cancers, the most frequent occurrence is observed in the presence of initial colon/rectum in 2-5% of patients, followed by breast, lung, prostate, and urinary bladder tumors (4,5). Particularly in obstructive cancers, ^{18}F-FDG PET/CT could be a valuable method for detecting synchronous colon tumors, with a high negative predictive value of 96.7% and accuracy of 87.5% (6). Diagnosis of second or more primary malignancies in patients with known cancer may be of significant importance for further therapeutic management (7) and can also accurately assess therapeutic response. In conclusion, PET/CT is a valuable hybrid technology that can more easily differentiate synchronous or metachronous tumors due to the combination of whole-picture visualization along with the different ^{18}F-FDG uptake patterns in oncological diseases. B) Follow-up ^{18}F-FDG PET/CT was performed after anterior rectal resection, transrectal polypectomy, and left kidney resection. Histological report was positive for 1. moderately differentiated adenocarcinoma of the rectum, pT3 pN0 LV0 Pn+ R0; 2. moderately differentiated adenocarcinoma of the cecum, pT1Nx, LV0 R0. 3. RCC, clear cell variant. The patient received targeted and osteomodulator therapy (sunitinib and denosumab). The MIP and axial and coronal fusion images of the follow-up scan show the metabolic and morphological progressive course of the disease, mainly involving lung and bone dissemination and persistence of metabolically active tumor formation with reduced size (due to partial resection).

Ethics

Informed Consent: Institutional review board approval was not required. Informed consent was obtained from each participant.

Footnotes

Authorship Contributions

Concept: P.N., V.H., Design: P.N., V.H., G.G., M.I., Data Collection or Processing: Y.G., S.V., G.G., E.R., Analysis or Interpretation: G.G., E.R., M.I., Literature Search: Y.G., S.V., G.G., Writing: P.N., V.H., M.I.

Conflict of Interest: No conflicts of interest were declared by the authors.

Financial Disclosure: The authors declare that this study has received no financial support.

References

1. Vogt A, Schmid S, Heinimann K, Frick H, Herrmann C, Cerny T, Omlin A. Multiple primary tumours: challenges and approaches, a review. ESMO Open. 2017;2:e000172.
2. Howlader N, Noone AM, Krapcho M, Garshell J, Miller D, Altekruse SF, Kosary CL, Yu M, Ruhl J, Tatalovich Z,Mariotto A, Lewis DR, Chen HS, Feuer EJ, Cronin KA (eds). SEER Cancer Statistics Review, 1975-2011, National Cancer Institute. Bethesda, MD, https://seer.cancer.gov/archive/csr/1975_2011/, based on November 2013 SEER data submission, posted to the SEER web site, April 2014. http://seer.cancer.gov/csr/1975_2011.
3. Rabbani F, Grimaldi G, Russo P. Multiple primary malignancies in renal cell carcinoma. J Urol. 1998;160:1255-1259.
4. Ringland CL, Arkenau HT, O'Connell DL, Ward RL. Second primary colorectal cancers (SPCRCs): experiences from a large Australian Cancer Registry. Ann Oncol. 2010;21:92-97.
5. Hayat MJ, Howlader N, Reichman ME, Edwards BK. Cancer statistics, trends, and multiple primary cancer analyses from the Surveillance, Epidemiology, and End Results (SEER) Program. Oncologist. 2007;12:20-37.
6. Maeda C, Endo S, Mori Y, Mukai S, Hidaka E, Ishida F, Kudo SE. The ability of positron emission tomography/computed tomography to detect synchronous colonic cancers in patients with obstructive colorectal cancer. Mol Clin Oncol. 2019;10:425-429.
7. Chun-Sing W, Nan-Jie G, Yiu-Ching C. Prevalence of synchronous second primary malignancy: identification using whole body PET/CT imaging. Clin Imaging. 2014;38:179-186.

Interesting Image

Mol Imaging Radionucl Ther 2025;34:58-60 *DOI:10.4274/mirt.galenos.2024.74875*

A Rare Malignancy; Primary Peritoneal Serous Carcinoma in Men with ^{18}F-FDG PET/CT and Histopathology

Nadir Bir Olgu; Histopatoloji ve ^{18}F-FDG PET/BT'de Erkek Primer Peritoneal Seröz Karsinomu

Büşra Özdemir Günay[1], Burak Günay[2], Nuray Can[3], Funda Üstün[4]

[1]Giresun Training and Research Hospital, Clinic of Nuclear Medicine, Giresun, Türkiye
[2]Kırklareli Training and Research Hospital, Clinic of Radiology, Kırklareli, Türkiye
[3]Trakya University Faculty of Medicine, Department of Pathology, Edirne, Türkiye
[4]Trakya University Faculty of Medicine, Department of Nuclear Medicine, Edirne, Türkiye

Abstract

Primary peritoneal serous carcinoma (PPSC) is a rare malignancy that mostly affects women. In males, there are only few reports in the literature. ^{18}F-fluorodeoxyglucose (^{18}F-FDG) positron emission tomography/computed tomography (PET/CT) is useful for evaluating the origin of the tumor, its extent, and distant metastasis. Moreover, ^{18}F-FDG PET/CT was helpful in distinguishing between PPSC and peritoneal carcinomatosis. We present a case of PPSC on ^{18}F-FDG PET/CT in a male with histopathological correlation.

Keywords: Peritoneal tumour, primary peritoneal serous carcinoma, ^{18}F-FDG PET/CT

Öz

Primer peritoneal seröz karsinom (PPSK) erkeklerde oldukça nadir görülen bir malignite olup ^{18}F-florodeoksiglukoz (^{18}F-FDG) pozitron emisyon tomografisi/bilgisayarlı tomografi (PET/BT) tümörün primer/sekonder ayrımında, hastalık yaygınlığının belirlenmesinde rol oynamaktadır. Tanıda histopatoloji ve görüntüleme birlikte değerlendirilir. Bu olguda PPSK tanısı olan bir erkek hastanın PET/BT bulgularını ve patolojisini sunduk.

Anahtar kelimeler: Peritoneal tümör, primer peritoneal seröz karsinom, ^{18}F-FDG PET/BT

Address for Correspondence: Büşra Özdemir Günay MD, Giresun Training and Research Hospital, Clinic of Nuclear Medicine, Giresun, Türkiye
E-mail: busraozdemir39@gmail.com **ORCID ID:** orcid.org/0000-0001-8540-0115
Received: 25.03.2024 **Accepted:** 05.06.2024 **Publication Date:** 07.02.2025

Cite this article as: Özdemir Günay B, Can N, Üstün F. A rare malignancy; primary peritoneal serous carcinoma in men with ^{18}F-FDG PET/CT and histopathology Mol Imaging Radionucl Ther. 2025;34:58-60.

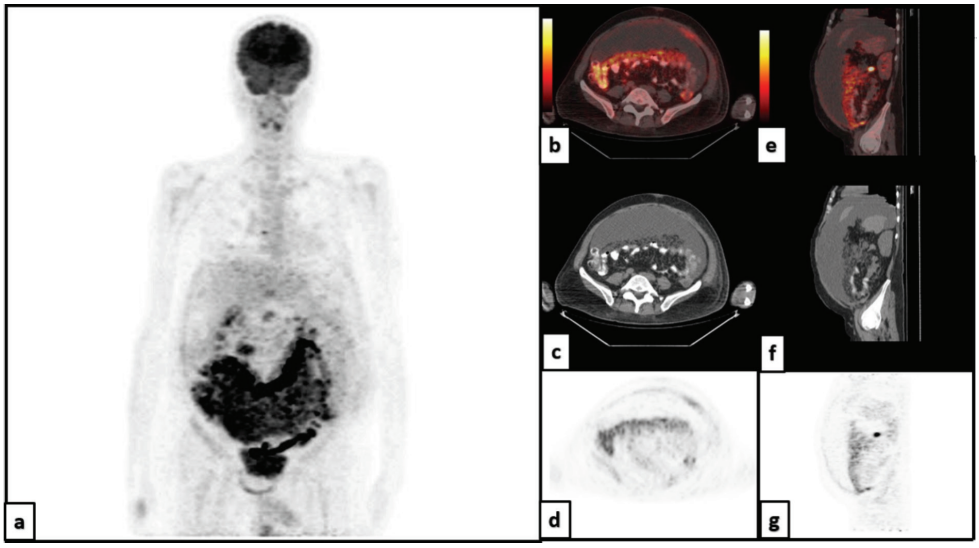

Figure 1. A 60-year-old man was admitted to the emergency department with progressive abdominal distention, and clinical assessment revealed the presence of ascites. Abdominal computed tomography showed peritoneal thickenings suggestive of peritoneal carcinomatosis. While undergoing gastro-colonoscopy and a testicular examination, the patient was referred to the nuclear medicine department for ^{18}F-fluorodeoxyglucose (^{18}F-FDG) positron emission tomography/computed tomography (PET/CT) and the radiology department for abdominal CT and magnetic resonance imaging (MRI) due to clinical suspicion of metastases. Maximum intensity projection (a) images, transaxial (b, c, d) sagittal (e, f, g) slices of fusion, and CT and PET/CT images of the abdomen showed multiple mild to moderate hypermetabolic nodular peritoneal thickening in the omentum and heterogeneity of the transverse mesocolon highly suggestive of peritoneal cancer with maximum standardized uptake value: 6.3. There was no other pathological finding in the rest of the body. True-cut biopsy was performed for the diagnosis and management of the therapy.

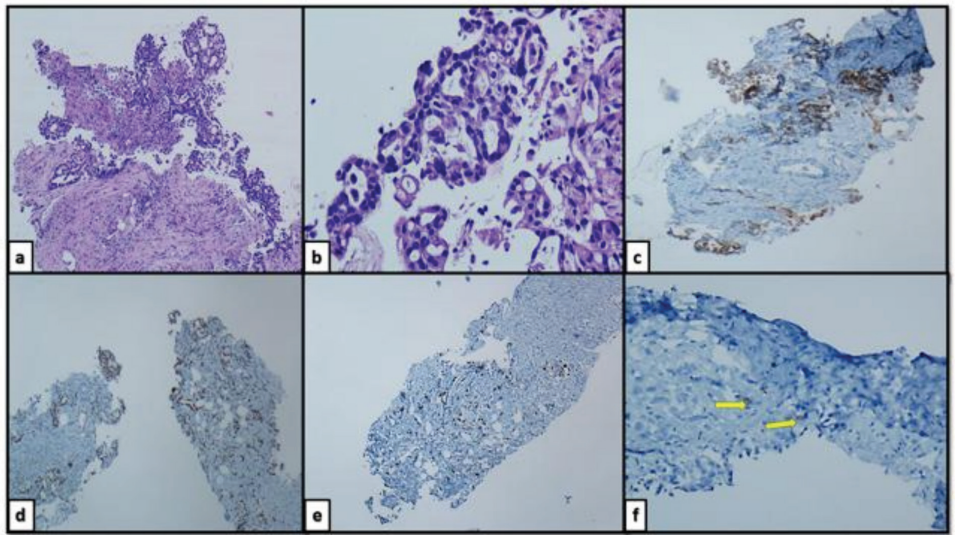

Figure 2. Histopathologic examination of a malignant epithelial tumor with cribriform architecture (a; hematoxylin & eosin x100, b; hematoxylin & eosin x400), diffuse p16 immune expression (c; immune peroxidase x100) and abnormal pattern of p53 observed in the tumor (d; immune peroxidase x200). A high proliferation index with Ki-67 (e; immune peroxidase x200) and increased mitotic activity in the tumor with PHH3 immunohistochemical staining (f; immune peroxidase x400) was noted. CK7, ESA, and CA 19.9 were positive; CDX2, SATB2, TTF1, CK20, HBME-1, calretinin, D2-40, B72.3, and ER were negative. P16 immunoexpression was diffuse and strong. An abnormal pattern of p53 immunoexpression (positivity in >80% cells) was observed. The current histopathological findings, together with clinical and radiological findings, were evaluated in favor of primary peritoneal serous carcinoma. Primary peritoneal serous carcinoma (PPSC) is a rare epithelial tumor that occurs almost exclusively in women (1,2). The male: female ratio ranged from 0.0018 to 0.0045 (3). There are only a few case reports of PPSC developing in men (4). Histopathological and cytological characteristics of these tumors are similar to those of epithelial ovarian cancer (2). Therefore, in addition to histopathological examination and imaging, ovarian cancer must be ruled out during diagnosis. Imaging methods such as CT, MRI, and PET/CT are used to confirm diagnosis, differentiate between primary peritoneal cancer and peritoneal metastasis, and determine the spread of the disease (5). Although not sufficient for diagnosis, ^{18}F-FDG PET/CT can assist in distinguishing between PPSC and peritoneal karsinomatosis (6). ^{18}F-FDG PET/CT is useful in evaluating the origin of the tumor, its extent, and distant metastasis (3).

Ethics

Informed Consent: Patient consent was obtained.

Footnotes

Authorship Contributions

Surgical and Medical Practices: B.Ö.G., B.G., F.Ü., Concept: N.C., F.Ü., Design: B.G., Data Collection or Processing: B.Ö.G., Analysis or Interpretation: B.G., N.C., Literature Search: B.Ö.G., Writing: B.Ö.G., F.Ü.

Conflict of Interest: No conflicts of interest were declared by the authors.

Financial Disclosure: The authors declare that this study has received no financial support.

References

1. Neuhausen SL, Shani H, Boker LK, Steele L, Silverman BG, Ottini L, Silvestri V, Laitman Y, Korach J, Perri T, Friedman E. Primary peritoneal serous carcinoma in men: A rare and non-BRCA-associated entity. Anticancer Res. 2017;37:3069-3072.
2. Levy AD, Arnáiz J, Shaw JC, Sobin LH. From the archives of the AFIP: primary peritoneal tumors: imaging features with pathologic correlation. Radiographics. 2008;28:583-607.
3. Guellil A, Jabi R, Mabrouk MY, Bouzayan L, Merhoum A, Del Gallo G, Godart C, Bouziane M. Primary peritoneal high-grade serous carcinoma in a man: A case report. Ann Med Surg (Lond). 2022;77:103605.
4. Gan J, Herzog J, Smith DA, Vos D, Kikano E, Tirumani SH, Ramaiya NH. Primary peritoneal serous carcinoma: a primer for radiologists. Clin Imaging. 2022;83:56-64.
5. Turlakow A, Yeung HW, Salmon AS, Macapinlac HA, Larson SM. Peritoneal carcinomatosis: role of (18)F-FDG PET. J Nucl Med. 2003;44:1407-1412.
6. Yun WS, Bae JM. Primary peritoneal serous carcinoma, an extremely rare malignancy: A case report and review of the literature. Oncol Lett. 2016;11:4063-4065.

Interesting Image

Mol Imaging Radionucl Ther 2025;34:61-63 *DOI:10.4274/mirt.galenos.2024.26486*

Diagnosis of Atypical Medullary Metastasis in Melanoma Using ^{18}F-FDG PET/CT

^{18}F-FDG PET/CT Kullanılarak Melanoma Bağlı Atipik Medüller Metastaz Tanısı Konması

Chaymae Bensaid, Salah Oueriagli Nabih, Kenza Bouzidi, Omar Ait Sahel, Yassir Benameur, Abderrahim Doudouh

Mohammed V Military Training Hospital, Clinic of Nuclear Medicine, Rabat, Morocco

Abstract

As part of the therapeutic evaluation, positron emission tomography/computed tomography (PET/CT) using ^{18}F-fluorodeoxyglucose (^{18}F-FDG) was performed on a 39-year-old patient with metastatic melanoma of the left thigh who was subsequently receiving immunotherapy. The examination revealed pathologic hypermetabolic foci in the lymph nodes and liver along with a highly suspicious pathologic hypermetabolic foci in the spinal marrow at the level of the first lumbar vertebra (L1). The presence of such a hypermetabolic focus can significantly decrease survival duration, highlighting the importance of early detection. PET/CT with ^{18}F-FDG proved to be more sensitive and specific than CT alone in identifying occult distant metastases, as the latter may underestimate malignant involvement of the spinal marrow.

Keywords: PET-^{18}F-FDG, melanoma, spinal marrow, metastasis

Öz

Terapötik değerlendirmenin bir parçası olarak, sol uylukta metastatik melanomu olan ve daha sonra immünoterapi alan 39 yaşındaki bir hastaya ^{18}F-florodeoksiglukoz (^{18}F-FDG) kullanılarak pozitron emisyon tomografisi/bilgisayarlı tomografi (PET/BT) uygulandı. Tetkik sonucunda lenf düğümleri ve karaciğerde patolojik hipermetabolik odakların yanı sıra, birinci lomber vertebra (L1) seviyesinde omurilik iliğinde oldukça şüpheli patolojik hipermetabolik odaklar ortaya çıktı. Böyle bir hipermetabolik odağın varlığı, sağkalım süresini önemli ölçüde azaltabilir ve bu da erken teşhisin önemini vurgular. ^{18}F-FDG'li PET/BT'nin, gizli uzak metastazları belirlemede tek başına BT'den daha duyarlı ve spesifik olduğu kanıtlanmıştır; zira BT, omurilikteki malign tutulumu saptayamayabilir.

Anahtar kelimeler: PET-^{18}F-FDG, melanom, spinal kemik iliği, metastaz

Address for Correspondence: Chaymae Bensaid MD, Mohammed V Military Training Hospital, Clinic of Nuclear Medicine, Rabat, Morocco
E-mail: chamabensaid@gmail.com **ORCID ID:** orcid.org/0009-0002-2164-0982
Received: 01.05.2024 **Accepted:** 05.06.2024 **Epub:** 17.07.2024 **Publication Date:** 07.02.2025

Cite this article as: Bensaid C, Nabih SO, Bouzidi K, Sahel OA, Benameur Y, Doudouh A. Diagnosis of atypical medullary metastasis in melanoma using ^{18}F-FDG PET/CT. Mol Imaging Radionucl Ther. 2025;34:61-63.

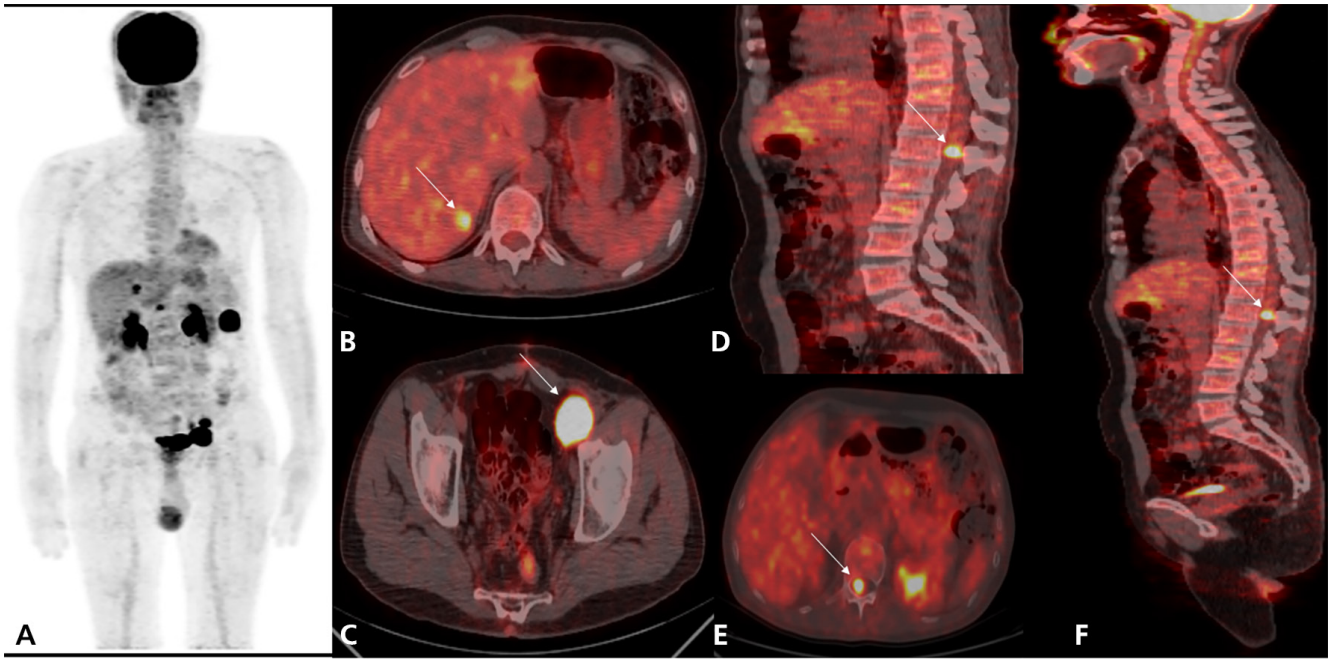

Figure 1. A 39-year-old patient underwent initial surgery in 2019 for melanoma of the left thigh, which was stage 4, followed by secondary surgery for metastatic left inguinal lymphadenopathy. Subsequently, the patient experienced pelvic lymph node recurrence and was placed on immunotherapy with pembrolizumab. As part of the therapeutic evaluation, a positron emission tomography/computed tomography (PET/CT) scan with ^{18}F-fluorodeoxyglucose (^{18}F-FDG) was performed, which showed the physiological and pathological distribution of the radiopharmaceutical (^{18}F-FDG) (maximum intensity projection; A) and revealed scintigraphic progression consistent with persistent disease. This condition was characterized by an increase in size and intensity of the hypermetabolic pathological left external iliac lymph node, measuring 36x29 mm with a maximum standardized uptake value (SUV_{max}) of 27 (fusion image in axial section; arrow; C). Additionally, hypermetabolic pathological foci were observed, including one in segment VII of the liver with an SUV_{max} of 8.6 (fusion image in axial section; arrow; B), and a highly suspicious intense intramedullary focus at the level of the first lumbar vertebra with an SUV_{max} of 9.5 (fusion images in axial and sagittal sections; arrow; D; E; F).

Malignant melanoma is considered one of the most lethal cancers (1), with a poor prognosis once metastasized. A rare site of metastasis for melanoma is the heart, spleen, and spinal marrow, which can significantly reduce survival time, underscoring the importance of early detection (2). Follow-up examinations using ^{18}F-FDG PET/CT have been employed to assess intramedullary lesions, especially in tumors characterized by high-grade malignancy, such as melanoma (3), and ideally must be diagnosed early and confirmed through dedicated magnetic resonance imaging (2).

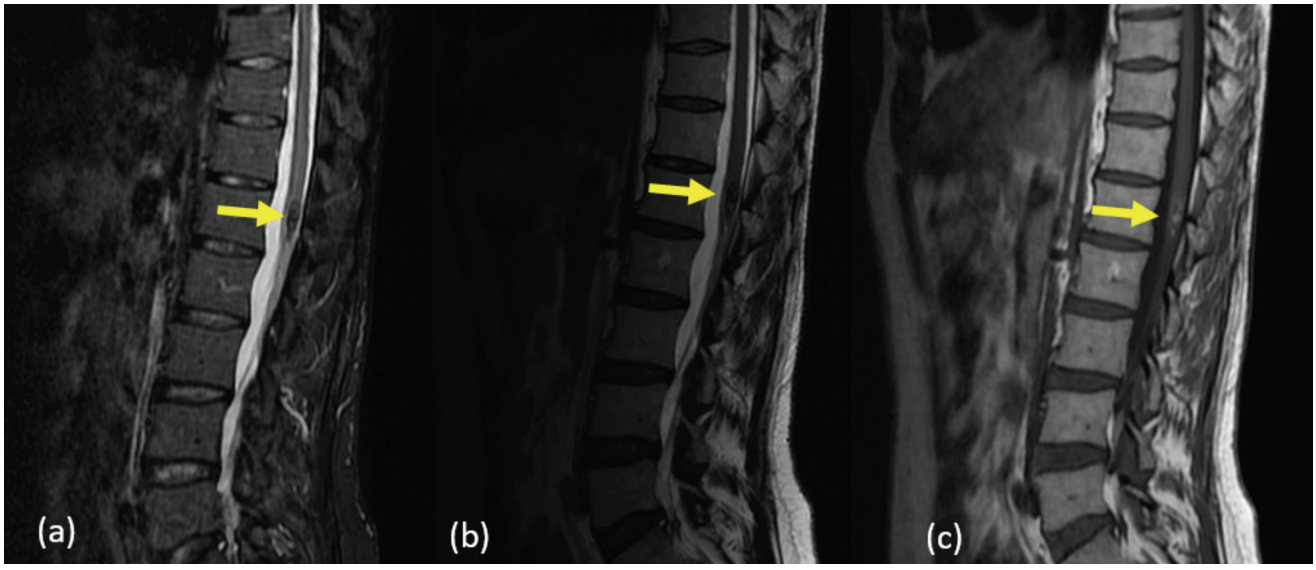

Figure 2. Our patient underwent spinal MRI in short T1 inversion recovery (STIR) sequence (a), in T2 weighting (b), and in T1 weighting without fat saturation (c), which revealed an intracanalicular, intramedullary lesion at the well-defined lobulated contours of the terminal cone at the level of the first lumbar vertebra in STIR and T2 hypointensity (sagittal section; arrow; a; b), and T1 hyperintensity (sagittal section; arrow; c), consistent with a secondary metastatic localization.

The disease course was characterized by the rapid onset of neurological symptoms a few months after diagnosis, followed by worsening and eventual demise.

Regular imaging follow-up is essential for monitoring therapeutic effectiveness and detecting new metastases in patients with malignant melanoma (4). However, there is significant variability in surveillance methods due to limited scientific data. Although no randomized trials have compared follow-up approaches with or without PET/CT imaging, a meta-analysis indicated PET/CT was superior to CT alone in identifying distant metastases, with higher sensitivity (86% vs. 63%) and specificity (91% vs. 78%) (2).

After conducting a comprehensive literature review, we found no similar cases of medullary metastasis from malignant melanoma demonstrated by PET/CT. To the best of our knowledge, we are the first case of this type. Our case highlights the role of ^{18}F-FDG PET/CT in the follow-up of metastatic melanoma by early diagnosis of spinal metastases, even before the onset of clinical symptoms. This underscores the importance of conducting further studies to compare the various imaging modalities used in the therapeutic assessment of metastatic malignant melanoma, particularly at atypical sites, as well as to evaluate their contributions.

Ethics

Informed Consent: Informed consents of the patient was obtained.

Footnotes

Authorship Contributions

Concept: C.B., S.O.N., K.B., O.A.S., Y.B., A.D., Design: C.B., S.O.N., O.A.S., Y.B., A.D., Data Collection or Processing: C.B., Analysis or Interpretation: C.B., S.O.N., A.D., Literature Search: C.B., Writing: C.B.

Conflict of Interest: No conflicts of interest were declared by the authors.

Financial Disclosure: The authors declare that this study has received no financial support.

References

1. Tsao H, Atkins MB, Sober AJ. Management of cutaneous melanoma. N Engl J Med. 2004;351:998-1012.
2. Vercellino L, Rivas A, Baroudjian B, Lebbé C, Merlet P. Role of FDG PET in the evaluation of locoregional and distant spread of melanoma staging. Nuclear Medicine. 2020;44:305-312.
3. Merhemic Z, Stosic-Opincal T, Thurnher MM. Neuroimaging of spinal tumors. Magn Reson Imaging Clin N Am. 2016;24:563-579.
4. Bier G, Hoffmann V, Kloth C, Othman AE, Eigentler T, Garbe C, La Fougère C, Pfannenberg C, Nikolaou K, Klumpp B. CT imaging of bone and bone marrow infiltration in malignant melanoma–challenges and limitations for clinical staging in comparison to 18FDG-PET/CT. Eur J Radiol. 2016;85:732-738.

Interesting Image

Mol Imaging Radionucl Ther 2025;34:64-65 *DOI:10.4274/mirt.galenos.2024.02259*

The Utility of ^{18}F-FDG PET/CT in Detecting Multiple Metastases in Papillary Renal Cell Carcinoma

Papiller Renal Hücreli Karsinomda Multipl Metastaz Saptanmasında ^{18}F-FDG PET/BT'nin Yararı

Melis Oflas, Duygu Has Şimşek, Serkan Kuyumcu, Murat Yılmaz Kıran, Yasemin Şanlı

İstanbul University, İstanbul Faculty of Medicine, Department of Nuclear Medicine, İstanbul, Türkiye

Abstract

The diagnostic performance of ^{18}F-fluorodeoxyglucose (^{18}F-FDG) positron emission tomography/computed tomography (PET/CT) for primary kidney tumors is limited. Nevertheless, ^{18}F-FDG PET/CT is valuable for staging renal cell carcinoma (RCC) when suspected metastases coexist, as one-third of patients with RCC have distant metastases upon diagnosis. Herein, we present a 53-year-old male patient with extensive ^{18}F-FDG-avid metastatic lesions and an ^{18}F-FDG-avid renal mass, which later revealed RCC.

Keywords: ^{18}F-FDG PET/CT, papillary renal cell carcinoma, metastasis, staging

Öz

Primer böbrek tümörlerinin tespitinde ^{18}F-florodeoksiglukoz (^{18}F-FDG) pozitron emisyon tomografisi/bilgisayarlı tomografinin (PET/BT) tanısal performansı sınırlıdır. Ancak, tanı anında renal hücreli karsinom (RCC) hastalarının üçte birinde uzak metastaz bulunduğundan dolayı metastaz şüphesi varlığında ^{18}F-FDG PET/BT, RCC evrelemesinde değerli bir yöntemdir. Burada; ^{18}F-FDG tutulumu gösteren yaygın metastazları bulunan ve ^{18}F-FDG tutulumu gösteren renal kitleden daha sonra RCC tanısı alan 53 yaşında erkek hasta sunulmuştur.

Anahtar kelimeler: ^{18}F-FDG PET/BT, papiller renal hücreli karsinom, metastaz, evreleme

Address for Correspondence: Melis Oflas MD, İstanbul University, İstanbul Faculty of Medicine, Department of Nuclear Medicine, İstanbul, Türkiye
E-mail: melis.oflas@istanbul.edu.tr **ORCID ID:** orcid.org/0000-0001-9796-3302
Received: 28.02.2024 **Accepted:** 05.06.2024 **Epub:** 17.07.2024 **Publication Date:** 07.02.2025

Cite this article as: Oflas M, Has Şimşek D, Kuyumcu S, Kıran MY, Şanlı Y. The utility of ^{18}F-FDG PET/CT in detecting multiple metastases in papillary renal cell carcinoma. Mol Imaging Radionucl Ther. 2025;34:64-65.

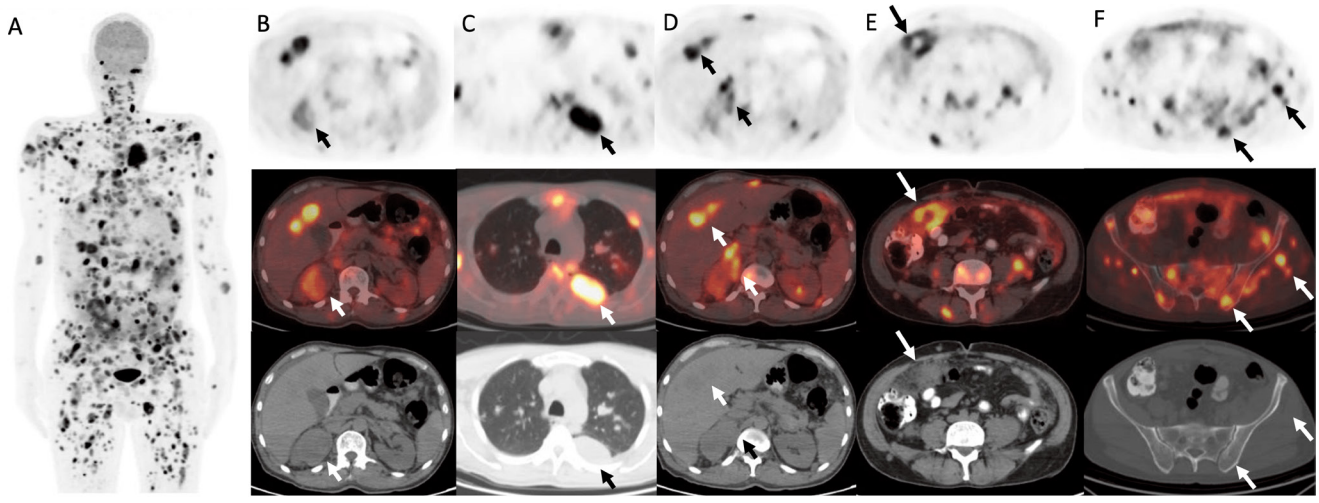

Figure 1. A 53-year-old male patient with no known comorbidity was admitted to the hospital with complaints of fever, night sweats, and fatigue for the last month. Upon detecting a suspicious mass in the right kidney and lung metastases on contrast-enhanced computed tomography (CT), ^{18}F-florodeoxyglucose (^{18}F-FDG) positron emission tomography (PET)/CT was performed (A) (1,2,3,4). In the PET/CT images, an exophytic localized renal mass in the upper pole of the right kidney exhibited increased ^{18}F-FDG uptake [maximum standardized uptake value (SUV_{max}): 5.5], which was considered suspicious for renal cell carcinoma (RCC) (B, arrows). In addition, multiple hypermetabolic parenchymal and pleural lesions in bilateral lungs (SUV_{max}: 11.9) (C, arrows), bilateral adrenal glands (SUV_{max}: 9.5) (D, arrows), liver parenchyma (SUV_{max}: 10.0) (D, arrows), peritoneum (SUV_{max}: 8.7), mesenterium (SUV_{max}: 13.1), and omentum (SUV_{max}: 11.1) (E, arrows), multiple bone metastases (SUV_{max}: 12.1), and soft tissue lesions in subcutaneous tissue and muscles (SUV_{max}: 14.6) (F, arrows). All lesions that could not be distinguished on CT images were distinguished on PET/CT images. A biopsy of the renal mass revealed papillary RCC (pRCC). A few days later, after pathological diagnosis, the patient was taken to the hospital because of worsening general condition and died in the intensive care unit due to hemodynamic deterioration. pRCC has a better outcome in localized disease than clear cell RCC (ccRCC). However, metastatic pRCC is associated with higher recurrence rates and lower survival than ccRCC (5). Moreover, various studies have reported that a higher SUV_{max} or presence of metastatic disease indicates shorter survival (6,7,8). Therefore, ^{18}F-FDG PET/CT is an efficient method for staging RCC, primarily for estimating the tumor load of metastatic disease.

Ethics

Informed Consent: Patient consent was obtained.

Authorship Contributions

Surgical and Medical Practices: M.O., M.Y.K., Concept: M.O., D.H.Ş., Y.Ş., Design: M.O., D.H.Ş., Y.Ş., Data Collection or Processing: M.O., M.Y.K., Analysis or Interpretation: M.O., S.K., Literature Search: M.O., S.K., Writing: M.O.

Conflict of Interest: No conflicts of interest were declared by the authors.

Financial Disclosure: The authors declare that this study has received no financial support.

References

1. Liu Y. The Place of FDG PET/CT in Renal cell carcinoma: value and limitations. Front Oncol. 2016;6:201.
2. Karivedu V, Jain AL, Eluvathingal TJ, Sidana A. Role of positron emission tomography imaging in metabolically active renal cell carcinoma. Curr Urol Rep. 2019;20:56.
3. Wang HY, Ding HJ, Chen JH, Chao CH, Lu YY, Lin WY, Kao CH. Meta-analysis of the diagnostic performance of [18F]FDG-PET and PET/CT in renal cell carcinoma. Cancer Imaging. 2012;12:464-474.
4. Mendhiratta N, Muraki P, Sisk AE Jr, Shuch B. Papillary renal cell carcinoma: review. Urol Oncol. 2021;39:327-337.
5. Connor Wells J, Donskov F, Fraccon AP, Pasini F, Bjarnason GA, Beuselinck B, Knox JJ, Rha SY, Agarwal N, Bowman IA, Lee JL, Pal SK, Srinivas S, Scott Ernst D, Vaishampayan UN, Wood LA, Simpson R, De Velasco G, Choueiri TK, Heng DYC. Characterizing the outcomes of metastatic papillary renal cell carcinoma. Cancer Med. 2017;6:902-909.
6. Xuan D, Wen W, Tian S, Piao M, Xu D, Liu L. Prognostic value of maximum standard uptake value, metabolic tumor volume, and total lesion glycolysis of 18F-FDG PET/CT in patients with renal carcinoma: a protocol for systematic review and meta analysis. Medicine (Baltimore). 2020;99:e19988.
7. Pankowska V, Malkowski B, Wedrowski M, Wedrowska E, Roszkowski K. FDG PET/CT as a survival prognostic factor in patients with advanced renal cell carcinoma. Clin Exp Med. 2019;19:143-148.
8. Wu C, Cui Y, Zhao Y, Chen X, Liao X, Di L, Yin L, Liu M, Wang R. Elevated tumor-to-liver standardized uptake value ratio (TLR) from preoperative 18F-FDG PET/CT predicts poor prognosis of patients with clear cell renal cell carcinoma after nephrectomy. Eur J Radiol. 2020;131:109218.

Interesting Image

Mol Imaging Radionucl Ther 2025;34:66-69 *DOI:10.4274/mirt.galenos.2024.96530*

A Rare Case of Synchronous Lobular Breast Carcinoma and Serous Psammocarcinoma of the Ovary Evaluated by ^{18}F-FDG PET/CT

^{18}F-FDG PET/BT ile Değerlendirilen Nadir Bir Senkron Lobüler Meme Karsinomu ve Over Seröz Psammokarsinomu Olgusu

Laure Al Mansour[1], Alexis Trecourt[2], Stela Asadurova[1], Anthime Flaus[1], Matthieu Dietz[1]

[1]Hospices Civils de Lyon, Service de Médecine Nucléaire, Lyon, France
[2]Hospices Civils de Lyon, Service de Pathologie Multi-Site, Lyon, France

Abstract

Serous psammocarcinoma of the ovary is a rare variant of ovarian serous carcinoma characterized by the presence of calcified peritoneal lesions, known as psammoma bodies. These calcified lesions may usually be considered benign on computed tomography but may show avidity for ^{18}F-fluorodeoxyglucose (^{18}F-FDG), which can be helpful in the diagnosis of this rare ovarian tumor. We present a rare case of serous psammocarcinoma of the ovary detected during the diagnostic work-up of lobular breast cancer using ^{18}F-FDG positron emission tomography/computed tomography.

Keywords: Psammocarcinoma, ovary, peritoneum, ^{18}F-FDG PET/CT

Öz

Overin seröz psammokarsinomu, psammoma cisimcikleri olarak bilinen kalsifiye peritoneal lezyonların varlığı ile karakterize edilen, over seröz karsinomunun nadir bir varyantıdır. Bu kalsifiye lezyonlar, bilgisayarlı tomografide genellikle iyi huylu olarak değerlendirilir ancak ^{18}F-florodeoksiglukoz (^{18}F-FDG) için avidite gösterebilir ve bu durum, bu nadir yumurtalık tümörünün tanısında yardımcı olabilir. Lobüler meme kanserinin tanısal incelemesi sırasında ^{18}F-FDG pozitron emisyon tomografisi/bilgisayarlı tomografi kullanılarak tespit edilen nadir bir over seröz psammokarsinomu olgusu sunulmuştur.

Anahtar kelimeler: Psammokarsinom, over, periton, ^{18}F-FDG PET/BT

Address for Correspondence: Matthieu Dietz MD, Hospices Civils de Lyon, Service de Médecine Nucléaire, Lyon, France
E-mail: matthieu.dietz@chu-lyon.fr **ORCID ID:** orcid.org/0000-0001-6041-2531
Received: 08.03.2024 **Accepted:** 23.06.2024 **Publication Date:** 07.02.2025

Cite this article as: Al Mansour L, Trecourt A, Asadurova S, Flaus A, Dietz M. A rare case of synchronous lobular breast carcinoma and serous psammocarcinoma of the ovary evaluated by ^{18}F-FDG PET/CT. Mol Imaging Radionucl Ther. 2025;34:66-69.

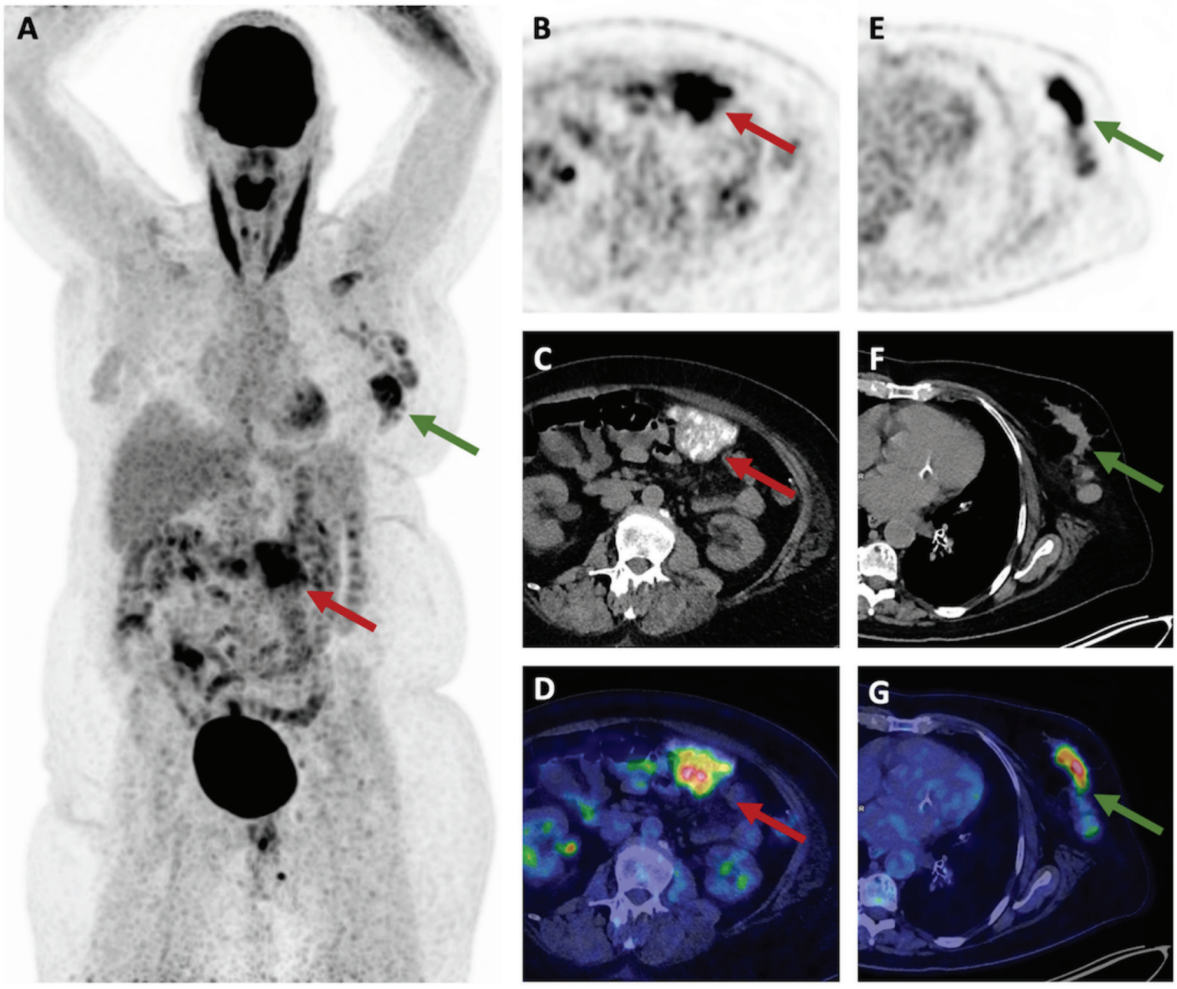

Figure 1. A 63-year-old woman underwent ^{18}F-fluorodeoxyglucose (^{18}F-FDG) positron emission tomography/computed tomography (PET/CT) for initial extension work-up of a lobular breast carcinoma. Maximum intensity projection (A), axial attenuation-corrected PET (E), transaxial CT (F), and fused PET/CT (G) images showing intense tracer uptake in the breast lesion (green arrows) associated with homolateral axillary lymph node involvement. Additionally, maximum intensity projection (A), axial attenuation-corrected PET (B), transaxial CT (C), and fused PET/CT (D) images revealed increased ^{18}F-FDG uptake by a large heavily calcified omental soft-tissue mass (red arrows), which was associated with less-FDG-avid disseminated calcified peritoneal lesions. Increased ^{18}F-FDG uptake in the calcified lesion was also observed in non-attenuation corrected images. No ovarian mass was detected.

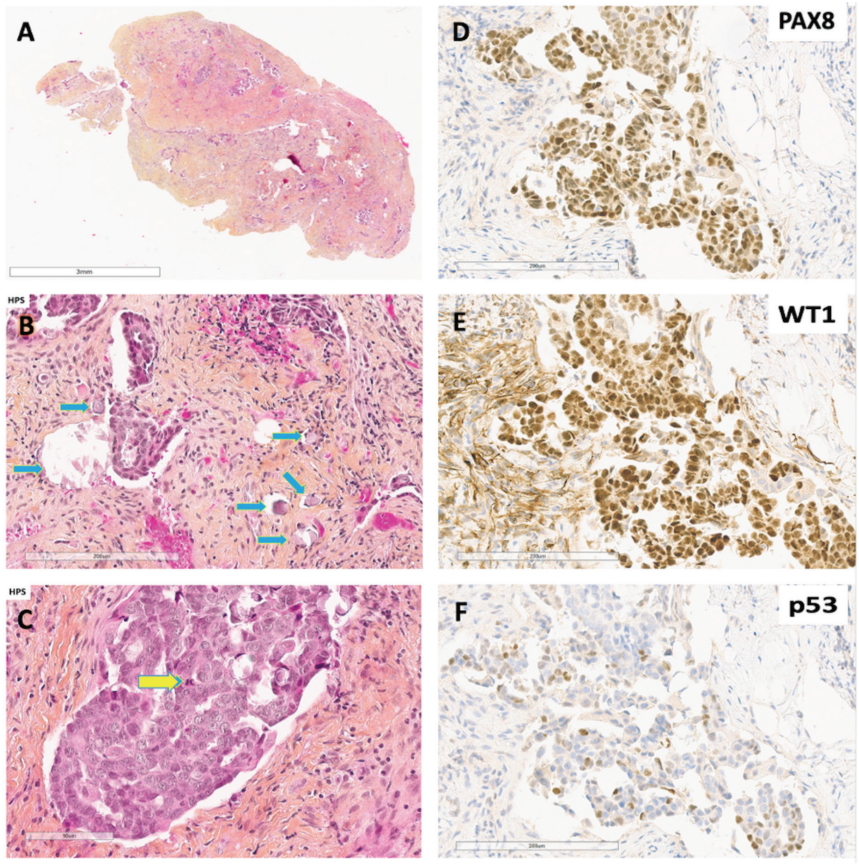

Figure 2. Histological examination of the peritoneal nodule revealed a desmoplastic stroma containing numerous tumor cell clusters [A, hematoxylin phloxine saffron staining (HES), x10 magnification]. At higher magnification (x180), clusters of tumor cells display micropapillary features and spherical, lamellated, concentric calcified structures corresponding to psammoma bodies (B, HES; blue arrows). Tumor cells were intermediate in size (C, HES; yellow arrow; x240 magnification). Immunohistochemical analysis showed intense and diffuse positivity for PAX8 and WT1, indicative of serous ovarian primary neoplasm (1). The expression of p53 was wild-type (D-F, magnification x200). The final diagnosis of this lesion was low-grade invasive serous carcinoma. The presence of psammoma bodies is characteristic of serous psammocarcinoma of the ovary, a rare variant of ovarian serous carcinoma (2,3,4). Low-grade serous carcinoma has a better prognosis (5,6,7). Calcified peritoneal lesions visualized on CT are explained by the presence of fine calcium particles in psammoma bodies (8,9). These lesions appear to show avidity for ^{18}F-FDG, although only a limited number of cases have been reported on ^{18}F-FDG PET/CT imaging (10,11,12,13). The visualization of a calcified lesion on conventional CT can be falsely reassuring, leading to misdiagnosis (14). This case reinforces the idea that ^{18}F-FDG PET/CT is useful for the diagnosis of this rare type of ovarian tumor.

Ethics

Informed Consent: A written informed consent was obtained.

Authorship Contributions

Concept: L.A.M., M.D., Design: L.A.M., M.D., Data Collection or Processing: L.A.M., A.T., S.A., A.F., M.D., Analysis or Interpretation: L.A.M., A.T., M.D., Literature Search: L.A.M., M.D., Writing: L.A.M., M.D.

Conflict of Interest: No conflicts of interest were declared by the authors.

Financial Disclosure: The authors declare that this study has received no financial support.

References

1. Liliac L, Carcangiu ML, Canevari S, Căruntu ID, Ciobanu Apostol DG, Danciu M, Onofriescu M, Amălinei C. The value of PAX8 and WT1 molecules in ovarian cancer diagnosis. Rom J Morphol Embryol. 2013;54:17-27.
2. Gilks CB, Bell DA, Scully RE. Serous psammocarcinoma of the ovary and peritoneum. Int J Gynecol Pathol. 1990;9:110-121.
3. Alanbay I, Dede M, Ustün Y, Karaşahin E, Deveci S, Günhan O, Yenen MC. Serous psammocarcinoma of the ovary and peritoneum: two case reports and review of the literature. Arch Gynecol Obstet. 2009;279:931-936.

4. Jena SK, Mishra P, Mohapatra V, Singh S. Bilateral Serous psammocarcinoma of ovary: rare variant low grade serous carcinoma. Case Rep Obstet Gynecol. 2015;2015:531242.
5. Aure JC, Hoeg K, Kolstad P. Psammoma bodies in serous carcinoma of the ovary. A prognostic study. Am J Obstet Gynecol. 1971;109:113-118.
6. Kühn W, Kaufmann M, Feichter GE, Schmid H, Hanke J, Rummel HH. Psammomabody content and DNA-flow cytometric results as prognostic factors in advanced ovarian carcinoma. Eur J Gynaecol Oncol. 1988;9:234-241.
7. Arole VC, Deshpande KA, Jadhav DB, Jogi A. Primary peritoneal psammocarcinoma. J Obstet Gynaecol Res. 2017;43:1366-1372.
8. Mitchell DG, Hill MC, Hill S, Zaloudek C. Serous carcinoma of the ovary: CT identification of metastatic calcified implants. Radiology. 1986;158:649-652.
9. Hiromura T, Tanaka YO, Nishioka T, Tomita K. Serous psammocarcinoma of the ovary: CT and MR findings. J Comput Assist Tomogr. 2007;31:490-492.
10. Ozulker T, Ozulker F, Ozpacaci T. 99mTc-MDP and 18F-FDG uptake in calcified metastatic lesions from ovarian papillary serous adenocarcinoma. Hell J Nucl Med. 2009;12:287-288.
11. Hu SL, Zhou ZR, Zhang YJ. Calcified metastases from ovarian carcinoma highlighted by F-18 FDG PET/CT: report of two cases. Abdom Imaging. 2012;37:675-679.
12. Dong A, Wang Y, Zuo C. FDG PET/CT in serous psammocarcinoma of the ovary. Clin Nucl Med. 2014;39:453-455.
13. Inanir S, Oksuzoglu K. FDG PET/CT Imaging of calcified sister mary joseph nodule. Clin Nucl Med. 2016;41:e458-e459.
14. Jeon G, Park SY. Primary peritoneal psammocarcinoma misdiagnosed as an heterotopic ossification: a case report. J Korean Soc Radiol. 2023;84:958-963.

Interesting Image

Mol Imaging Radionucl Ther 2025;34:70-72 *DOI:10.4274/mirt.galenos.2024.47135*

Pseudoprogression Shown on ^{18}F-FDG PET/CT After Pembrolizumab Treatment in a Case of Metastatic Bladder Cancer

Metastatik Mesane Kanserli Bir Olguda Pembrolizumab Tedavisi Sonrası ^{18}F-FDG PET/BT'de Gösterilen Psödoprogresyon

Fulya Kaya[1], Halil Kömek[1], İbrahim Hakkı Dursun[2], Veysi Şenses[1], Cihan Gündoğan[1]

[1]*University of Health Sciences Türkiye, Gazi Yaşargil Training and Research Hospital, Clinic of Nuclear Medicine, Diyarbakır, Türkiye*
[2]*Bower Hospital, Clinic of Medical Oncology, Diyarbakır, Türkiye*

Abstract

A 57-year-old man diagnosed with a metastatic bladder tumor was initiated on pembrolizumab treatment. ^{18}F-fluorodeoxyglucose (^{18}F-FDG) positron emission tomography/computed tomography (PET/CT) imaging performed to evaluate treatment response showed numerical-dimensional and metabolic increase in the metastatic lesions. In the ^{18}F-FDG PET/CT imaging performed 8 weeks later due to suspicion of pseudoprogression, a significant regression of the lesions was observed, and the patient was diagnosed with pseudoprogression. Pseudoprogression should be kept in mind when ^{18}F-FDG PET/CT is performed after the use of immunotherapy, and evaluation with follow-up PET/CT is recommended to confirm that the patient has hyperprogression or pseudoprogression.

Keywords: Immunotherapy, pseudoprogression, bladder cancer, pembrolizumab, PET/CT

Öz

Metastatik mesane tümörü tanılı 57 yaşında erkek hastaya pembrolizumab tedavisi başlandı. Tedavi yanıtının değerlendirilmesi için yapılan ^{18}F-florodeoksiglukoz (^{18}F-FDG) pozitron emisyon tomografisi/bilgisayarlı tomografi (PET/BT) görüntülemesinde, metastatik lezyonlarda sayısal-boyutsal ve metabolik artış izlendi. Psödoprogresyon şüphesi nedeniyle 8 hafta sonra yapılan ^{18}F-FDG PET/BT görüntülemesinde, lezyonların belirgin gerilediği görüldü ve psödoprogresyon tanısı konuldu. İmmünoterapi kullanımı sonrası yapılan ^{18}F-FDG PET/BT'de psödoprogresyon akılda tutulup hastanın hiper veya psödoprogrese olduğunu göstermek için takip PET/BT ile değerlendirme önerilir.

Anahtar kelimeler: İmmünoterapi, psödoprogresyon, mesane kanseri, pembrolizumab, PET/BT

Address for Correspondence: Fulya Kaya MD, University of Health Sciences Türkiye, Gazi Yaşargil Training and Research Hospital, Clinic of Nuclear Medicine, Diyarbakır, Türkiye
E-mail: fulyakaya450@gmail.com **ORCID ID:** orcid.org/0009-0005-4303-4993
Received: 27.02.2024 **Accepted:** 23.06.2024 **Publication Date:** 07.02.2025

Cite this article as: Kaya F, Kömek H, Dursun İH, Şenses V, Gündoğan C. Pseudoprogression shown on ^{18}F-FDG PET/CT after pembrolizumab treatment in a case of metastatic bladder cancer. Mol Imaging Radionucl Ther. 2025;34:70-72.

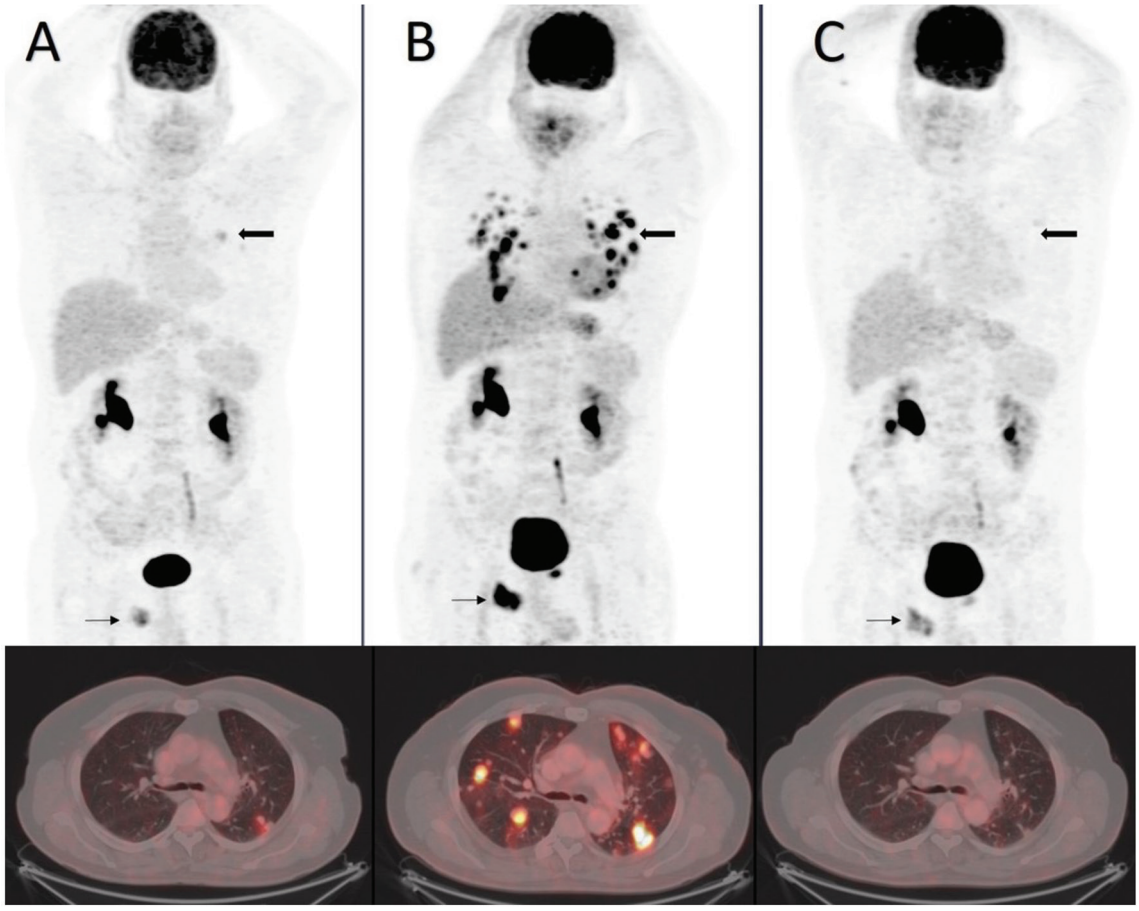

Figure 1. A 57-year-old man with high-grade papillary urothelial carcinoma who underwent transurethral resection of the bladder received gemstabin, cisplatin, and zolendronic acid due to lung and bone metastases in the initial staging. ^{18}Flourine-fluorodeoxyglucose (^{18}F-FDG) positron emission tomography/computed tomography (PET/CT) imaging [A: maximum intensity projection (MIP) and axial fusion] performed to evaluate treatment response showed increased ^{18}F-FDG uptake in multiple nodular lesions (thick arrows) [maximum standardized uptake value (SUV_{max}): 4.4], the largest of which was 11x8 mm in both lungs and lytic lesion (thin arrow) (SUV_{max}: 8.2) in the right ischium. Because there was a numerical progression in lung metastases compared with the previous PET/CT imaging (not shown), pembrolizumab treatment was initiated as second-line treatment. After 4 cycles of pembrolizumab treatment (after 3 months), PET/CT imaging (B: MIP and axial fusion) showed markedly increased intense ^{18}F-FDG uptake in multiple nodular lesions (thick arrows) (SUV_{max}: 15.4), the largest of which was 23x23 mm in both lungs and lytic-sclerotic lesions (thin arrow) (SUV_{max}: 15.6) in the left pubic-right ischial bones. In the multidisciplinary oncology council, the patient was considered pseudoprogression, and pembrolizumab treatment was continued. PET/CT imaging 8 weeks later (C: MIP and axial fusion) showed significant numerical and metabolic regression of nodular lesions (thick arrows) in both lungs, the largest of which regressed to 11x11 mm in size, and low ^{18}F-FDG uptake was observed in the nodules (SUV_{max}: 2.2). Reduced ^{18}F-FDG uptake was observed in the right ischial and left pubic bones (thin arrow) (SUV_{max}: 7) compared with the previous study. The patient was diagnosed with pseudoprogression, and treatment was continued. Immune checkpoint inhibitors have a wide range of indications, and their frequency of use is increasing (1). Overexpression of programed cell death protein-1 (PD-1)/programed cell death ligand 1 (PD-L1) in muscle invasive bladder cancer (MIBC) tissue was found to be associated with high ^{18}F-FDG uptake in the tumor (2). A recent study prospectively investigated the value of ^{18}F-FDG PET/CT for predicting lymph node metastasis (LNM) in MIBC patients receiving neoadjuvant pembrolizumab. PET/CT results were compared with histopathological findings, and the sensitivity to detect LNM was found to be 27% and 37.5%, and the specificities were 97% and 98% for ^{18}F-FDG PET/CT before and after pembrolizumab, respectively (3). Pseudoprogression describes the phenomenon of marked disease progression (increase in size and ^{18}F-FDG-affinity of lesions) on ^{18}F-FDG PET scan within 12 weeks of the start of immunotherapy, with a reduction in tumor burden if immunotherapy is continued (4). The incidence of pseudoprogression in urothelial cancer ranges from 1.5% to 17% (5). A new category of unconfirmed progression (iUPD) has been created in the immune-based therapeutics Response Evaluation Criteria in Solid Tumors and requires confirmation of progression (increase in size or number of lesions) on follow-up imaging. This treatment is usually recommended after 4-8 weeks following an initial study showing significant disease progression (6). The role of pseudoprogression on ^{18}F-FDG PET/CT in patients with MIBC treated with immunotherapy requires further investigation.

Ethics

Informed Consent: Informed consent was obtained from the patient.

Authorship Contributions

Concept: H.K., C.G., Design: H.K., C.G., İ.H.D., Data Collection or Processing: F.K., V.Ş., İ.H.D., Literature Search: F.K., C.G., V.Ş., Writing: F.K., C.G.

Conflict of Interest: No conflicts of interest were declared by the authors.

Financial Disclosure: The authors declare that this study has received no financial support.

References

1. Vaddepally RK, Kharel P, Pandey R, Garje R, Chandra AB. Review of Indications of FDA-approved immune checkpoint inhibitors per NCCN Guidelines with the level of evidence. Cancers (Basel). 2020;20:12(3):738.
2. Chen R, Zhou X, Liu J, Huang G. Relationship between the expression of PD-1/PD-L1 and 18F-FDG uptake in bladder cancer. Eur J Nucl Med Mol Imaging. 2019;46(4):848-854.
3. Marandino L, Capozza A, Bandini M, Raggi D, Farè E, Pederzoli F, Gallina A, Capitanio U, Bianchi M, Gandaglia G, Fossati N, Colecchia M, Giannatempo P, Serafini G, Padovano B, Salonia A, Briganti A, Montorsi F, Alessi A, Necchi A. [18F]Fluoro-Deoxy-Glucose positron emission tomography to evaluate lymph node involvement in patients with muscle-invasive bladder cancer receiving neoadjuvant pembrolizumab. Urol Oncol. 2021;39(4):235.e15-235.e21.
4. Jia W, Gao Q, Han A, Zhu H, Yu J. The potential mechanism, recognition and clinical significance of tumor pseudoprogression after immunotherapy. Cancer Biol Med. 2019;16(4):655-670.
5. Soria F, Beleni AI, D'Andrea D, Resch I, Gust KM, Gontero P, Shariat SF. Pseudoprogression and hyperprogression during immune checkpoint inhibitor therapy for urothelial and kidney cancer. World J Urol. 2018;36(11):1703-1709.
6. Gandy N, Arshad MA, Wallitt KL, Dubash S, Khan S, Barwick TD. Immunotherapy-related adverse effects on 18F-FDG PET/CT imaging. Br J Radiol. 2020;93(1111):20190832

Interesting Image

Mol Imaging Radionucl Ther 2025;34:73-75 *DOI:10.4274/mirt.galenos.2024.48264*

Primary Pulmonary Liposarcoma: A Case Report

Primer Pulmoner Liposarkom: Bir Olgu Sunumu

Huimin Li[1], Zhehao Lyu[2]

[1]Inner Mongolia Autonomous Region People's Hospital, Clinic of Nuclear Medicine, Hohhot, Inner Mongolia Autonomous, People's Republic of China

[2]The First Afliated Hospital of Harbin Medical University, Department of Nuclear Medicine, Harbin, Heilongjiang, People's Republic of China

Abstract

Primary liposarcoma of the lung is extremely rare. To date, only 24 cases have been reported in the English literature. Herein, we present a case of well-differentiated pulmonary liposarcoma that was misdiagnosed as teratoma on positron emission tomography/computed tomography (CT) and contrast-enhanced CT. Radical surgery with left superior lobectomy and mediastinal lymph node dissection were performed. The patient experienced recurrence and distant metastases 33 months after surgery. He was alive at the time of writing this report (36 months postoperatively). To our knowledge, this is the first case report of pulmonary well-differentiated liposarcoma.

Keywords: Primary pulmonary liposarcoma, positron emission tomography/computed tomography, well-differentiated liposarcoma

Öz

Akciğerin primer liposarkomu son derece nadirdir. Bugüne kadar, İngilizce literatürde sadece 24 olgu bildirilmiştir. Bu olgu sunumunda, pozitron emisyon tomografisi/bilgisayarlı tomografi ve kontrastlı CT'de teratom olarak yanlış teşhis edilen iyi farklılaşmış bir pulmoner liposarkom olgusu sunulmaktadır. Sol üst lobektomi ve mediastinal lenf nodu diseksiyonu ile radikal cerrahi uygulanmıştır. Hastada operasyondan 33 ay sonra nüks ve uzak metastazlar görülmüştür. Bu olgu sunumu yazıldığı sırada hasta hala hayattaydı (ameliyattan 36 ay sonra). Bildiğimiz kadarıyla, bu olgu bildirilen ilk iyi farklılaşmış pulmoner liposarkom olgusudur.

Anahtar kelimeler: Primer pulmoner liposarkom, pozitron emisyon tomografisi/bilgisayarlı tomografi, iyi farklılaşmış liposarkom

Address for Correspondence: Zhehao Lyu, The First Afliated Hospital of Harbin Medical University, Department of Nuclear Medicine, Harbin, Heilongjiang, People's Republic of China

E-mail: lyuzhehao@hrbmu.edu.cn **ORCID ID:** orcid.org/0009-0005-3160-2623

Received: 14.05.2024 **Accepted:** 21.07.2024 **Publication Date:** 07.02.2025

Cite this article as: Li H, Lyu Z. Primary pulmonary liposarcoma: a case report. Mol Imaging Radionucl Ther. 2025;34:73-75.

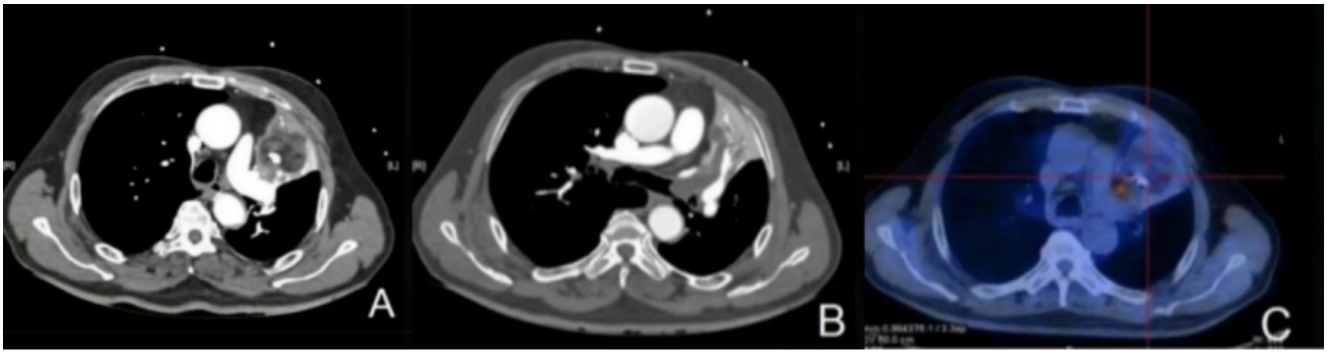

Figure 1. A 72-year-old male presented with complaints of shortness of breath for 2 weeks. Contrast-enhanced computed tomography of the chest (A and B) revealed an irregularly shaped, mixed-density mass with multiple components of soft tissue density, nodular calcification, and some areas of very low density (-51 H to -89 Hounsfield units), suggesting fat in the superior lobe of the left lung, involving the left main bronchus and left superior lobular bronchus, resulting in atelectasis of the left superior lobe. Positron emission tomography/computed tomography [PET/CT(C)] showed most of the mass to be non-fluorodeoxyglucose uptake, with hypermetabolic foci in the lateral portion with a maximum standardized uptake value of 6.2. PET/CT showed no distant metastases or other lesions.

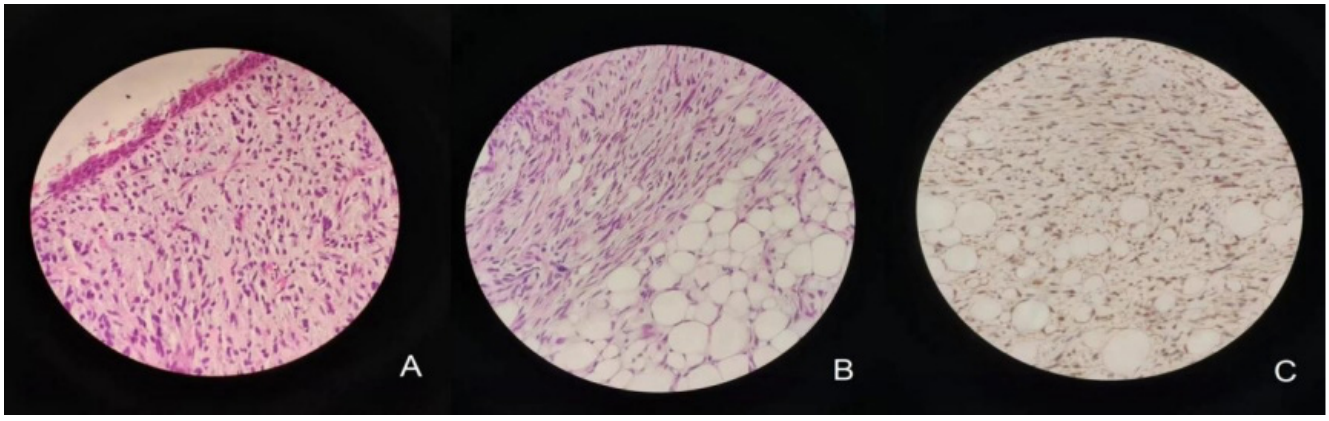

Figure 2. The patient underwent radical surgery, including left superior lobectomy and mediastinal lymph node dissection. Sudan III staining revealed that the tumor cells consisted of spindle cells and well-differentiated, nearly mature fat cells (A and B). Immunohistochemical staining of the tumor was positive for S-100 protein, Vimentin, Smooth muscle actin, and cyclin-dependent kinase 4 (CDK4) (C); scattered positive for MDM2 and CD34; and negative for cytokeratin, desmin, MelanA, and HMB45. The postoperative pathological diagnosis was well-differentiated spindle cell liposarcoma.

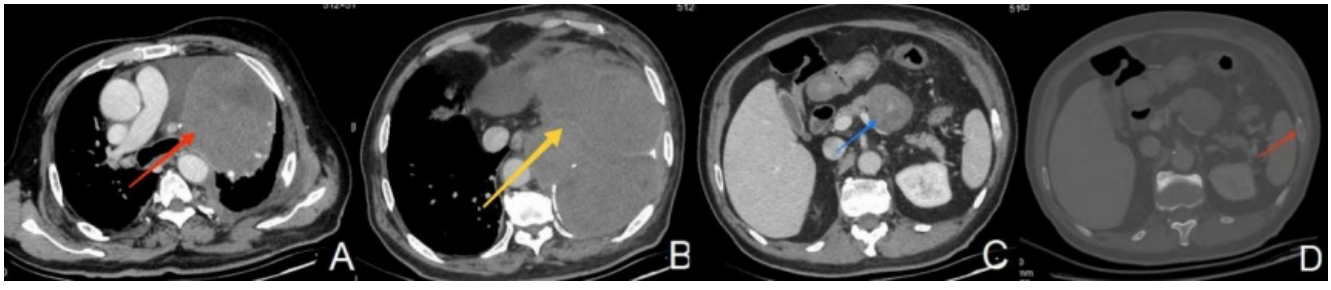

Figure 3. Local recurrence (A, red arrow), pleural metastasis (B, yellow arrow), pancreatic metastasis (C, blue arrow), and bone metastasis (D, red arrow) were found 33 months after the operation. The patient was alive at the time of writing this report (36 months postoperatively).

Primary liposarcoma of the lung is an extremely rare malignancy, accounting for approximately 0.2% of all pulmonary tumors (1). Lipomatosis and asbestosis may be pathogenic factors (2); According to the World Health Organization Classification of Soft Tissue Tumors (2020 edition), liposarcomas can be divided into five types: well-differentiated, dedifferentiated, myxoid, pleomorphic, and mixed (3); Well-differentiated liposarcoma tumors contain a large amount of fat, usually ≥ 75% of the tumor volume (4). Although well-differentiated liposarcomas have certain imaging characteristics, they still need to be differentiated from other lung tumors, especially those with fatty components such as teratomas, hamartomas, and other mesenchymal-derived tumors (5). Preoperative imaging examination is difficult to correctly diagnose, and the final diagnosis depends on the immunohistochemical results. Immunohistochemistry of well-differentiated liposarcoma was positive for Vimentin, S-100, MDM2, and CDK4 (2). The preferred treatment for primary pulmonary liposarcoma is radical resection and lymph node dissection (2,4). Well-differentiated liposarcoma was the least invasive of the five pathological subtypes. The 5-year survival rate of well-differentiated liposarcomas is 87.1% (6) and the recurrence rate is 40-50% (7). The median survival time of patients with primary intrathoracic liposarcoma according to the well-differentiated subtypes was 174 months (8).

Ethics

Informed Consent: An informed consent was obtained from the patient.

Authorship Contributions

Concept: H.L., Design: H.L., Data Collection or Processing: Z.L., Analysis or Interpretation: Z.L., Literature Search: Z.L., Writing: H.L.

Conflict of Interest: No conflicts of interest were declared by the authors.

Financial Disclosure: The authors declare that this study has received no financial support.

References

1. Li B, Xin Z, Li Z, Zhang X. Giant pulmonary pleomorphic liposarcoma: A case report and literature review. Asian J Surg. 2023;46:1109-1110.
2. Dey T, Khosla D, Kumar D, Chatterjee D, Madan R, Singh H, Singh H, Kapoor R. Rare case of primary pulmonary pleomorphic liposarcoma treated with multimodal therapy. Ochsner J. 2021;21:431-435.
3. Choi JH, Ro JY. The 2020 WHO classification of tumors of soft tissue: selected changes and new entities. Adv Anat Pathol. 2021;28:44-58.
4. Said M, Migaw H, Hafsa C, Braham R, Golli M, Moussa A, Zakhama A, Elkamel A, Gannouni A. Imaging features of primary pulmonary liposarcoma. Australas Radiol. 2003;47:313-317.
5. Stark P, Eber CD, Jacobson F. Primary intrathoracic malignant mesenchymal tumors: pictorial essay. J Thorac Imaging. 1994;9:148-155.
6. Oh YJ, Yi SY, Kim KH, Cho YJ, Beum SH, Lee YH, Suh JS, Hur H, Kim KS, Kim SH, Choi YD, Shin KH, Jun HJ, Kim SJ, Lee J, Park SH, Noh SH, Rha SY, Kim HS. Prognostic model to predict survival outcome for curatively resected liposarcoma: a multi-institutional experience. J Cancer. 2016;7:1174-80.
7. Henricks WH, Chu YC, Goldblum JR, Weiss SW. Dedifferentiated liposarcoma: a clinicopathological analysis of 155 cases with a proposal for an expanded definition of dedifferentiation. Am J Surg Pathol. 1997;21:271-281.
8. Fu Z, Yang K, Yang X, Chen S, Wang W, Chen D, Zhao J, Li Z, Feng Q, Zhou Z, Wang L, Gao S, Liang J. Primary intrathoracic liposarcoma: a clinical analysis of 31 cases. Cancer Commun (Lond). 2019;39:15.

Interesting Image

Mol Imaging Radionucl Ther 2025;34:76-78 *DOI:10.4274/mirt.galenos.2024.46547*

Pyomyositis as Presentation of Chemoport-related Infection in Breast Carcinoma: ^{18}F-FDG PET/CT Findings

Meme Karsinomunda Kemoport ile İlişkili Enfeksiyon Olarak Piyomiyozit: ^{18}F-FDG PET/BT Bulguları

Vijay Singh[1], Dinesh Srivastava[2], Neha Kotarya[2], Manish Ora[2], Sanjay Gambhir[2]

[1]All India Institute of Medical Sciences (AIIIMS), Rishikesh, India
[2]Sanjay Gandhi Post Graduate Institute of Medical Sciences (SGPGIMS), Lucknow, India

Abstract

A Chemoport is frequently utilized in oncological patients for administering chemotherapy. However, inadequate care can lead to various infectious and non-infectious complications. Infection commonly presents as a local infection that can lead to life-threatening septicemia. Early diagnosis and intervention are necessary to reduce morbidity and mortality. We report a patient with breast cancer who underwent ^{18}F-fluorodeoxyglucose positron (^{18}F-FDG) positron emission tomography/computed tomography (PET/CT) due to suspicion of metastatic disease. ^{18}F-FDG-PET/CT revealed pyomyositis involving multiple skeletal muscles and septic emboli in the lungs and identified the chemoport as a possible source of infection. The infection source was confirmed and the patient responded to anti-microbiological therapy.

Keywords: Chemoport-related infection, breast cancer, ^{18}F-FDG PET/CT, pyomyositis, methicillin-resistant staphylococcus aureus

Öz

Kemoterapi portu, onkolojik hastalarda kemoterapi uygulamak için sıklıkla kullanılır. Ancak, yetersiz bakım çeşitli enfeksiyöz ve enfeksiyöz olmayan komplikasyonlara yol açabilir. Enfeksiyon genellikle lokal bir enfeksiyon olarak ortaya çıkar ve bazen yaşamı tehdit eden septisemiye yol açabilir. Morbidite ve mortaliteyi azaltmak için erken tanı ve müdahale gereklidir. Metastatik hastalık şüphesiyle ^{18}F-florodeoksiglukoz (^{18}F-FDG) pozitron emisyon tomografisi/bilgisayarlı tomografi (PET/BT)'ye giren bir meme kanseri hastası bildirilmiştir. ^{18}F-FDG PET/BT ile çok sayıda iskelet kasını tutan piyomiyozit ve akciğerlerde septik emboli ortaya kondu ve kemoport olası bir enfeksiyon kaynağı olarak tanımlandı. Enfeksiyon kaynağı doğrulandı ve hasta anti-mikrobiyal tedaviye yanıt verdi.

Anahtar kelimeler: Kemoport ile ilişkili enfeksiyon, meme kanseri, ^{18}F-FDG PET/BT, piyomiyozit, metisiline dirençli staphylococcus aureus

Address for Correspondence: Manish Ora, Sanjay Gandhi Post Graduate Institute of Medical Sciences (SGPGIMS), Lucknow, India
E-mail: drmanishora@yahoo.com **ORCID ID:** orcid.org/0000-0002-9748-2215
Received: 20.05.2024 **Accepted:** 21.07.2024 **Publication Date:** 07.02.2025

Cite this article as: Singh V, Srivastava D, Kotarya N, Ora M, Gambhir S. Pyomyositis as presentation of chemoport-related infection in breast carcinoma: ^{18}F-FDG PET/CT findings. Mol Imaging Radionucl Ther. 2025;34:76-78.

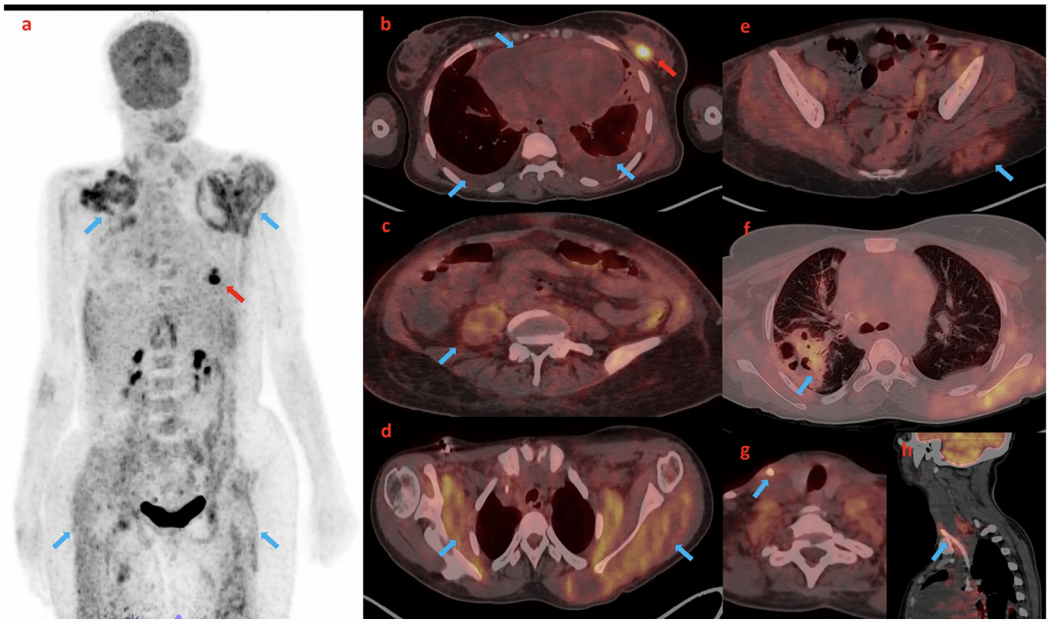

Figure 1.
A 23-year-old female presented with a left breast lump associated with nipple discharge. She had a history of lumpectomy six months ago (histopathology was not available). Mammography revealed a lump in the left breast. A core biopsy confirmed infiltrating ductal carcinoma, grade III (Ki-67 index: 70-80%). Clinical staging was CT4bN1M0. A Chemoport was placed for neoadjuvant chemotherapy. The treatment plan consisted of four cycles of Epirubicin+Cyclophosphamide, followed by four cycles of docetaxel, and subsequent surgery. The patient remained asymptomatic during the chemotherapy regimens. She developed fever, cough, difficulty breathing, chills, and rigors four days after the last dose of docetaxel. Bilateral crepitations were observed. Chest X-ray revealed lung lesions with pericardial effusion. ^{18}F-fluorodeoxyglucose positron (^{18}F-FDG) positron emission tomography/computed tomography (PET/CT) maximum intensity projection image (a) shows ^{18}F-FDG-avidity in the left breast region (red arrow). Multiple areas of increased uptake are noted around the shoulders and both thighs (blue arrow). Axial Fused ^{18}F-FDG PET/CT image (b) revealed an ^{18}F-FDG-avid lesion in the left breast (red arrow) with pericardial effusion and bilateral pleural effusion (blue arrow), ^{18}F-FDG-avid hypodense collection in the right psoas muscle (c). Similar heterogeneous density bulky muscles were noted in the bilateral periscapular region (d), bilateral iliopsoas, right gluteal muscles, and subcutaneous region of the left gluteal region (e). A lung abscess with an air-fluid level is noted in the right lower lobe (f). Linear ^{18}F-FDG avidity was noted along the catheter line (g, h). Pus was found along the catheter line. Aspiration Cytology of the Scapular Muscle revealed Methicillin-resistant Staphylococcus aureus. The Chemoport was removed. The broad-spectrum antibiotics Meropenem and Teicoplanin were initiated. She responded within 24 hours with improvement in symptoms.

An implantable chemoport device is used to administer chemotherapies with the aim of reducing the need for frequent venipunctures. Common complications include thrombosis, catheter obstruction, extravasation, catheter migration, and catheter fracture infection (1,2,3,4). These conditions may be associated with significant morbidity and mortality. The incidence of central venous access port-related infection ranges from 0.21 to 0.66 per 1000 catheter days (3,5). Hematogenous seeding may cause endocarditis, suppurative thrombosis, osteomyelitis, and metastatic site infections (4). *Staphylococcus*, *Gram-negative bacilli*, and Candida are the predominant pathogens (4,5). Although rare, extensive pyomyositis can also occur (6). General treatment principles involve blood and catheter cultures, initiating empirical intravenous antimicrobial therapy, device removal if clinically indicated, and tailoring the antimicrobial spectrum based on culture results (4).

Ethics

Informed Consent: Informed consent was obtained.

Footnotes

Authorship Contributions

Concept: V.S., M.O., Design: V.S., D.S., N.K., M.O., S.G., Data Collection or Processing: V.S., D.S., N.K., M.O., S.G., Analysis or Interpretation: V.S., D.S., N.K., M.O., S.G., Literature Search: V.S., M.O., Writing: V.S., M.O.

Conflict of Interest: No conflicts of interest were declared by the authors.

Financial Disclosure: The authors declare that this study has received no financial support.

References

1. Machat S, Eisenhuber E, Pfarl G, Lenz K, Payer F, Duran C, Längle F, Reiner CS, Ketteler H, Betz M. Complications of central venous port systems: a pictorial review. Insights Imaging. 2019;10:86.
2. Mittal GS, Sundriyal D, Naik NB, Bansal D, Khandelwal N, Singh K, Rathi A, Gupta A, Kapoor R. Totally implantable venous access device (Chemoport) in oncology: study of 168 polyurethane Chemoport catheter system. South Asian J Cancer. 2021;10:261-4.
3. Aparna S, Ramesh S, Appaji L, Ghosh P, Chatterjee N, Manohar S. Complications of Chemoport in children with cancer: Experience of 54,100 catheter days from a tertiary cancer center of Southern India. South Asian J Cancer. 2015;4:143-5.
4. Sousa B, Furlanetto J, Hutka M, Baggott S, Bassam T, Chiappino C, Mavri V. ESMO Guidelines committee. Central venous access in oncology: ESMO clinical practice guidelines. Ann Oncol. 2015;26:152-68.
5. Wang TY, Lee KD, Chen PT, Lai JH, Chang MC, Su HC, Lee YC, Chang YT. Incidence and risk factors for central venous access port-related infection in Chinese cancer patients. J Formos Med Assoc. 2015;114:1055-60.
6. Nakayama Y, Sugiyama A, Yamamoto T, Matsumoto Y, Kinoshita A, Mori N, Sakamoto M. Pyomyositis in a patient undergoing chemotherapy for gastric cancer: a case report and literature review. Case Rep Oncol. 2021;14:1220-7.

Interesting Image

Mol Imaging Radionucl Ther 2025;34:79-81 *DOI:10.4274/mirt.galenos.2024.37929*

Omental Cake in Non-Hodgkin's Disease: ^{18}F-FDG PET-CT Findings

Non-Hodgkin Lenfomada Omental Kek: ^{18}F-FDG PET-BT Bulguları

Manale Otmani, Salah Oueriagli Nabih, Omar Ait Sahel, Yassir Benameur, Abderrahim Doudouh

Mohammed V Military Training Hospital, Clinic of Nuclear Medicine, Souissi University, Rabat, Fas

Abstract

Neoplastic infiltration of the omentum is mostly caused by metastatic ovarian, gastric, colon, or pancreatic cancer. Lymphomatous infiltration of the omentum is rare because the omentum lacks a lymphoid component. To date, lymphomatous involvement of the omentum has only been reported in patients with non-Hodgkin lymphoma. Peritoneal lymphomatosis remains a rare presentation of malignant lymphoma characterized by diffuse peritoneal lesions and is frequently accompanied by ascites and mesenteric lesions. In this review, we aimed to illustrate the case of a 72 year old mal patient diagnosed with aggressive large B-cell lymphoma, adressed for initial extension assessment in whom ^{18}F-fluorodeoxyglucose positron emission tomograph/computed tomography found unusual omental and mesenteric involvement.

Keywords: ^{18}F-FDG PET-CT, non-Hodgkin's lymphoma, omental cake

Öz

Omentumun neoplastik infiltrasyonu çoğunlukla metastatik over, gastrik, kolon veya pankreas kanserinden kaynaklanır. Omentumun lenfomatöz infiltrasyonu nadirdir çünkü omentumda lenfoid bir bileşen yoktur. Bugüne kadar, omentumun lenfomatöz tutulumu yalnızca non-Hodgkin lenfomalı hastalarda bildirilmiştir. Peritoneal lenfomatozis, yaygın peritoneal lezyonlarla karakterize ve sıklıkla asit ve mezenterik lezyonlarla birlikte görülen malign lenfomanın nadir bir sunumu olmaya devam etmektedir. Bu derlemede, agresif büyük B-hücreli lenfoma tanısı almış, ilk ekstansiyon değerlendirmesi için başvuran ve ^{18}F-florodeoksiglukoz pozitron emisyon tomografisi/bilgisayarlı tomografide alışılmadık omental ve mezenterik tutulum bulunan 72 yaşında bir erkek hastayı bildirmeyi amaçladık.

Anahtar kelimeler: ^{18}F-FDG PET-BT, non-Hodgkin lenfoma, omental kek

Address for Correspondence: Manale Otmani, Mohammed V Military Training Hospital, Clinic of Nuclear Medicine, Souissi University, Rabat, Fas
E-mail: otmanale2014@gmail.com **ORCID ID:** orcid.org/0009-0006-4574-9105
Received: 06.06.2024 **Accepted:** 21.07.2024 **Publication Date:** 07.02.2025

Cite this article as: Otmani M, Nabih SO, Sahel OA, Benameur Y, Doudouh A. Omental cake in non-hodgkin's disease: ^{18}F-FDG PET-CT findings. Mol Imaging Radionucl Ther. 2025;34:79-81.

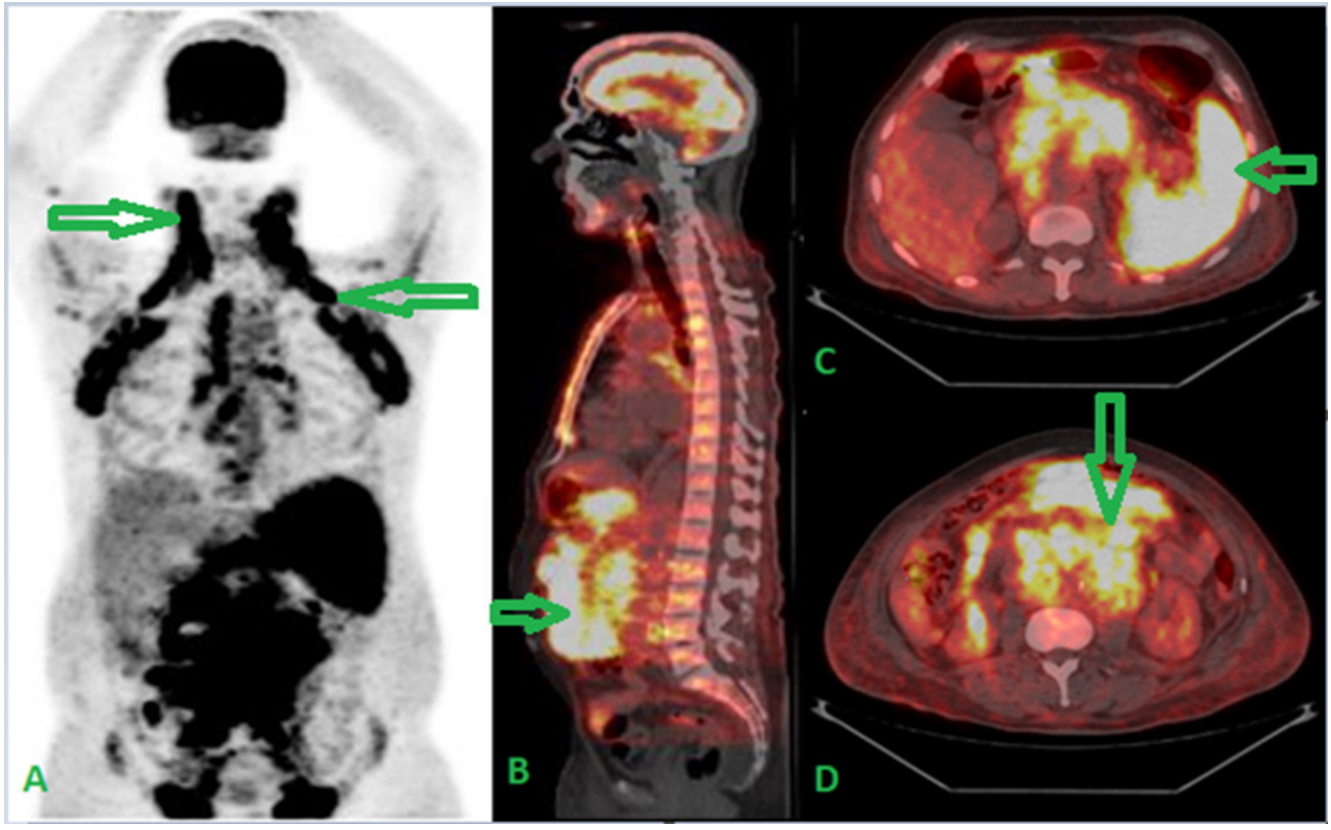

Figure 1. A 72 year old mal patient diagnosed with aggressive large B-cell lymphoma, adressed for initial extension assessment. A whole body ^{18}F-fluorodeoxyglucose (^{18}F-FDG)-positron emission tomograph (PET) scan showed the presence of lymph node involvement of almost all the lymph nodes above and below the diaphragm (A; maximum intensity projection; arrows), diffuse splenic damage [C; fused axial section PET- computed tomography (CT); arrow] and intense ^{18}F-FDG uptake in the pelvis with epiploic and mesenteric nodular foci (B; fused coronal image PET-CT; arrow) and (D; fused axial section PET-CT arrow) eliciting SUV_{max} up to 14.9, suggesting diffuse peritoneal lymphomatosis. This case illustrates an extraordinary presentation of peritoneal lymphomatosis visualized on PET-CT and an uncommon aspect of "^{18}F-FDG-avid omentum cake" in non-Hodgkin's lymphoma. The greater omentum is a fibrous, fatty membrane structure formed by the continuation of the peritoneal surface of the anterior and posterior viscera. It extends downward from the stomach and folds in on itself, covering the small intestine and attaching to the upper side of the transverse colon (1). Neoplastic infiltration of the omentum is most commonly caused by metastatic ovarian, gastric, colon, or pancreatic cancer. Lymphomatous infiltration of the omentum is rare because the omentum lacks a lymphoid component. To date, lymphomatous involvement of the omentum has only been reported in patients with non-Hodgkin lymphoma (1). Since most lymphomas are usually metabolically active, PET using ^{18}F-FDG is very useful for early diagnosis and staging (2). PET-CT may be useful in the assessment of lymphomatous peritoneal tumor infiltration, as outlined in several published studies of other malignancies (3). Peritoneal lymphoma is radiologically characterized by diffuse peritoneal thickening and mass, and is associated with ascites in most cases. Intestinal wall thickening, retroperitoneal lymphadenopathy, and hepatosplenomegaly are also frequently observed (4). Peritoneal involvement is critical for accurate staging and treatment planning, as peritoneal involvement can be cured with appropriate therapeutic intervention and may result in death if treatment is delayed (5), which in our case highlights the value and the performances of PET-CT in initial staging and evaluation of the extent of the disease.

Ethics

Informed Consent: An informed consent was obtained from the patient.

Footnote

Authorship Contributions

Concept: M.O., S.O.N., O.A.S., Y.B., A.D., Design: M.O., S.O.N., O.A.S., Y.B., A.D., Data Collection or Processing: M.O., Analysis or Interpretation: M.O., S.O.N., A.D., Literature Search: M.O., O.A.S., Writing: M.O.

Conflict of Interest: No conflicts of interest were declared by the authors.

Financial Disclosure: The authors declare that this study has received no financial support.

References

1. Jacobs JE, Salhany KE, Fox KR, Birnbaum BA. Omental caking in Hodgkin's disease. Computed tomography findings. Clin Imaging. 1996;20:253-255.
2. Hutchings M, Barrington SF. PET/CT for therapy response assessment in lymphoma. J Nucl Med. 2009;50:21S-30S.
3. Turlakow A, Yeung HW, Salmon AS, Macapinlac HA, Larson SM. Peritoneal carcinomatosis: role of (18)F-FDG PET. J Nucl Med. 2003;44:1407-1412.
4. Karaosmanoglu D, Karcaaltincaba M, Oguz B, Akata D, Ozmen M, Akhan O. CT findings of lymphoma with peritoneal, omental and mesenteric involvement: peritoneal lymphomatosis. Eur J Radiol. 2009 2009;71:313-317.
5. Ichikawa S, Fukuhara N, Saito K, Onodera K, Onishi Y, Yokoyama H, Ichinohasama R, Harigae H. Diffuse Large B-cell Lymphoma Presenting as Peritoneal Lymphomatosis: A Case Report and Literature Review. Intern Med. 2022;61:2057-2060.

Interesting Image

Mol Imaging Radionucl Ther 2025;34:82-84 *DOI:10.4274/mirt.galenos.2024.46667*

Nasolacrimal Metastasis from Parotid Ductal Carcinoma Detected by ^{18}F-FDG PET/CT

^{18}F-FDG PET/BT ile Parotis Duktal Karsinomu Kaynaklı Nazolakrimal Metastaz Saptanması

Kexia Fang[1], Jianqiang Li[1], Guodong Feng[1], Xiang Guo[1], Yumin Zheng[2]

[1]*Zibo Municipal Hospital, Department of Nuclear Medicine, Shandong, China*

[2]*Beijing Hospital, National Center of Gerontology, Institute of Geriatric Medicine, Chinese Academy of Medical Sciences, Department of Nuclear Medicine, Beijing, China*

Abstract

A 39-year-old woman presented with left neck masses for 4 months and epiphora of the left eye for 3 weeks. Ultrasonography revealed a mass in the left parotid gland and multiple cervical lymph nodes. Biopsy of the mass in the left parotid gland revealed infiltrating ductal carcinoma. ^{18}F-fluorodeoxyglucose positron emission tomography/computed tomography scan was undertaken, which showed a mass in the left parotid gland and multiple cervical lymph nodes with high metabolism. A nodule in the left nasolacrimal duct with high metabolism was observed. The nodule was surgically removed and pathologically confirmed as metastatic parotid ductal carcinoma.

Keywords: Nasolacrimal tumor, metastasis, parotid ductal carcinoma, ^{18}F-FDG, PET/CT

Öz

Otuz dokuz yaşındaki kadın hasta 4 aydır boynunun sol tarafında kitleler çıkması ve 3 haftadır sol gözünde epifora şikayeti ile başvurdu. Ultrasonografi sol parotis bezinde kitle ve çok sayıda büyümüş servikal lenf nodu olduğunu ortaya koydu. Sol parotis bezindeki kitlenin biyopsisi infiltre duktal karsinom iyi uyumlu idi. ^{18}F-florodeoksiglukoz pozitron emisyon tomografisi/bilgisayarlı tomografi taraması yapıldı ve sol parotis bezinde kitle ve yüksek metabolizmaya sahip çok sayıda servikal lenf nodu görüldü. Sol nazolakrimal kanalda yüksek metabolizmaya sahip bir nodül gözlendi. Nodül daha sonra cerrahi olarak çıkarıldı ve patolojik olarak metastatik parotis duktal karsinomu olarak doğrulandı.

Anahtar kelimeler: Nazolakrimal tümör, metastaz, parotis duktal karsinomu, ^{18}F-FDG, PET/BT.

Address for Correspondence: Yumin Zheng, Beijing Hospital, National Center of Gerontology, Institute of Geriatric Medicine, Chinese Academy of Medical Sciences, Department of Nuclear Medicine, Beijing, China
E-mail: yuminzhengcn@163.com **ORCID ID:** orcid.org/0000-0002-5294-4981
Received: 29.05.2024 **Accepted:** 21.07.2024 **Publication Date:** 07.02.2025

Cite this article as: Fang K, Li J, Feng G, Guo X, Zheng Y. Nasolacrimal metastasis from parotid ductal carcinoma detected by ^{18}F-FDG PET/CT. Mol Imaging Radionucl Ther. 2025;34:82-84.

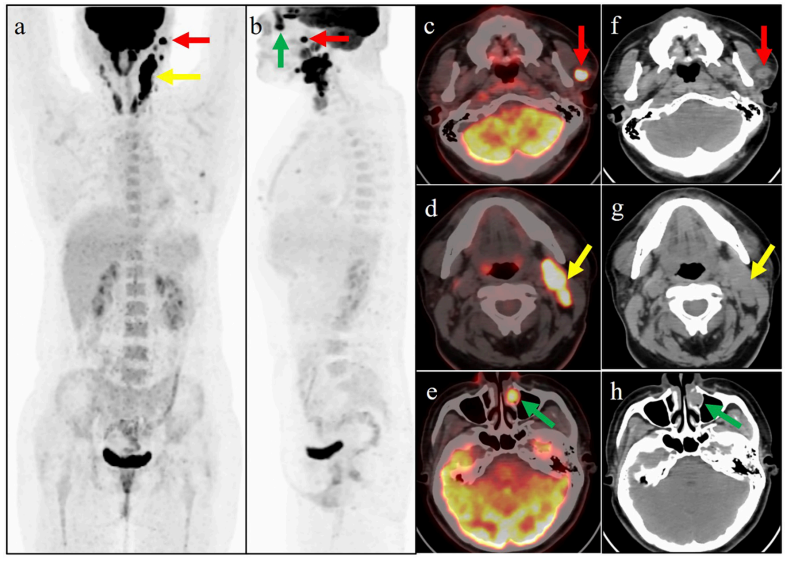

Figure 1. A 39-year-old woman presented with left neck masses for 4 months and epiphora of the left eye for 3 weeks. Ultrasonography revealed a mass in the left parotid gland and multiple cervical lymph nodes. The biopsy pathology of the mass in the left parotid gland revealed infiltrating ductal carcinoma. ^{18}F-florodeoksiglukoz (^{18}F-FDG) positron emission tomography/computed tomography scan was then performed for staging. The maximum-intensity projection image (a: anteroposterior) shows some areas of intense ^{18}F-FDG activity in the left parotid region with an SUV_{max} of 24.0 (red arrow) and the left side of neck with SUV_{max} of 22.3 (yellow arrow). The left lateral MIP image (b) shows a focus of intense activity behind the nose, with an SUV_{max} of 17.3 (green arrow). On the axial images (c-e: fused PET/CT; f-h: CT), the red arrow corresponded well to the mass of the left parotid, the yellow arrow pointed to multiple cervical lymph nodes, and the green arrow corresponded to the nodule of the left nasolacrimal duct, which was surgically removed. Subsequently, the lesion was pathologically and immunohistochemically confirmed as metastatic parotid ductal carcinoma.

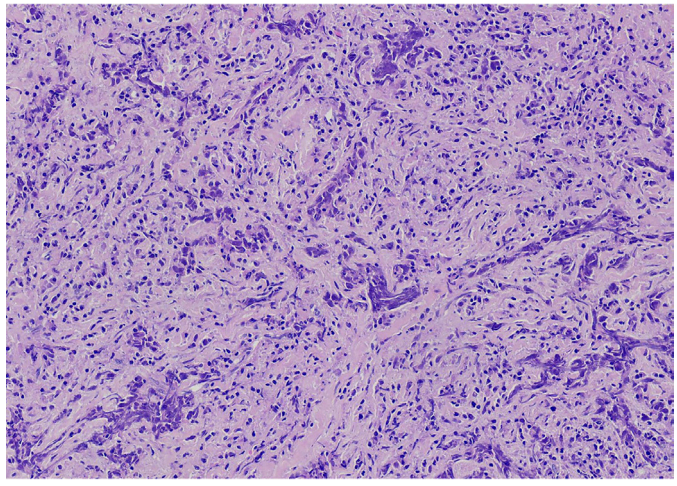

Figure 2. Histologically, the nasolacrimal duct specimen (hematoxylin and eosin stain, original magnification x200) showing mesenchyma infiltrated by strip-shaped invasive ductal carcinoma cells with the typical feature of irregular nested infiltrate. The most common clinical symptoms of lacrimal sac and duct tumors are epiphora, recurrent dacryocystitis, epistaxis, and/or lacrimal sac mass. These non-specific clinical manifestations often lead to the misdiagnosis of lacrimal sac tumors such as dacryocystitis (1). Tumors of the lacrimal sac and duct are divided into primary and secondary tumors. Primary malignant epithelial neoplasms include squamous cell carcinoma (SCC), transitional cell carcinoma, adenocarcinoma, adenoid cystic carcinoma, poorly differentiated carcinoma, and primary melanomas (2,3). The most common malignant lacrimal sac tumors are of epithelial origin, with the majority being SCC (4,5,6). Secondary tumors can occur from any cutaneous or paranasal sinus lesion or from distant organs, in the case of metastatic tumors, and may include carcinomas or melanomas (7,8). Our case indicates that metastatic tumors should be considered when high ^{18}F-FDG accumulation is observed in the nodule of the lacrimal duct, especially when accompanied by other abnormal ^{18}F-FDG uptake lesions.

Ethics

Informed Consent: Written informed consent has been obtained from the patient.

Footnote

Authorship Contributions

Surgical and Medical Practices: J.L., Concept: Y.Z., Design: Y.Z., Data Collection or Processing: G.F., Analysis or Interpretation: Y.Z., Literature Search: X.G., Writing: K.F.

Conflict of Interest: No conflict of interest was declared by the authors.

Financial Disclosure: There were no sources of funding for this work.

References

1. Lee LN, Scott AR, Chan AW, Frankenthaler RA. Management of transitional cell carcinoma of the lacrimal sac: a multidisciplinary approach to orbit sparing treatment. Laryngoscope. 2010;120(Suppl 4):161.
2. El-Sawy T, Frank SJ, Hanna E, Sniegowski M, Lai SY, Nasser QJ, Myers J, Esmaeli B. Multidisciplinary management of lacrimal sac/nasolacrimal duct carcinomas. Ophthalmic Plast Reconstr Surg. 2013;29:454-457.
3. Subramaniam SS, Anand R, Mellor TK, Brennan PA. Primary Lacrimal Sac Melanoma With Metastatic Cervical Disease: A Review of the Literature and Case Report. J Oral Maxillofac Surg. 2017;75:1438-1441.
4. Zhang R, Qian J, Meng F, Yuan Y, Bai M, Bi Y, Xu B, Yuan Y, Hong R. A Staged Procedure in the Treatment of Primary Lacrimal Sac Epithelial Malignancy: A Retrospective Cases Analysis. Ophthalmic Plast Reconstr Surg. 2019;35:187-192.
5. Song X, Wang J, Wang S, Wang W, Wang S, Zhu W. Clinical analysis of 90 cases of malignant lacrimal sac tumor. Graefes Arch Clin Exp Ophthalmol. 2018;256:1333-1338.
6. Kumar VA, Esmaeli B, Ahmed S, Gogia B, Debnam JM, Ginsberg LE. Imaging Features of Malignant Lacrimal Sac and Nasolacrimal Duct Tumors. AJNR Am J Neuroradiol. 2016;37:2134-2137.
7. Sia KJ, Tang IP, Kong CK, Tan TY. Nasolacrimal relapse of nasopharyngeal carcinoma. J Laryngol Otol. 2012;126:847-850.
8. Ding J, Sun H, Xin Y, Li D. Metastatic hepatocellular carcinoma mimicking acute dacryocystitis. Can J Ophthalmol. 2018;53:132-134.

Interesting Image

Mol Imaging Radionucl Ther 2025;34:85-87 *DOI:10.4274/mirt.galenos.2024.68095*

Unexpected Detection of Cephalad Renal Ectopia Due to Large Omphalocele Containing the Liver on Tc-99m DMSA Scintigraphy

Tc-99m DMSA Sintigrafisinde Sefalad Renal Ektopi: Karaciğer İçeren Geniş Omfalosel Olgusu ve Beklenmeyen Bulgular

Zeynep Işık, Cansu Küçüker, Murat Fani Bozkurt

Hacettepe University Faculty of Medicine, Department of Nuclear Medicine, Ankara, Türkiye

Abstract

Omphalocele is a congenital abdominal wall defect with herniation of abdominal viscera into a sac. Tc-99m DMSA renal cortical scan is a functional imaging technique used for detecting parenchymal defects, mostly in patients with recurrent urinary tract infection as well as congenital renal abnormalities. Renal anomalies are known to accompany omphalocele. In this retrospective study, we present a case of cephalad renal ectopia as observed on Tc-99m DMSA scintigraphy in a patient with omphalocele due to a large hernia sac containing most of the liver; and we review the renal abnormalities associated with omphalocele in the literature.

Keywords: Omphalocele, cephalad renal ectopia, Tc-99m DMSA, liver, renal abnormality

Öz

Omfalosel; abdominal organları içerebilen herni kesesinin izlendiği bir konjenital abdominal duvar defektidir. Sıklıkla ek konjenital anomaliler eşlik eder ve çeşitli sendromlarla ilişkilidir. Tc-99m DMSA sintigrafisi böbrek parankimini görüntülemede kullanılan bir fonksiyonel görüntülemedir, tekrarlayan idrar yolu enfeksiyonu hastalarında geniş kullanımı olmasının yanında konjenital renal anomalilerde de kullanılmaktadır. Sık tekrarlayan idrar yolu enfeksiyonu nedeni ile başvuran, omfalosel tanısı olan hastamızda Tc-99m DMSA sintigrafisinde sefalad renal ektopi saptandı, ayrıca karaciğerin büyük kesimini içeren geniş herni kesesi izlendi, Bu çalışmada Tc-99m DMSA sintigrafisinde karşılaştığımız bulguları sunmanın yanında omfalosel ve buna ikincil gelişen renal anomalileri değerlendirdik.

Anahtar kelimeler: Omfalosel, sefalad renal ektopi, Tc-99m DMSA, karaciğer, renal anomali

Address for Correspondence: Zeynep Işık, Hacettepe University Faculty of Medicine, Department of Nuclear Medicine, Ankara, Türkiye
E-mail: zeynepisik@hacettepe.edu.tr **ORCID ID:** orcid.org/0009-0000-8818-6441
Received: 12.02.2024 **Accepted:** 22.07.2024 **Publication Date:** 07.02.2025

Cite this article as: Işık Z, Küçüker C, Bozkurt MF. Unexpected detection of cephalad renal ectopia due to large omphalocele containing the liver on Tc-99m DMSA scintigraphy. Mol Imaging Radionucl Ther. 2025;34:85-87.

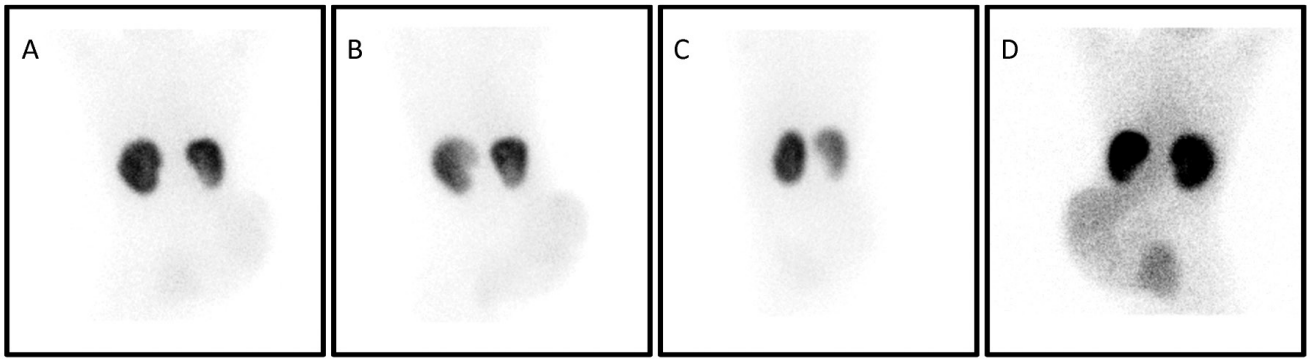

Figure 1. A 6-year-old girl with omphalocele was referred to our clinic with the diagnosis of recurrent urinary tract infection (UTI) after a Tc-99m DMSA scan. The Tc-99m DMSA scan revealed minimally decreased Tc-99m DMSA uptake in the lower pole of the right kidney, which may be suggestive of a parenchymal defect due to UTI and otherwise quite normal Tc-99m DMSA biodistribution throughout both kidneys. However, the kidneys appeared to be located more cranially than their normal expected position within the abdomen, along with an impression suspicious of a rotational anomaly seen on posterior, right posterior oblique, and left posterior oblique projections (Figure 1A, B, C) respectively. To our knowledge, there was also an unusual Tc-99m DMSA uptake in the right abdominal quadrant, with a laterally bulging appearance. The pattern of the uptake was homogeneous, and its intensity was lower than that of Tc-99m DMSA uptake in the kidneys, and the intensity of such uptake was more prominent on the anterior projection image (Figure 1D). Thus, these findings suggest that the uptake may not be due to an ectopic kidney as a component of supernumerary kidneys. Upon physical examination, a large hernia sac with an omphalocele was observed in the area.

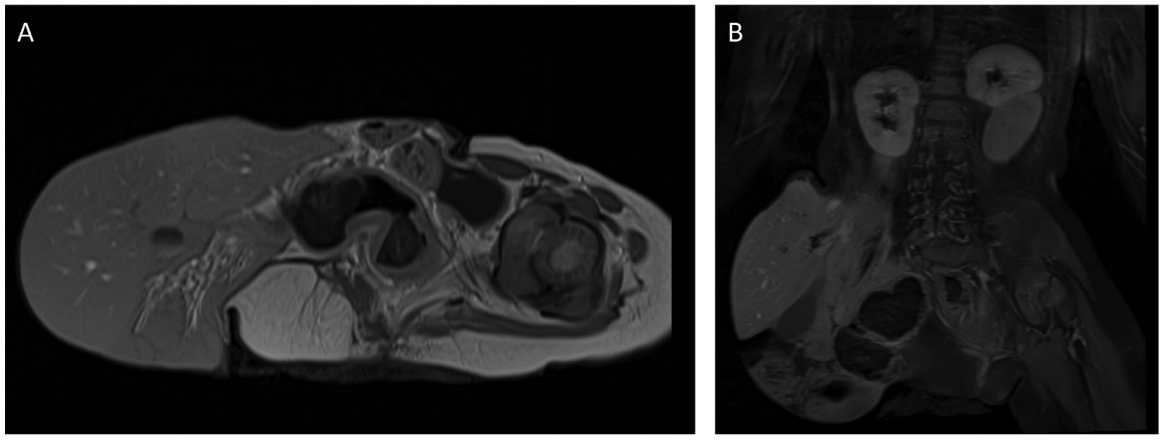

Figure 2. Magnetic resonance imaging (Figures 2a axial, 2b coronal) revealed a large omphalocele that included most of the liver, corresponding to the faint but homogeneous Tc-99m DMSA uptake in the right quadrant of the abdomen (Figure 2a). The kidneys were located just below the diaphragm, consistent with cephalad renal ectopia, and the liver was mostly located within the omphalocele sac (Figure 2b). Omphalocele is an abdominal wall defect characterized by herniation of the abdominal viscera into a sac (1). During fetal development, omphalocele occurs when gut contents fail to rotate and return to the abdominal cavity (2). It is a rare congenital defect that shows a severity spectrum from small umbilical hernia to large sac with evisceration of all abdominal organs, as in our case (3). Omphalocele is frequently associated with syndromes and a variety of additional congenital abnormalities, including chromosomal abnormalities, cardiac, pulmonary, gastrointestinal, musculoskeletal manifestations, and neural tube defects (3,4,5,6). In addition, associated renal anomalies can be observed. The kidneys migrate from the pelvis to the upper abdomen during normal fetal development. The liver plays an important role in the normal position of the kidneys as it arrests the ascent of the kidneys. Omphalocele containing the liver has been accounted for excessive migration, which is finally stopped by the diaphragm, resulting in cephalad renal ectopia (7,8). Our patient had a neural tube defect, right lower extremity agenesia, cephalad renal ectopia, and omphalocele. To the best of our knowledge, this is the first case of a laterally protruded large omphalocele containing most of the liver that was diagnosed with cephalad renal ectopia on a Tc-99m DMSA scan.

Ethics

Informed Consent: An informed consent was obtained from the patient.

Footnotes

Authorship Contributions

Surgical and Medical Practices: Z.I., C.K., Concept: Z.I., M.F.B., Design: Z.I., M.F.B., Data Collection or Processing: Z.I., C.K., Analysis or Interpretation: Z.I., M.F.B., Literature Search: Z.I., C.K., M.F.B., Writing: Z.I., C.K., M.F.B.

Conflict of Interest: No conflicts of interest were declared by the authors.

Financial Disclosure: The authors declare that this study has received no financial support.

References

1. Fernbach SK. Neonatal Gastrointestinal Radiology. In:Textbook of Gastrointestinal Radiology W.B. Saunders; 2008:2203-2233.
2. Zahouani T, Mendez MD. Omphalocele. In: StatPearls [Internet]. Treasure Island (FL): StatPearls. 2021 Jan–.
3. Gaca M, Bissett GS. Diseases of the Pediatric Abdominal Wall, Peritoneum, and Mesentery. In: Textbook of Gastrointestinal Radiology. W.B. Saunders. 2008: 2371-2381.
4. Bence CM, Wagner AJ. Abdominal wall defects. Transl Pediatr. 2021;10:1461-1469.
5. Conner P, Vejde JH, Burgos CM. Accuracy and impact of prenatal diagnosis in infants with omphalocele. Pediatr Surg Int. 2018;34:629-633.
6. Corey KM, Hornik CP, Laughon MM, et al. Frequency of anomalies and hospital outcomes in infants with gastroschisis and omphalocele. Early Hum Dev. 2014;90:421-424.
7. Connolly LP, Connolly SA, Treves ST. Renal malposition secondary to omphalocele shown on hepatobiliary scintigraphy. Clin Nucl Med. 2001;26:546-548.
8. Pinckney LE, Moskowitz PS, Lebowitz RL, et al. Renal malposition associated with omphalocele. Radiology. 1978;129:677-682.

Letter to the Editor

Mol Imaging Radionucl Ther 2025;34:88-89 *DOI:10.4274/mirt.galenos.2024.60566*

A Different Scintigraphic Perspective on the Systolic Function of the Left Ventricle-I

Sol Ventrikülün Sistolik Fonksiyonuna Sintigrafik Olarak Farklı Bir Bakış Açısı-I

Alper Özgür Karaçalıoğlu

University of Health Sciences Türkiye, Gülhane Faculty of Medicine, Department of Nuclear Medicine, Ankara, Türkiye

Keywords: Exponential decay, time-volume curve, the left ventricle, gMPI

Anahtar kelimeler: Üstsel azalma, zaman-hacim eğrisi, sol ventrikül, gMPS

Dear Editor,

Exponential decay refers to the process of decreasing an amount by a constant percentage rate over time. A leaking container is an example of a non-steady-state fluid system, which behaves exponentially. In this system, the height decreases as the liquid flows out of the cylinder, resulting in a decrease in current. The gravitational potential energy-density gradient is proportional to the height of the fluid inside the container, and this is the driving force of the leaking water from the container (1). The left ventricle can be considered a leaking container, and the contractility of the myocardium is the driving force for ejecting the blood volume from the cavity into the aorta. As seen on the Wiggers diagram, not all volumes and pressures recorded in the left ventricle increase or decrease linearly (2). For this reason, the model described in the manuscript (3), seems to be reasonable to express the systolic ejection dynamics of the left ventricle.

When the pulse rate increases from 60 to 72, the Ec value increases when we recalculate the values for an imaginary patient. "t" value of the imaginary patient [end-diastolic volume (EDV) 100 mL, end-systolic volume (ESV): 40 mL cycle time 6.4/16] for 60 bpm is (6.4/16x1000) 400 ms. Ec value of the imaginary patient for 60 bpm is [40/100= e -k(0.4)] 2.29/s. "t" value of the imaginary patient for 72 bpm is (6.4/16x833) 333 ms. Ec value of the imaginary patient for 72 bpm is [40/100= e -k (0.333)] 2.75/s. When we apply a similar pulse increase to a study patient with real values (EDV: 125 mL, ESV: 35 mL, cycle time 5.5/16), we obtain similar increase in results. For 60 bpm, "t" value is (5.5/16x1000) 343 ms. Ec value for 60 bpm is [35/125= e -k (0.343)] 3.7 / s. For 72 bpm, "t" value is (5.5/16x833) 286 ms. Ec value for 72 bpm is [35/125= e -k (0.286)] 4.4/s. It can be observed that, if all parameters remain constant, the Ec value increases as the pulse increases. This means that the heart can do the same job in less time and perform better. In other words, when the pulse rate increases, a negative development such as "falling into the ischemic category" does not occur.

The "t" value, which shows systole time in the decay formula, takes the patient's heart rate into account for calculating the cycle and systole time.

The cycle time (ms)=60bpm x 1000ms/pulse (bpm) of a patient

The systole time= the cycle time x distance (EDV-ESV)/16.

Ec is a systolic functional parameter of the left ventricle, and while it does not provide information about left ventricular perfusion, it seems to have the potential to detect systolic

Address for Correspondence: Address for Correspondence: Alper Özgür Karaçalıoğlu, University of Health Sciences Türkiye, Gülhane Faculty of Medicine, Department of Nuclear Medicine, Ankara, Türkiye
E-mail: aokaracali@gata.edu.tr **ORCID ID:** orcid.org/0000-0003-2683-804X
Received: 02.01.2024 **Accepted:** 02.01.2024 **Publication Date:** 07.02.2025

Cite this article as: Karaçalıoğlu ÖA. A Different scintigraphic perspective on the systolic function of the left ventricle-1. Mol Imaging Radionucl Ther. 2025;34:88-89.

dysfunction caused by any perfusion disorder. Depending on the size, the infarct area affects the systolic function of the left ventricle. Therefore, it is expected to reduce the percentage of the left ventricular emptying per unit time.

This letter to the editor was prepared in response to the author's criticisms (4) about the article referenced with number 3.

Footnotes

Author Contributions

Financial Disclosure: The author declared that this study has received no financial support.

References

1. https://phys.libretexts.org/Courses/University_of_California_Davis/UCD%3A_Physics_7B_-_General_Physics/5%3A_Flow_Transport_and_Exponential_-working_copy/5.09%3A_Exponential_Fluid_Flow
2. Mitchell JR, Wang JJ. Expanding application of the wiggers diagram to teach cardiovascular physiology. Adv Physiol Educ. 2014;38:170-175.
3. Karaçalıoğlu AÖ, Çınar A. A Different Scintigraphic Perspective on the Systolic Function of the Left Ventricle-1. Mol Imaging Radionucl Ther. 2023;32:206-213.
4. Taşçı C. About the article titled "a different scintigraphic perspective on the systolic function of the left ventricle-1". Mol Imaging Radionucl Ther. 2024;33:66-67.